Dissertation

Submitted to the
Combined Faculties for the Natural Sciences and for Mathematics
of the Ruperto-Carola University of Heidelberg, Germany
for the Degree of
Doctor of Natural Sciences

Presented by
Ann-Cathrin Hofer (M.Sc.)
Born in Heidelberg, Germany

Oral Examination: 12th of September 2016

Regulatory T cells protect the neonatal liver and secure the hepatic circadian rhythm

Referees

1st Referee: Prof. Dr. Peter Angel

2nd Referee: Dr. Markus Feuerer

This dissertation was performed and written during the period from November 2012 to May 2016 in the German Cancer Research Center (DKFZ) under the supervision of Prof. Dr. Peter Angel and direct supervision of Dr. Markus Feuerer. The dissertation was submitted to the Combined Faculties for the Natural Sciences and for Mathematics of the Ruperto-Carola University of Heidelberg, Germany in June 2016.

German Cancer Research Center (DKFZ)
Immune Tolerance (D100)
Im Neuenheimer Feld 280
69120 Heidelberg, Germany

Confirmation

Hereby, I confirm that I have written this thesis independently, using only the results of my investigation unless otherwise stated. Furthermore, I declare that I have not submitted this thesis for a degree to any other academic or similar institution.

Parts of this dissertation have been submitted for publishing:

> Regulatory T cells protect the liver early in life and safeguard the hepatic circadian rhythm
> Ann-Cathrin Hofer, Thomas Hielscher, David M. Richards, Michael Delacher, Ulrike Träger, Sophia Föhr, Artyom Vlasov, Marvin Wäsch, Marieke Esser, Annette Kopp-Schneider, Achim Breiling, Frank Lyko, Ursula Klingmüller, Peter Angel, Jakub Abramson, Jeroen Krijgsveld & Markus Feuerer

Parts of the experiments in this dissertation were performed in collaboration with other research groups as follows:

- CG methylation analysis with the 454 pyrosequencing technology:
  Division of Epigenetics, DKFZ, Heidelberg
  Dr. Achim Breiling & Prof. Dr. Frank Lyko
- Quantitative differential proteomics experiments:
  Genome Biology Unit, EMBL, Heidelberg
  Sophia Föhr and Dr. Jeroen Krijgsveld
- Bioinformatic analysis of microarray data
  Division of Biostatistics, DKFZ, Heidelberg
  Thomas Hielscher and Annette Kopp-Schneider
- Mdr2$^{-/-}$ liver microarray data
  Division of Signal Transduction and Growth Control, DKFZ, Heidelberg
  Prof. Dr. Peter Angel

(Place/Date) (Signature)

Table of content

1 Summary 1

2 Zusammenfassung 2

3 Introduction 3

3.1 The immune system 3

3.1.1 The innate immune response 3

3.1.2 The adaptive immune response 4

3.2 Regulatory T cells 6

3.2.1 Thymic-derived T_{reg} cells 7

3.2.2 Thymus-derived versus peripheral-induced T_{reg} cells 10

3.2.3 Heterogeneity idea of T_{reg} cell 11

3.2.4 Tissue-specialized T_{reg} cells 13

3.3 Liver cells 16

3.4 Circadian rhythm 18

3.4.1 Circadian rhythm pathway 18

3.4.2 Lymphocytes and the circadian rhythm 22

4 Aim of study 23

5 Methods 24

5.1 Mice 24

5.1.1 Keeping 24

5.2 Tissue sample preparation 24

5.2.1 Cell depletion 24

5.2.2 Tissue isolation and sample preparation 25

5.2.3 AutoMACS cell purification 25

5.2.4 Blood samples 25

5.3 Cell culture techniques 26

5.3.1 Primary hepatocyte isolation 26

5.4 Flow cytometry 26

5.5 Fluorescence-activated cell sorting (FACS) 27

5.5.1 *In vivo* proliferation assay 27

5.6 Epigenetics 28
5.6.1 Purification and bisulfite conversion of genomic DNA 28
5.7 Proteomics 29
5.7.1 Protein digestion, labeling of peptides with stable isotopes (TMT) and fractionation 29
5.7.2 LC-ESI-MS/MS analysis 29
5.7.3 Protein identification and quantification 30
5.8 PCR techniques 30
5.8.1 RNA isolation and cDNA synthesis 30
5.8.2 Quantitative real-time PCR 31
5.8.3 RNA expression profiling 31
5.9 Bioinformatic and statistical analysis 31
5.9.1 Bioinformatic and statistical analysis of proteomic data 31
5.9.2 Bioinformatics and statistical analysis of microarray data 32
5.9.3 General statistical analysis 33

6 Materials 34

6.1 Mice 34
6.2 Antibodies 35
6.3 Cytokines 36
6.4 Kits 37
6.5 Bisulfite Primer 38
6.6 Quantitative real-time PCR primer 39
6.7 Reagents 40
6.8 Plasticware and consumables 42
6.9 Buffers and solutions 43
6.10 Equipment 44
6.11 Software 45

7 Results 46

7.1 Hepatic regulatory T cells 46
7.2 The neonatal liver 59
7.3 Neonatal T_{reg} cells protect homeostasis and metabolic liver function 68

7.4 T_{reg} cells influence the circadian rhythm 74

8 Discussion 92

8.1 The neonatal liver 92

8.2 Neonatal hepatic T_{reg} cells 93

8.3 Where does the enlarged T_{reg} cell population in the liver of neonatal mice come from? 95

8.4 Hepatic T_{reg} cell depletion 97

8.5 Removal of T_{reg} cells affects the circadian rhythm 98

8.6 Hepatic macrophages, liver inflammation and the circadian rhythm 100

8.7 Conclusion and perspectives 103

9 References 106

10 Appendix 120

11 Abbreviations 123

12 Acknowledgments 128

List of Figures

Figure 1: T_{reg} cell subsets. 12
Figure 2: Circadian rhythm. 19
Figure 3: Molecular mechanisms of the circadian clock. 21
Figure 4: Diphtheria toxin injection scheme. 24
Figure 5: T_{reg} cell sorting scheme. 27
Figure 6: T_{reg} cell gating strategy in liver, spleen and lung. 47
Figure 7: T_{reg} cells in liver, spleen and lung of neonatal mice. 48
Figure 8: Hepatic T_{reg} cells in neonatal mice are thymus-derived. 49
Figure 9: Hepatic T_{reg} cells in neonatal NOD mice. 50
Figure 10: CD44 surface expression of T_{reg} and T_{conv} cells in liver, spleen and lung. 52
Figure 11: $CD11a^{+}$ T_{reg} and T_{conv} cells in liver and spleen. 53
Figure 12: Proliferative activity of T cell populations in liver, lung and spleen measured by flow cytometry staining with Hoechst 33342-A. 55
Figure 13: Proliferative activity and TCR stimulation of hepatic T_{reg} cells. 56
Figure 14: Gene expression analysis of hepatic T_{reg} cells. 58
Figure 15: Gene expression in neonatal and adult livers. 59
Figure 16: NK cells, macrophages and monocytes in the neonatal liver. 61
Figure 17: Gene expression in neonatal and adult primary hepatocytes. 62
Figure 18: Hepatic gene expression in $MyD88^{-/-}$, $Trif^{-/-}$, $Tlr4^{-/-}$ and $Rag2^{-/-}$ mice. 64
Figure 19: The neonatal liver. 66
Figure 20: Proliferative activity in neonatal primary hepatocytes. 67
Figure 21: T_{reg} cell depletion in neonatal and adult livers. 69
Figure 22: Gene expression in neonatal livers was strongly affected after T_{reg} cell depletion. 70
Figure 23: Expression of transcriptions factors in the livers of T_{reg}-depleted mice. 71

Figure 24: T_{reg} cell depletion in neonatal livers induced changes in expression of genes involved in metabolic liver function. 73
Figure 25: Loss of T_{reg}-mediated control induced elevated levels of core-clock gene expression in the liver. 75
Figure 26: Disturbed circadian gene expression in T_{reg}-depleted livers. 77
Figure 27: Different patterns of altered circadian gene expression in T_{reg}-depleted livers. 78
Figure 28: RAIN algorithm identified altered circadian gene expression in T_{reg}-depleted livers. 79
Figure 29: T_{reg} cell depletion induced altered expression of circadian genes involved in metabolic processes. 81
Figure 30: Development block of mature B and T cells had no influence on the hepatic circadian gene expression. 83
Figure 31: Loss of macrophages did not mimic T_{reg} cell depletion induced changes in circadian gene expression. 84
Figure 32: Cytokine or dexamethasone treatment did not result in alteration of *Rev-Erb-α* gene expression. 85
Figure 33: Gene expression of *in vitro* cultured primary hepatocytes. 87
Figure 34: Circadian gene expression in livers of $Mdr2^{-/-}$ mice. 88
Figure 35: Hepatic T_{reg} cell frequency 7 days after T_{reg} cell depletion. 89
Figure 36: Normalized circadian gene expression after return of T_{reg} cells in the liver. 90
Figure 37: Liver inflammation after return of hepatic T_{reg} cells. 91
Figure 38: T_{reg} cells safeguard the circadian rhythm in the liver tissue. 100
Figure 39: Identification of two new non-classical functions of T_{reg} cells in the liver tissue. 105

List of Tables

Table 1:	List of antibodies	35
Table 2:	List of cytokines	36
Table 3:	List of Kits	37
Table 4:	List of Bisulfite Primer	38
Table 5:	List of Sybr Primer	39
Table 6:	List of Reagents	40
Table 7:	List of Plasticware and consumables	42
Table 8:	List of buffers and solutions	43
Table 9:	List of equipment	44
Table 10:	List of software used for analysis	45
Table 11:	Comparison of Cyp proteins expressed in the liver of neonatal versus adult mice assessed by quantitative mass spectrometry analysis	120
Table 12:	List of cluster of genes following the dysregulated pattern of *Per1* expression during T_{reg} cell depletion	121
Table 13:	List of cluster of genes following the dysregulated pattern of *Rev-Erb-*α expression during T_{reg} cell depletion	122

1 Summary

Regulatory T cells (T_{reg} cells) play a crucial role in the immune system by controlling the establishment and maintenance of immune tolerance and homeostasis. T_{reg} cells have been described to perform additional non-immunological functions beyond their classical functions in peripheral tissues. In this context, best examples are the specialized T_{reg} cell population in visceral adipose tissue (VAT). The VAT-resident T_{reg} cells gain the ability to control metabolic parameters. To further extent the concept of tissue-resident T_{reg} cells, we aimed to analyze the phenotype and function of T_{reg} cells in the liver tissue.

We observed a significant accumulation of hepatic T_{reg} cells in neonatal mice at around day 10 after birth. With progressive maturation of the mice the T_{reg} frequency normalized. The neonatal hepatic T_{reg} cells were highly proliferative as demonstrated by cell cycle measurements. Furthermore, the cells showed the characteristic T_{reg} cell methylation pattern of the Foxp3 locus. The T_{reg} cell accumulation in the neonatal liver occurred in an immature liver with strongly proliferating hepatocytes, a low-grad inflammatory signature and changes in key gene expression.

Depletion of T_{reg} cells with the associated loss of T_{reg}-mediated immune control induced major changes in the liver, including increased expression of immune-related genes and genes regulating the circadian clock such as *Rev-Erb-*α or *Per1*. The circadian expression of approximately 400 genes in the liver was affected by the ablation of T_{reg} cells.

Our results indicate that T_{reg} cells are important to secure the circadian rhythm of genes regulating the hepatic clock as well as clock-controlled genes. Furthermore, the presence of T_{reg} cells is required for a normal expression of genes involved in liver metabolism, especially in the neonatal phase of the mice. Therefore, we propose that T_{reg} cells do not only control the inflammatory state of the liver, but are also critical for the establishment and maintenance of liver homeostasis.

2 Zusammenfassung

Regulatorische T-Zellen (T_{regs}) spielen eine wichtige Rolle im Immunsystem da sie für die Etablierung und Aufrechterhaltung der Immuntoleranz sowie der Immunhomöostase im Gewebe verantwortlich sind. T_{regs} können neben ihren klassischen Funktionen zusätzlich nicht-immunologische Funktionen in peripheren Geweben ausführen. Ein bekanntes Beispiel für gewebe-spezialisierte T_{reg} Populationen sind die T_{regs} im viszeralen Fettgewebe. Diese Zellen haben die Fähigkeit metabolische Parameter im Fettgewebe zu steuern. Unser Ziel war es den Phänotyp sowie die Funktion von T_{regs} im Lebergewebe zu analysieren, um das Konzept der gewebe-spezialisierten T_{regs} weiter zu entwickeln.

Wir beobachteten eine signifikante Anreicherung von T_{regs} in der Leber von neugeborenen 10 Tage alten Mäusen. Die T_{reg} Frequenz in der Leber normalisierte sich mit fortschreitender Reifung der Mäuse. Zellzyklus-Messungen demonstrierten, dass die T_{regs} in der neonatalen Leber stark proliferierten. Des Weiteren zeigten die Zellen ein für T_{regs} charakteristisches Methylierungsmuster des *Foxp3* Lokus auf. Die signifikante Anreicherung von T_{regs} erfolgte in einer unreifen, neonatalen Leber mit stark proliferierenden Hepatozyten, einer niedriggradigen Entzündungssignatur sowie einer veränderten Expression von Lebergenen.

Depletion von T_{regs} induzierte eine starke Veränderung der Genexpression der Leber. Die Expressionen von Immun-Genen sowie Regulatoren der zirkadianen Uhr, wie zum Beispiel *Rev-Erb-*α oder *Per1*, erhöhten sich stark durch den Verlust der T_{reg}-vermittelnden Immunkontrolle. Die zirkadiane Expression von rund 400 Lebergenen war durch den Verlust von T_{regs} in der Leber beeinträchtigt.

Unsere Ergebnisse deuten an, dass T_{regs} wichtig für die sichere Ausführung des zirkadianen Rhythmus von Lebergenen, welche die zirkadiane Uhr regulieren oder von der zirkadianen Uhr kontrolliert werden, sind. Des Weiteren sind T_{regs} erforderlich für eine ungestörte Expression von Genen des Leberstoffwechsels, besonders in der Leberentwicklung von neonatalen Mäusen. Basierend auf diesen Ergebnissen kommen wir zu dem Schluss, dass T_{regs} nicht nur den Entzündungszustand der Leber kontrollieren, sondern auch eine entscheidende Rolle in der Etablierung und Erhaltung der Leber-Homöostase spielen.

3 Introduction

3.1 The immune system

The mammalian immune system protects our body from diseases using layered defense mechanisms with increasing specificity, whereby different tissue, cellular and molecular components all work together. Besides pathogens like viruses, bacteria, fungi or parasites, the immune system is also challenged with damaged or cancerous cells of the host itself. Allergies, autoimmune diseases or infections with pathogens can result from impaired function of the immune system. The vertebrate immune system can be divided into two parts: the innate and the adaptive immune system (Murphy et al., 2008; Alberts et al. 2008).

3.1.1 The innate immune response

Innate immune responses serve as a first line of host defense in a non-specific manner. Three different mechanisms of the innate immune defense are involved in the clearance of infections before the adaptive immune systems needs to be called into play to work together to eliminate the pathogens (Alberts et al. 2008). Physical and chemical barriers build the first line of defense for pathogens. For example, skin and mucosal epithelia as well as the acidic pH of the stomach block access of microorganisms to the vertebrate host. The second mechanism of the innate immune defense involves cell-intrinsic responses. Cells such as neutrophils, macrophages or dendritic cells (DC) take up pathogens via phagocytosis und use different mechanisms to destroy pathogens. For example, engulfed pathogens are digested after fusion of the phagosome with the lysosome. The third mechanism of the innate immune defense includes a specialized set of phagocytic cells that helps to clear the body of pathogens and infected cells. Professional phagocytic cells recognize conserved structures expressed on the surface of pathogens through a complex and overlapping molecular network of pattern-recognition receptors (PRRs) (Alberts et al. 2008). Receptor ligation results in activation of complement cascades to opsonize the pathogen. Moreover, secretion of cytokines,

chemokines and co-stimulatory molecules leads to local inflammation and chemotactic attraction of further immune cells to site of inflammation (Akira, Uematsu, and Takeuchi 2006). Natural killer (NK) cells are involved in the destruction of infected cells by inducing apoptosis. When the innate immune response fails to clear or keep the infection at bay, the adaptive immune response comes into play and both work together to eliminate the infection. Nevertheless, the innate immune defense plays a critical role in controlling early infections because of the delayed activation of the adaptive immune defense (Alberts et al. 2008).

3.1.2 The adaptive immune response

In comparison to the unspecific immune response mounted by the innate system, the adaptive immune response is pathogen-specific and provides long-lasting memory. While invading pathogens as well as their toxic product are destroyed by adaptive immune responses, several mechanisms are in place to avoid immune responses directed against self-molecules. Two different types of immune responses -*antibody response* and *T cell-mediated immune response*- can be distinguished, which are performed by different classes of lymphocytes (Alberts et al. 2008).

During the antibody response, bone marrow-derived B cells become activated and secrete antibodies to opsonize pathogens (Alberts et al. 2008).

In the T cell-mediated immune response naïve thymus-derived T cells, expressing either the surface co-receptor CD4 or CD8, circulate in the bloodstream and peripheral lymphoid organs until the cells recognize a specific antigen with their T cell receptor (TCR). Antigens are presented on the surface of antigen-presenting cells (APCs) by the major histocompatibility complex (MHC) (Alberts et al. 2008). Besides the binding to their specific antigen, T cells require distinct cytokine co-stimulation and CD28-dependent co-stimulation mediated by the binding to the APC surface proteins CD80 or CD86. T cell differentiation into different effector T cells subtypes depends on the kind of pathogen (Murphy, Travers, and Walport 2008).

$CD8^+$ T cells recognize a complex of MHC class I molecules and peptides from intra-cellular pathogens such as viruses (Alberts et al. 2008). Stimulated $CD8^+$ T cells differentiate into cytotoxic T lymphocytes (CTLs), killing infected host cells by the release of cytotoxic granules such as granzymes or perforins (Jenkins and Griffiths 2010).

$CD4^+$ T cells recognize extra-cellular peptides presented by MHC class II molecules and differentiate upon stimulation into different CD4 effector subsets such as T helper 1 (T_{H1}), T_{H2} and T_{H17} cells (Alberts et al. 2008, Murphy et al., 2008). T helper cell subsets fulfill different functions to help regulating immune responses such as inducing B cell antibody class switch, helping to activate CTLs or maximizing bactericidal activity of macrophages (Alberts et al. 2008). The different subsets are characterized by different transcription factors and cytokine secretion patterns. The transcription factor T-bet and the secretion of Interleukin- (IL-) 2 and interferon (INF)-γ characterize the T_{H1} subset, which is induced through the cytokines IL-12 and INF-γ. IL-4 induce the differentiation of T_{H2} cells, characterized by the expression of the transcription factor GATA3 and the release of IL-4, IL-13 and IL-5 (Koch et al. 2009; Campbell and Koch 2011). The T_{H17} lineage is induced by exposure to the transforming growth factor β (TGF-β) and IL-6. T_{H17} cells express the transcription factor RORγT and secret IL-17 (Korn et al. 2009).

The natural killer T (NKT) cells are another lymphocyte cell type, which is important for the adaptive immune response. Like the T helper cell subsets, the $NK1.1^+CD4^+$ cells develop in the thymus and carry a TCR consisting of one α- and one β-chain. Glycosphingolipid-activated NKT cells secret IFN-γ and IL-4, mobilize CD4 and CD8 T cell responses by activation of DCs, and activate NK cells as well as antibody production by B cells (Bendelac, Savage, and Teyton 2007).

Regulatory T (T_{reg}) cells, a subpopulation of $CD4^+$ conventional T cells (T_{conv} cells), regulate both the innate and the adaptive immune responses to foreign and self-antigens and prevent autoimmunity (Hori, Takahashi, and Sakaguchi 2003; Fontenot, Gavin, and Rudensky 2003). T_{reg} cells are in the focus of this thesis and will be explored in detail in the following chapters of this introduction.

3.2 Regulatory T cells

T_{reg} cells modulate both the innate and the adaptive immune responses to foreign and self-antigens and limit the extent of inflammation while also preventing autoimmunity. Thereby, T_{reg} cells play a central role in the immune system by controlling the establishment and maintenance of immunologic tolerance and homeostasis (Feuerer, Hill, et al. 2009; Hori, Takahashi, and Sakaguchi 2003).

T_{reg} cells represent around 3 - 5% of the entire T cell pool and are characterized by high expression of the IL-2 receptor molecule α (CD25) and the lineage marker transcription factor forkhead box P3 (Foxp3) (Hori, Takahashi, and Sakaguchi 2003; Fontenot, Gavin, and Rudensky 2003). It is now well established that deficiency or dysfunction of T_{reg} cells, due to loss-of-function mutations in the *Foxp3* gene, are responsible for various autoimmune diseases, allergies and other sometimes fatal immune disorders in mice and human. Scurfy mice, carrying a mutated *Foxp3* gene, develop multi-organ autoimmunity and lymphoproliferation, which leads to the death of the mice by the age of 24 days (Brunkow et al. 2001; Godfrey et al. 1991). The counterpart in humans is the fatal immune dysregulation polyendocrinopathy enteropathy (IPEX) syndrome, which is developed in humans with an X-linked *FOXP3* mutation (Bennett et al. 2001).

T_{reg} cells have conserved suppressive mechanisms to exert their immunosuppressive functions (Vignali, Collison, and Workman 2008). One mechanism of T_{reg}-mediated suppression is the secretion of cytokines such as IL-10, IL-35 and TGF-β, which have inhibitory effects on T_{conv} cells. Another mechanism of T_{reg}-mediated suppression is the induction of apoptosis in target cells in a granzyme A or B- and perforin-dependent manner (Grossman et al. 2004; Gondek et al. 2005). The high expression of the surface receptor CD25 on T_{reg} cells can also contribute to the T_{reg} cell suppressive capacity by consuming local IL-2, which results in starving of other IL-2-dependent T_{conv} cells (Oberle et al. 2007). Furthermore, the T_{reg}-mediated direct transfer of the second messenger cyclic adenosine monophosphate (cAMP) into target cells and the generation of adenosine by the expression of the ectoenzymes CD39- and CD73 on the T_{reg} cell surface result in T_{reg}-mediated suppression of target cells (Vignali, Collison, and Workman 2008). To inhibit the activation of T_{conv} cells, T_{reg} cells use different mechanism to suppress the T_{conv}-activating DCs. The CD4 homologue lymphocyte activation gene 3 (Lag3) interacts with MHC class II molecules on DCs to block

their maturation and thereby activation of T_{conv} cells (Liang et al. 2008). Furthermore, the surface molecule cytotoxic T lymphocyte associated protein 4 (Ctla-4) on T_{reg} cells is important for T_{reg}-mediated suppression of DCs. Engagement of Ctla-4 with the surface receptors of the B7 family (CD80/CD86) on DCs leads to expression and release of the inhibitory enzyme indoleamine 2, 3-dioxygenase (Ido) and results in suppression of T_{conv} cells (Mellor and Munn 2004). There are two different main pathways for the generation of T_{reg} cells *in vivo*. The majority of functionally mature Foxp3$^+$ T_{reg} cells are produced in the thymus. The remaining part of the T_{reg} cells is generated in the periphery, where naïve CD4$^+$Foxp3$^-$ T cells develop into periphery-derived CD4$^+$Foxp3$^+$ T_{reg} (pT_{reg}) cells under certain conditions (Abbas et al. 2013).

3.2.1 Thymic-derived T_{reg} cells

The majority of T_{reg} cells is like all other types of T cells thymic-derived. The thymus establishes immune tolerance by eliminating potentially autoreactive T cells from the T cell pool as well as by generating the tolerance-mediating population of thymic (t)T_{reg} cells (Hsieh, Lee, and Lio 2012; Josefowicz, Lu, and Rudensky 2012). T cells stem from the common lymphoid progenitors (CLPs), which in turn develop from pluripotent hematopoietic stem cells (HSCs) in the bone marrow. After migration to the thymus, CLPs give rise to thymocytes, which undergo highly controlled selection processes to differentiate into different types of mature T cells. Double negative (DN) thymocytes do neither express T cell receptors (TCRs) nor the surface co-receptors CD4 and CD8 (Miller 2011). Depending on their CD25 and CD44 expression DN cells are divided into four subsequent developmental stages (DN1-DN4). During these stages the first gene arrangement takes place to express TCRα, TCRβ and TCRδ chains. Thereby, the cells commit their T cell lineage to either $\alpha\beta$T cells or $\gamma\delta$T cells. After TCRβ rearrangement, thymocytes committed to the $\alpha\beta$T cell lineage start to express a pre-TCR complex, composed of the TCRβ chain, a pre-Tα molecule and the receptor CD3. These thymocytes differentiate into double-positive (DP) cells by co-expressing CD4 and CD8. DP cells start to rearrange their *Tcra* gene to express a surface $\alpha\beta$ TCR on their surface. To further maturate into specialized

CD4 or CD8 single-positive cells, DP cells undergo positive and negative selection processes (Murphy et al., 2008).

The interaction of high affinity TCRs with self-peptides presented by MHCs plays a central role in the generation of thymus-derived T cells. During positive selection, DP T cells recognize MHC class I or II molecules presented by cortical thymic epithelial cells (cTECs). Interaction of DP T cells with MHC class I molecules on the surface of cTECs leads to the development of single-positive CD8 T cells, whereas interaction with MHC class II molecules results in CD4 T cell lineage commitment. DP T cells, which fail to recognize MHC I or II molecules with their TCRs undergo apoptosis (Josefowicz, Lu, and Rudensky 2012; Taniuchi 2009).

Negative selection helps to eliminate potentially autoreactive T cells. Medullary thymic epithelial cells (mTECs) and other thymic APCs present a broad range of self-peptide:MHC complexes towards the positively selected $CD4^+$ or $CD8^+$ T cells. mTECs are able to express a broad repertoire of mRNA transcripts encoding proteins characteristic of differentiated cell-types (Miller 2011), which is promoted by the transcription factor autoimmune regulator (AIRE). Positively selected $CD4^+$ or $CD8^+$ T cells with a strong interaction between their TCR and the self-peptid:MHC complex are driven into apoptosis to eliminate potentially autoreactive T cells. $CD4^+$ or $CD8^+$ T cells with low to moderate TCR affinity towards self-antigen survive this selection process (Josefowicz, Lu, and Rudensky 2012; Klein et al. 2014). However, $CD4^+$ T cells with a medium TCR affinity that lies between the signal strength required for positive selection and clonal deletion are able to escape deletion and differentiate into $CD25^+Foxp3^-CD4^+$ tT_{reg} cell precursors (Josefowicz, Lu, and Rudensky 2012). In addition, TCR stimulation leads to activation of the nuclear receptor 4a1 (Nr4a1). Experiments using a transgenic reporter mouse, which express the green fluorescent protein (GFP) under the control of the Nr4a1 promoter verified that differentiation into tT_{reg} cells requires a higher signaling strength as compared to T_{conv} cells (Moran et al. 2011). However, the exact mechanism that leads to tT_{reg} cell generation or clonal deletion of self-reactive T cells are still not well defined.

Additionally to the TCR activation, costimulatory signals via CD28 play a central role in tT_{reg} cell differentiation. CD28 deficiency results in a massive decrease in T_{reg} cell frequency (Salomon et al. 2000). Furthermore, CD28 was shown to regulate tT_{reg} cell development and function due to its central cell-intrinsic role in

the induction of *Foxp3*, *Gitr* and *Ctla-4* in DP thymocytes (Tai et al. 2005; Campbell and Koch 2011). In addition to the TCR- and CD28-dependent tT_{reg} cell differentiation, $CD4^+$ thymocytes require IL-2 and IL-15 exposure to develop into mature $CD25^+Foxp3^+CD4^+$ tT_{reg} cells (Campbell and Koch 2011; Fontenot et al. 2005). These common γ-chain cytokines, as well as other stimuli such as TGF-β activate the transcriptional machinery regulating *Foxp3* gene expression. IL-2 and TGF-β stimulation as well as co-stimulation via CD28 is essential for tT_{reg} differentiation but dispensable for T_{conv} cell development in the thymus (Fontenot et al. 2005).

Several signaling pathways get activated downstream of TCR and CD28 signaling and lead to activation of distinct transcriptions factors such as NFκB, Ap-1 and Nfat. cRel, a transcription factor of the NFκB family seems to bind to the conserved non-coding sequence 3 (CNS3) promoter region and thereby initiates *Foxp3* expression (Zheng et al. 2010). Activation of the AKT-mTOR pathway has been described to have an inhibitory effect on *Foxp3* expression (Haxhinasto, Mathis, and Benoist 2008). Furthermore, the Nr4a family members have been identified as critical transcription factors for the regulation of *Foxp3* expression, since deficiency of *Nr4a1*, *Nr4a2* and *Nr4a3* leads to the complete loss of *Foxp3* expression (Sekiya et al. 2013).

The development of tT_{reg} cells is generally delayed compared to T_{conv} cells during ontogeny in the thymus. It has been shown that around day 4 after birth, the $CD25^+$ T cell percentage among total $CD3^+$ T cells in the spleen increases. Day 3 thymectomized mice show a reduced and delayed percentage of $CD25^+$ T cells in the spleen in comparison to control mice (Asano et al. 1996). Furthermore, these thymectomized mice develop severe autoimmune diseases resulting from the selective reduction in T_{reg} cells relative to self-reactive T cells, which can be inhibited by injection of peripheral T_{reg} cells from adult mice (Suri-Payer et al. 1998; Itoh et al. 1999; Asano et al. 1996; Fontenot et al. 2005). In conclusion, T_{reg} cells which start to migrate from the thymus into the periphery after day 3, are essential for inducing and maintaining self-tolerance.

Recently, the important role of Aire in modulating the tT_{reg} cell repertoire in the early life of mice has been described. A unique subpopulation of Aire-dependent perinatal tT_{reg} cells has been identified, which play a critical role for the induction of immune self-tolerance (Yang et al. 2015). Aire is necessary during the neonatal

window to prevent the development of multi-organ autoimmunity and induce long-lasting tolerance (Guerau-de-Arellano et al. 2009). T_{reg} cell depletion during the first 10 days after birth using the NOD.Foxp3-DTR system results in multi-organ autoimmunity, which is normally typical for Aire-deficient mice on the NOD background. Mice depleted of T_{reg} cells at a later time-point show no dramatic outcome (Yang et al. 2015). Moreover, through a tamoxifen inducible T_{reg} cell lineage-tracer system using the NOD.Foxp3eGFP-Cre-ERT2xR26Y reporter mouse, it has been shown that neonatally generated and tagged T_{reg} cells stably persist in adult mice and show distinct functional and phenotypic properties such as higher activation and proliferation capacities, increased expression of genes associated with T_{reg} cell effector function, more suppressive properties as well as different T cell receptor repertoires (Yang et al. 2015). T_{reg} cells generated in the neonatal age window play an important role in maintaining self-tolerance, since neonatal generated and tagged T_{reg} cells are able to reserve the autoimmune phenotype after their injection in Aire-deficient mice. In contrast, prevention of the typical Aire autoimmune pathology cannot be achieved following transfer of thymus- or periphery-derived T_{reg} cells from older mice. Thereby, this study demonstrate that Aire seems to be critical for the induction of a unique subpopulation of tT_{reg} cells during the neonatal age period (Yang et al. 2015).

3.2.2 Thymus-derived versus peripheral-induced T_{reg} cells

Following development in the thymus, T_{reg} cells as well as T_{conv} cells enter the periphery to circulate through peripheral non-lymphoid tissues and secondary lymphoid tissues such as spleen and lymph nodes. A smaller part of the T_{reg} cell population is generated in the periphery. Hereby, $Foxp3^{-}CD4^{+}$ T_{conv} cells can be stimulated with TGF-β and IL-2 and activated through specialized APCs to convert into pT_{reg} cells. A phenomenon well described for gut and colon microenvironment (Yadav, Stephan, and Bluestone 2013; Lee, Bautista, and Hsieh 2011; Lathrop et al. 2011). While both pT_{reg} and tTr_{eg} cells express similar levels of Foxp3, the two populations can be discriminate based on their expression of the transcription factor Helios of the Ikaros family and the cell surface transmembrane glycoprotein Neuropilin-1 (Nrp1; CD304) (Thornton et al. 2010; Yadav et al. 2012). Both Helios

and Nrp1 are dominantly expressed in tT_{reg} cells and absent or reduced in pT_{reg} cells (Yadav et al. 2012). Moreover, recent studies have described that during tT_{reg} cell differentiation characteristic DNA demethylation patterns are induced upon TCR stimulation. tT_{reg} cells feature a specific demethylation pattern in characteristic T_{reg} cell signature genes such as *Foxp3* (Ohkura et al. 2012). Demethylation of CpG islands in the CNS2 of the *Foxp3* gene is essential to promote stable *Foxp3* gene expression (Zheng et al. 2010). *In vitro* induced T_{reg} (iT_{reg}) cells and pT_{reg} cells fail to demethylate the CNS2 region and eventually lose *Foxp3* expression (Hori 2011). Therefore, the CNS2 region is termed T_{reg}-specific demethylated region (TSDR). The analysis of the methylation status of the CNS2 region in the Foxp3 gene is another important marker to discriminate between tT_{reg} cells, iT_{reg} cells, pT_{reg} cells as well as T_{conv} cells (Ohkura et al. 2012).

3.2.3 Heterogeneity idea of T_{reg} cell

It is known that $CD4^+$ T_{conv} cells develop into different T helper subsets depending on distinct cytokine signals the cells receive during activation. For example, T_{H1} cells develop in the presence of IFN-γ and IL-12, whereas IL-4 is necessary for T_{H2} cell differentiation (Campbell and Koch 2011). T_{reg} cells also are a heterogeneous population. The first T_{reg} cell subsets were identified in secondary lymphoid tissues such as spleen and lymph nodes (Feuerer et al. 2010; Josefowicz, Lu, and Rudensky 2012; Feuerer, Hill, et al. 2009). Genome wide transcriptional profiling and functional characterization studies identified that distinct T_{reg} cell subsets in secondary lymphoid tissue can differ in the expression of transcription factors, such as T-bet, Gata3, Stat3 and Bcl6 that also have essential roles in the respective T helper subset (T_{H1}, T_{H2}, T_{H17} and follicular T helper cells (T_{FH})) (Fig. 1) (Josefowicz, Lu, and Rudensky 2012). It was shown that deletion of these transcription factors leads to impaired suppression of the respective T_{conv} cell subsets. For example, suppression of T_{H2} responses is disabled in Irf4- or Gata3-depleted T_{reg} cells (Wohlfert et al. 2011; Zheng et al. 2009). Therefore, the matched symmetry of expression patterns between T_{conv} cell subsets and T_{reg} cell subsets expands and supports T_{reg} cell functions.

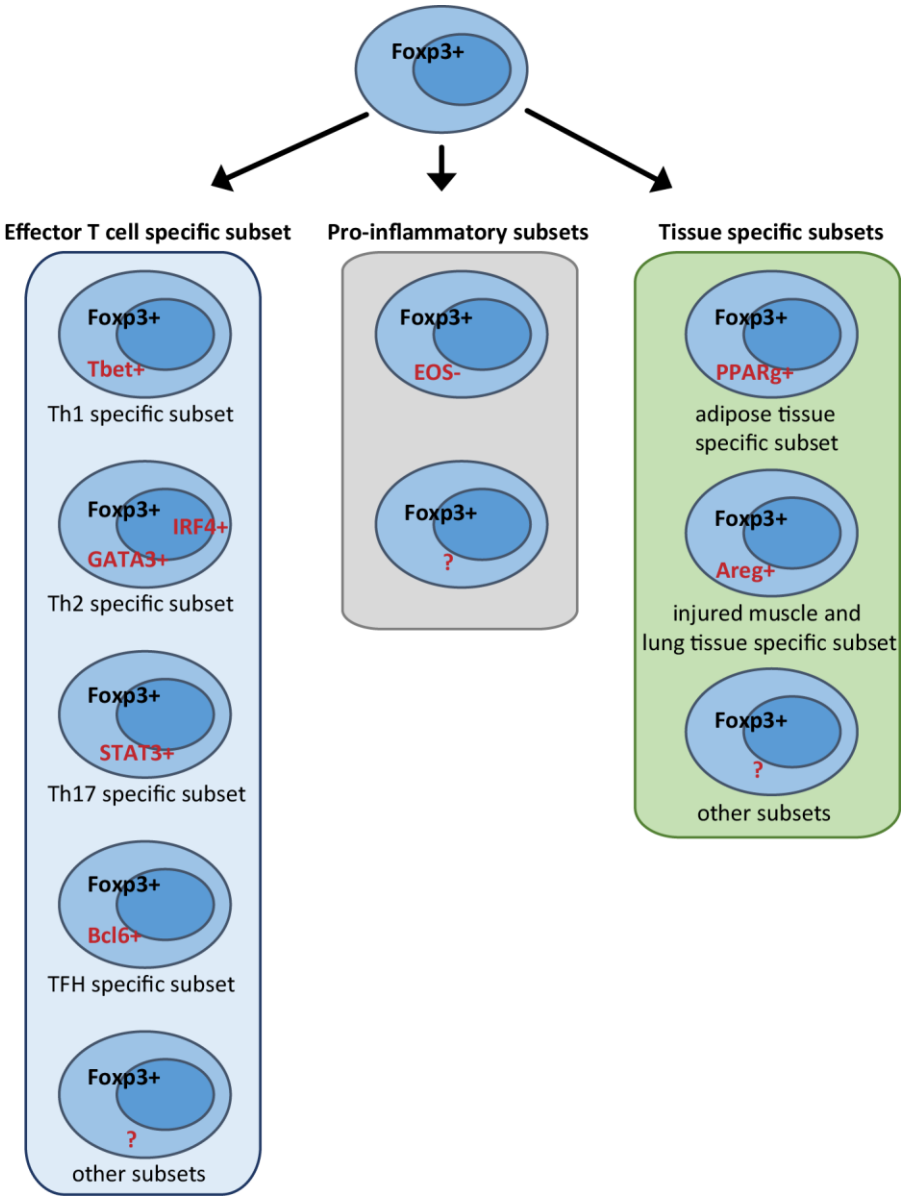

Figure 1: T_{reg} cell subsets. Functional T_{reg} cell subsets are determined by expression of distinct transcriptions factors.

The heterogeneous T_{reg} cell subset idea has been extended by the introduction of a novel concept of tissue-resident T_{reg} cells (Burzyn et al. 2013; Burzyn, Benoist, and Mathis 2013; Cipolletta et al. 2012; Feuerer, Herrero, et al. 2009). Distinct features make each of the tissue-resident T_{reg} cells unique such as the expression of distinct chemokine receptors, effector molecules, transcription factors as well as TCR repertoires (Burzyn, Benoist, and Mathis 2013). Specialized tissue-resident T_{reg} cell populations have been described in several non-lymphoid tissues like

adipose tissue, muscle, skin and lung (Burzyn et al. 2013; Cipolletta et al. 2012; Arpaia et al. 2015; Scharschmidt et al. 2015). In these peripheral tissues, T_{reg} cells perform non-classical T_{reg} cell functions like helping to control metabolic homeostasis in adipose tissue or inducing tissue repair in injured muscles (Burzyn et al. 2013; Arpaia et al. 2015; Cipolletta et al. 2012; Feuerer, Herrero, et al. 2009).

3.2.4 Tissue-specialized T_{reg} cells

Visceral adipose tissue

One of the well described examples of tissue-resident T_{reg} cells is the T_{reg} cell population in visceral adipose tissue (VAT). The T_{reg} cell frequency in VAT is notably higher as compared to lymphoid tissue. VAT-resident T_{reg} cells represent around 50% of the $CD4^+$ T cell pool, whereas only up to 5 to 15% of the $CD4^+$ T cell population in spleen and lymph node are T_{reg} cells (Burzyn, Benoist, and Mathis 2013). T_{reg} cell colonization in the visceral adipose tissue happens in the first weeks of life and is later independent of thymic input (Kolodin et al. 2015). It has been reported that in addition to the expression of classical T_{reg} cell signature genes, T_{reg} cells in the visceral adipose tissue differently express more than two thousand genes, leading to a unique functional T_{reg} cell phenotype (Burzyn, Benoist, and Mathis 2013; Feuerer, Herrero, et al. 2009). For example, specific chemokine receptors such as CCR1, CCR2 and CCR9, as well as the immunomodulatory cytokine IL-10 are overexpressed in VAT-resident T_{reg} cells. Another feature of VAT-resident T_{reg} cells are the distinct TCR sequences, which show little overlap to their counterparts in lymphoid tissue (Feuerer, Herrero, et al. 2009). VAT-resident T_{reg} cells are able to take up fat droplets via the expression of CD36 and perform non-immunological functions such as controlling metabolic parameter in adipose tissue. (Feuerer et al. 2010; Cipolletta et al. 2012; Burzyn, Benoist, and Mathis 2013). Furthermore, these cells are able to modulate obesity-associated insulin resistance, pro-inflammatory cytokine secretion as well as cell infiltration in visceral adipose tissue (Feuerer, Herrero, et al. 2009; Cipolletta et al. 2012). The key driver of this VAT-resident T_{reg} cell phenotype is the peroxisome proliferator-activated receptor-γ (PPAR-γ), which normally functions as a “master

regulator" of adipocyte differentiation (Feuerer, Herrero, et al. 2009; Cipolletta et al. 2012). *In vitro* it has been shown that up-regulation of the VAT T_{reg} cell signature is induced by interaction of PPAR-γ with Foxp3 (Feuerer, Herrero, et al. 2009; Cipolletta et al. 2012). Deficiency of PPAR-γ in T_{reg} cells leads to a reduced number of T_{reg} cells in visceral adipose tissue as well as to an under-representation of the specific signature of VAT-resident T_{reg} cells (Feuerer, Herrero, et al. 2009; Cipolletta et al. 2012). It is still not completely known how and where the specialized phenotype of VAT-resident T_{reg} cells is generated. One could speculate that once T_{reg} cells enter the visceral adipose tissue, a VAT-specific gene expression prolife is induced which leads to a distinct T_{reg} cell signature.

Injured muscle tissue

The introduction of T_{reg} cells specialized in muscle-repair further extended the concept of tissue-resident T_{reg} cells (Burzyn et al. 2013). T_{reg} cells in healthy muscle tissue make up a small population of around 10% of the $CD4^+$ T cell pool. Most of the studies describing the muscle-resident T_{reg} cell phenotype and function are done under pathological conditions. Accumulation of lymphocytes in muscle tissue is known to occur in human Duchenne muscular dystrophy (DMB) patients (Tidball and Villalta 2010) and dystrophic muscles of dytrophin-deficient mice harboring a muscular dystrophy (*mdx)* mutation (Eghtesad et al. 2011). Dystrophic muscle of mdx mice and human DMB patient show an elevated percentage of activated T_{reg} cells (Vetrone et al. 2009). Muscle-resident T_{reg} cells have the function to modulate dystrophinopathy by controlling the balance between type 1 and type 2 inflammatory responses. Osteopontin seems to regulate T_{reg} cell number or stability since osteopontin-deficient mdx mice have elevated muscular *Foxp3* mRNA level (Vetrone et al. 2009). Depletion of CD25-expressing cells in mdx mice increased inflammatory responses in the injured muscle combined with impaired muscle fiber regeneration (Burzyn et al. 2013). However, an elevated T_{reg} cell frequency and IL-10 concentration are observed after treatment with IL-2/anti-IL-2 mAb complexes, which results in decreased myofiber injury (Villalta et al. 2014). Therefore, T_{reg} cells play an important role in limiting muscle damage

by suppressing the development of type 1 inflammatory responses.
Recently, Burzyn and colleagues describe that T_{reg} cells rapidly accumulate in skeletal muscle after acute muscle injury induced via the administration of cardiotoxin (Burzyn et al. 2013). The T_{reg} cell frequency increased to about 50% of the entire T cell pool within seven weeks, long after local tissue inflammation has declined. Microarray-based-gene expression studies reveal that T_{reg} cells in injured muscle tissue have a unique gene expression profile closely related to VAT-resident T_{reg} cells with high expression levels of amphiregulin and IL-10 (Burzyn et al. 2013). Muscle T_{reg} cells contribute to repair processes in injured muscles, since the epidermal growth factor receptor (EGF-R) ligand amphiregulin enhances the differentiation of muscle cell precursors as well as lowers the expression of proteins associated with fibrosis, (Burzyn et al. 2013). Collectively, T_{reg} cells play a critical role once acute muscle damage has occurred by actively enhancing muscle repair.

Virus-infected lung tissue

The T_{reg} cell population in virus infected-lung tissue is another example for specialized T_{reg} cells in peripheral tissues that are able to adopt distinct effector mechanisms matching their target cells or tissues. In addition to the above described finding of amphiregulin-expressing T_{reg} cells specialized in muscle-repair, influenza-infected lungs harbor a T_{reg} cell population that has an essential role in tissue protection, depending on their production of amphiregulin. Depletion of T_{reg} cells leads to the loss of T_{reg}-derived amphiregulin in influenza-infected lungs and therefore to an elevated level of acute lung damage with unaffected viral load and T cell responses (Arpaia et al. 2015).
T_{reg} cells act as a kind of universal monitor of mucosal barriers. Through the ability to rapidly respond to tissue damage and to retain lung structural and functional integrity during tissue damage, the cells are able to promote tolerance and tissue repair (Arpaia et al. 2015).

3.3 Liver cells

The liver is one of the largest internal organ of the body. Besides the efficient metabolism of nutrients, digestion and detoxification, a further liver function is the maximization of immune surveillance (Jenne and Kubes 2013; Crispe 2003). Around 80% of the incoming blood arrives in the portal vein. The other 20% of the blood passing though the liver is coming from the hepatic artery. The hepatic sinusoid combines the two blood supplies and the blood is transported to the central vein between plates of hepatocytes through spaces that are lined by liver sinusoidal endothelium cells (LSECs) (Jenne and Kubes 2013; Crispe 2003).

The permanent exposure to food and microbial products from the intestine leads to a tolerogenic state of the liver (Tiegs and Lohse 2010; Crispe 2003). Several mechanisms, including the expression of immunosuppressive cytokines and induction of T_{reg} cells, mediate the induction and maintenance of tolerance in the liver. In the late 1960s, long-term acceptance of liver allografts without immunosuppression demonstrated the first time the tolerant feature of the liver (Edwards-Smith et al. 1996).

Hepatocytes represent with around 80% of all liver cells the largest cell population in the liver. Studies have identified that hepatocytes as non-immune cells are capable of expressing innate immune receptors on their surface, leading to the induction of innate immune responses in the hepatocytes (Seki and Brenner 2008). With the production of acute-phase proteins and complement molecules, hepatocytes serve as a first line of defense against pathogens (Bode et al. 2012; Jenne and Kubes 2013; Crispe 2003). In addition, the expression of MHC I and II molecules on the surface of hepatocytes maximizes the capacity to activate lymphocytes, such as T cells (Warren et al. 2006; Crispe 2003; Jenne and Kubes 2013).

Kupffer cells are another major liver cell population. These cells are liver-resident macrophages and compromise about 35% of the non-parenchymal cells in the liver and around 80 - 90% of all tissue macrophages in the entire body (Crispe 2003). In contrast to typical macrophages, which are actively crawling through tissue to search for pathogens, Kupffer cells are located in the vasculature, adherent to LSECs, where they are directly exposed to blood and able to catch bacteria (Jenne and Kubes 2013). Kupffer cells act as APCs and detect and internalize pathogens through a set of surface receptors including scavenger receptors, Toll like

receptors (TLRs), complement receptors as well as antibody receptors (Jenne and Kubes 2013). Receptor signaling results in activation of Kupffer cells and production of cytokines and chemokines. Moreover, expression of MHC I, MHC II and costimulatory molecules on their surface contribute to activation and proliferation of T cells and NKT cells (Crispe 2003).

Besides Kupffer cells and hepatocytes, the liver contains also a small population of hepatic stellate cells, which represent around 5 - 8% of the total liver cell pool (Jenne and Kubes 2013). These cells act in an APC-like manner through endocytosis of exogenous antigens and by expressing low amounts of molecules such as MHC I, MHC II, CD80 and CD86, which are required for antigen presentation to T cells (Vinas et al. 2003; Winau et al. 2007). Hepatic stellate cells are also able to induce cytokine production in T cells, NK cells and NKT cells. (Jenne and Kubes 2013).

Approximately one third of all lymphocytes in the liver are NK cells (Jenne and Kubes 2013). NK cells respond to several cell-surface ligands on infected or damaged cells (Notas, Kisseleva, and Brenner 2009; Jenne and Kubes 2013). During liver damage NK cells seem to have a crucial role in T cell recruitment (Toyabe et al. 1997). Activated NK cells release perforin and granzyme as well as different cytokines. Secretion of IFN-γ results in induction of a multi-step cytokine/chemokine cascade to recruit T cells. Additionally, the liver contains an abundant number of NKT cells, expressing NK1.1 as well as the IL-2 receptor and an intermediate density of $\alpha\beta$ TCRs (MacDonald 2002).

Liver DCs are able to function as APCs and activate T cells. However, this function appears to be less efficient partly due to the local immunesuppressive cytokine milieu in the liver, including liver cell-secreted IL-10 (Sana et al. 2014). Contact of DCs with LSECs and hepatocytes further results in a reduced capacity of T cell activation. DC-derived IL-10 promotes a shift from T_{H1}- to T_{H2}-immune responses and the development of T_{reg} cells (Bamboat et al. 2009).

Around 50% of liver-resident lymphocytes express a TCR. In contrast to the CD4:CD8 ratio in the blood and lymphoid tissues, the liver is enriched with $CD8^+$ T cells (Jenne and Kubes 2013). Most of CD4 and CD8 T cells in the liver have an activated phenotype. They circulate through liver sinusoids and are able to interact with Kupffer cells and LSECs. Moreover, the liver contains one of the largest

accumulations of $\gamma\delta$ T cells, representing around 15 - 25% of all hepatic T cells (Nemeth, Baird, and O'Farrelly 2009).

Hepatic T_{reg} cells have been extensively studied under pathological conditions. For example, a high T_{reg} cell frequency among $CD4^+$ T cells is observed in chronic Hepatitis C virus (HCV)-infected patients as well as in mice and patient suffering from hepatocellular cancer (HCC) and is often connected to a poor prognosis for the patients (Wang et al. 2016; Unitt et al. 2005). On the other side, autoimmune diseases such as autoimmune hepatitis (AIV) or primary biliary cirrhosis (PBC) show a reduction of T_{reg} cell numbers (Lan et al. 2006; Ward et al. 2007; Erhardt et al. 2007). However, less is known about the function of T_{reg} cells in a healthy liver.

3.4 Circadian rhythm

3.4.1 Circadian rhythm pathway

Circadian rhythms are known as physiological processes occurring with a repeating period close to 24 hours (Duguay and Cermakian 2009; Scheiermann, Kunisaki, and Frenette 2013). It is hypothesized that circadian rhythms have been shaped in aerobic organisms to anticipate oxygen level changes in the environment induced by the solar magnetic activity cycle and phototrophic bacteria (Edgar et al. 2012; Scheiermann, Kunisaki, and Frenette 2013). Circadian rhythms ensure synchronization of internal physiology with external physiology to maintain homeostasis. Prokaryotes, fungi, algae, plants and mammals show physiological processes under circadian control (Scheiermann, Kunisaki, and Frenette 2013; Edgar et al. 2012).

In mammals up to 10% of the genome is under control of circadian rhythms, which are endogenously generated and maintained by the central clock located in the suprachiasmatic nucleus (SCN) of the hypothalamus (Arjona et al. 2012). There the central clock receives input from the retina and coordinates hormonal, biochemical and behavioral rhythms in other tissues to mediate their synchronization to external environment (Fig. 2) (Scheiermann, Kunisaki, and Frenette 2013; Ferrell and Chiang 2015). Daily light/dark cycles are the main Zeitgeber (german: “time giver”) inducing synchronization to a 24 hour rhythm (Fortier et al. 2011; Scheiermann, Kunisaki, and Frenette 2013).

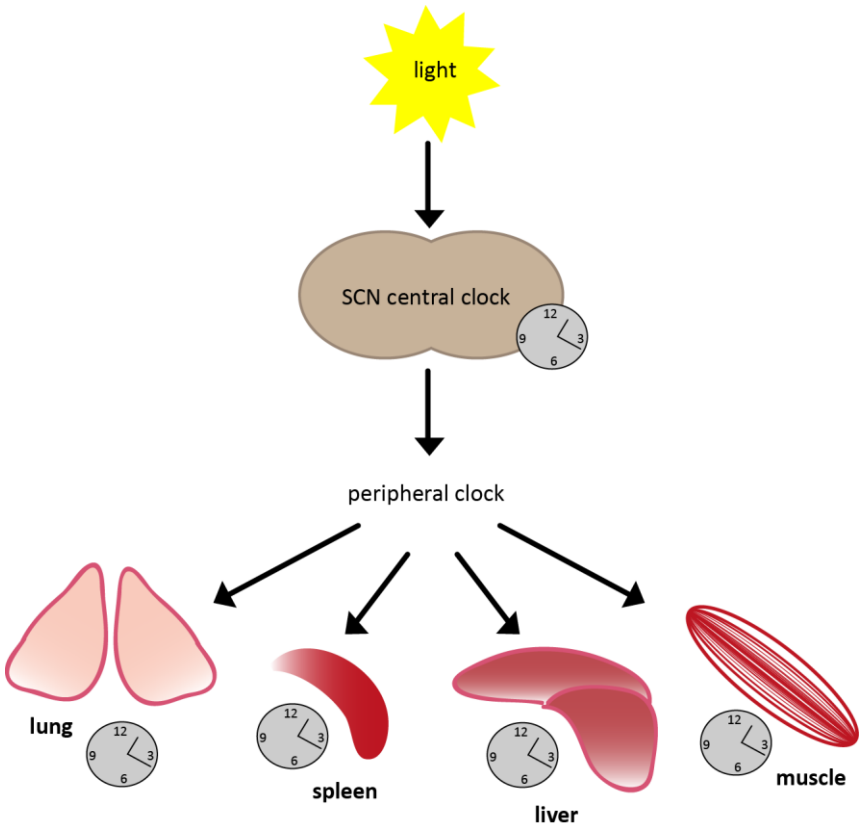

Figure 2: Circadian rhythm. Circadian rhythms are synchronized by `Zeitgeber´. These are external cues, such as light, synchronizing the endogenous rhythm to a 24-hour light–dark cycle. Light is processed via the retina and leads to the synchronization of rhythms in the master clock of the organism located in the hypothalamic suprachiasmatic nuclei (SCN). Peripheral clocks can be synchronized by the SCN central clock through humoral and neural output systems, but otherwise are able to oscillate autonomously by using the same molecular components (Scheiermann, Kunisaki, and Frenette 2013).

At the molecular level, the clock is controlled by auto-regulatory transcription-translation feedback loops (Fig. 3). The core-clock genes circadian locomotor output cycles kaput (Clock) and brain and muscle Arnt-like 1 (Bmal1) build a heterodimer, which translocates into the nucleus and binds to canonical Enhancer box (E-box) promoter sequences of target genes to initiate circadian processes, including their own transcription (Ferrell and Chiang 2015; Scheiermann, Kunisaki, and Frenette 2013). Heterodimers of negative regulator genes, such as Period 1 and 2 (Per1 and 2) or Cry1 and 2 (Cryptochrome1 and 2) translocate back to the nucleus to interact with Clock/Bmal1 to inhibit transcription. In the second auto-regulatory transcription-translation feedback loop the activating nuclear retinoid-related orphan receptor α (Rorα) competes with the negative regulators Rev-Erbα- and β for the binding to the Ror response element (Rore) binding site in the Bmal1 promoter to activate or repress Bmal1 expression (Ferrell and Chiang 2015). In addition to these core-clock genes, many other genes are known to be under direct circadian control of the clock. These clock-controlled genes require important regulatory elements such as E-box and Rore sequences to drive their expression in a circadian manner (Partch, Green, and Takahashi 2014).

Peripheral clocks are observed in various peripheral tissues, including the liver, lung, heart, pancreas, and white adipose tissue (Storch et al. 2002; Dibner and Schibler 2015; Haspel et al. 2014; Kohsaka et al. 2007). Even cultured primary cells can show periodic expression of core-clock genes (Molyneux et al. 2015). Although, peripheral clocks are known to be synchronized by the central clock, they are additionally able to oscillate autonomously by using the same molecular components. In the liver around 10% of genes are under circadian control, including genes involved in liver metabolisms such as regulation of glucose, lipid and nutrient homeostasis (Solt et al. 2012; Cho et al. 2012; Chaves et al. 2014; Yoshitane et al. 2014).

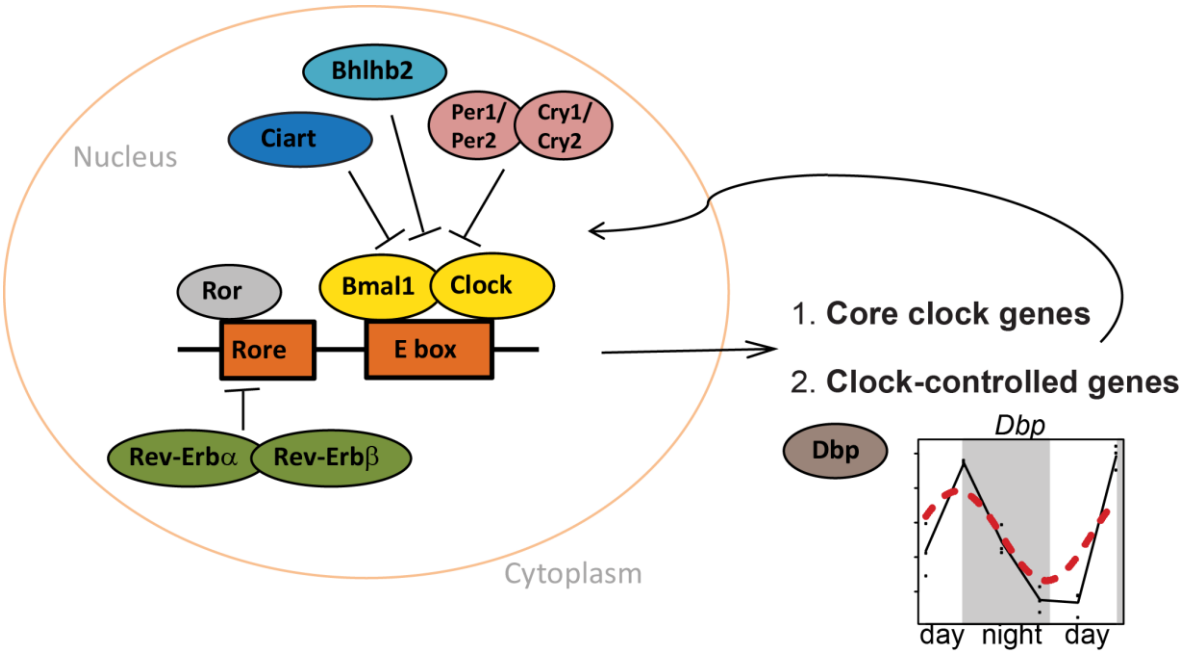

Figure 3: Molecular mechanisms of the circadian clock. Expression of the core-clock genes *Clock* (circadian locomotor output cycles kaput) and *Bmal1* (brain and muscle ARNT-like 1) leads to the heterodimerization of Bmal1 and Clock in the cytoplasm. After the heterodimer translocated into the nucleus, it binds to canonical E-box sequences (CACGTG) in core-clock genes and clock-controlled genes to drive circadian processes and their own expression. Other core-clock genes, controlling the expression of the Clock/Bmal1 heterodimer are positive regulators, such as the retinoic acid receptor-related orphan receptor (Ror), which induce the expression of Bmal1 by binding to Ror response elements (Rores) in the Bmal1 promoter. Negative regulators such as Per (period circadian protein) and Cry (cryptochrome) build heterodimers and inhibit the binding of Bmal1/Clock to core-clock genes or clock-controlled genes. In a second autoregulatory feedback loop, the transcription of Rev-Erb-α and Rev-Erb-β is induced to inhibit Bmal1 transcription and competes with Ror for binding to Rores. This pathway stabilizes the clock, and can also directly drive circadian rhythms. After a period of time, the regulatory heterodimers are degraded and another transcription cycle is activated (Scheiermann, Kunisaki, and Frenette 2013). Other recently described negative regulators are Ciart and Bhlhb2. Ciart interacts with Bmal1 and represses Clock-Bmal1 activity in the nucleus, whereas Bhlhb2 is able to interact with Bmal1 and compete for E-box binding sites.

3.4.2 Lymphocytes and the circadian rhythm

It has also been reported that immune cells have an intrinsic clock, which is important for certain functions such as migration, cytokine release and differentiation (Arjona and Sarkar 2006; Scheiermann, Kunisaki, and Frenette 2013; Nguyen et al. 2013; Yu et al. 2013). For example, lymphocytes show different oscillation pattern over the day in the blood of humans and rodents (Depres-Brummer et al. 1997; Dimitrov et al. 2009). Furthermore, innate immune responses of NK cells as well as the cytokine release of macrophages in response of bacterial antigens are controlled by core-clock genes (Arjona and Sarkar 2006; Hayashi, Shimba, and Tezuka 2007; Keller et al. 2009).

Although these data show that the immune cell's intrinsic clock modifies their function, little is known about whether immune cells are able to control the circadian rhythm of other cells in peripheral organs such as the liver.

4 Aim of study

To further extent the concept of specialized tissue-resident T_{reg} cells, we aimed to analyze and characterize T_{reg} cells and their function in the liver tissue. So far, only little is known about T_{reg} cells in the liver environment under non-pathological conditions, particularly in neonatal mice at an age of 10 days. Therefore, on the one hand we were focusing on the functional characterization and development of hepatic T_{reg} cells and on the other hand we wanted to examine if and how T_{reg} cells influence the liver function.

5 Methods

5.1 Mice

5.1.1 Keeping

Mice were 9 - 11 day-old or 5 - 7 week-old at the time of the experiments. All mice were cared for under the specific-pathogen free conditions in the animal facility of the DKFZ. All animal experiments were reviewed and approved by the governmental committee for animal experimentation in Karlsruhe, Germany.

5.2 Tissue sample preparation

5.2.1 Cell depletion

T_{reg} cells or macrophages were depleted by intraperitoneal injection of 40 ng/g body weight diphtheria toxin (DT) (Sigma) on two consecutive days (Fig. 4). For the 24 h time point single injection was used.

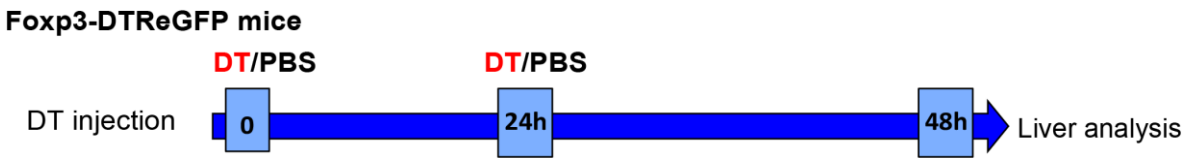

Figure 4: Diphtheria toxin injection scheme. DT was injected into Foxp3-DTReGFP mice on two consecutive days. Afterwards the liver tissue was analyzed by performing flow cytometry, RNA microarray and proteomic analysis.

5.2.2 Tissue isolation and sample preparation

For tissue isolation, mice were sacrificed and perfused with 10 ml of PBS by heart puncture. Liver, spleen and lung were removed and mechanically dispersed.
Liver suspension was digested for 30 min at 37°C in DMEM (Life Technologies) plus 1 mg/ml collagenase type IV (C5138, Sigma), 0.5% (w/v) BSA (Sigma) and 20 µg/ml DNase I (Roche). Samples were enriched for liver T cells by centrifugation through a Percoll gradient (40 and 80% solutions; GE Healthcare). After centrifugation (20 min, 4°C, 1500 g, without break and acceleration) T cells were found between the two Percoll layers and washed with PBS.
Ammonium chloride-potassium bicarbonate (ACK) lysis buffer was used to lyse erythrocytes in spleen and lung samples.

5.2.3 AutoMACS cell purification

For sorting of cells, liver and spleen samples were pre-purified with magnetic cell separation after digestion or ACK lysis treatment. Cells were labeled with CD45 microbeads (Miltenyi). Samples were subjected to positive selection for $CD45^+$ cells on an autoMACS Pro Separator (Miltenyi) and subsequently stained for FACS sorting.
For Kupffer cell analysis in the liver samples, cells were purified with magnetic beads after digestion. Cells were labeled with CD45 microbeads (Miltenyi) and isolated on an autoMACS Pro Separator (Miltenyi) system.

5.2.4 Blood samples

Blood was collected from sacrificed mice with heparin-coated syringes. Blood plasma was collected by centrifugation (10 min; 3 000 rpm). ALT and AST levels were measured by photometric analysis on the ADVIA 2400 system (Siemens Healthcare Diagnostics). Analysis was performed at the Zentrallabor, Medical Clinic-1, Analysezentrum, University Clinic Heidelberg.

5.3 Cell culture techniques

5.3.1 Primary hepatocyte isolation

Livers of anesthetized mice were perfused for 5 min with EGTA buffer (pH 7.2; 8 ml/min) following a 5 min perfusion with collagenase solution (collagenase type IV, Sigma; 1.2 mg/ml; 8ml/min) through the venae porta. Livers were extracted and liver capsule was carefully opened. Primary mouse hepatocytes were isolated and cultured in serum-free Williams' Medium E. The viability of isolated hepatocytes was determined by trypan blue exclusion. Only cell preparations with a viability > 80% were used for experiments. The isolated cells were seeded in adhesion media on 6-well collagen type I-coated culture dishes at a density of $9x10^5$ cells per well . Four hours after isolation, the primary hepatocytes were cultured in Williams Medium E supplemented with 2 mM L-glutamine (Invitrogen) and 1% penicillin and streptomycin (Invitrogen). Different stimuli were added: dexamethasone (100 nM; Sigma), TNF-α, IL-6, IL-10, TGF-β or IFN-γ (50ng/ml; Peprotech).

5.4 Flow cytometry

For surface staining cells were labeled with antibodies for 30 min in FACS buffer at 4°C. For intracellular Foxp3 and Helios staining, the intracellular Foxp3 staining buffer set (eBioscience) was used. Cells were treated with the fixation buffer for 30 min at 4°C in the dark. Afterwards, the cells were intracellular stained with Fix/Perm buffer and the Foxp3 or Helios antibodies for 45 min at room temperature in the dark. Unstained or anti-CD4 single stained spleen cells (in the colors corresponding to the staining panel) were used for compensation. Cells were filtered and then analyzed using the BD Bioscience Canto II, LSR Fortessa or LSR II.

5.5 Fluorescence-activated cell sorting (FACS)

For FACS-purification of cells the BD Biosciences FACSAria I, II or III instruments were used. After pre-purification with magnetic cell separation, surface of cells were stained (Fig. 5) and kept cold at 4 °C. After sorting, purity of cell sorts was controlled through post-sort analysis. Data were analyzed with Tree Star FlowJo (Treestar).

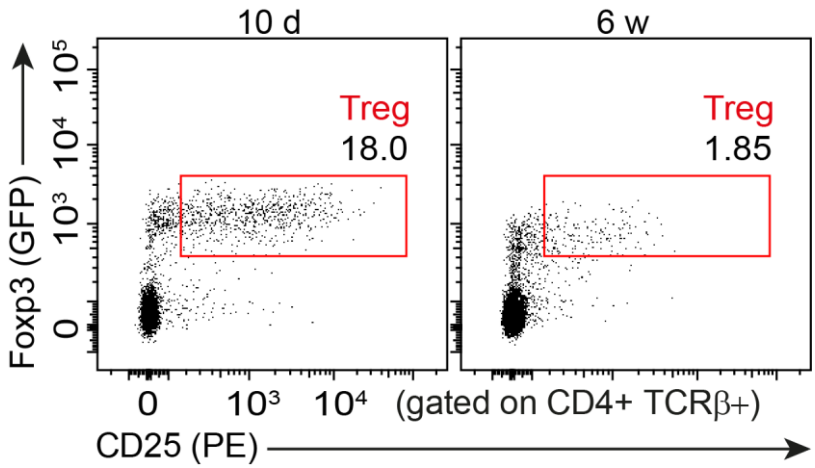

Figure 5: T_{reg} cell sorting scheme. Foxp3⁺CD25⁺CD4⁺TCRb⁺ T_{reg} cells were purified out of liver and spleen of 10 day-old (10 d) and 6 week-old (6w) Foxp3-DTReGFP mice.

5.5.1 *In vivo* proliferation assay

We used two methods for analysis of the *in vivo* proliferative activity of the T_{reg} cells or hepatocytes. First, we analyzed DNA-contents with Hoechst 33342 (Life Technologies) and determined cell cycle indices (G_2-M+S/G_1-G_0). Second, we i.v. injected EdU (5-ethynyl-2′-deoxyuridine), dissolved in sterile PBS at a dose of 1 mg per mouse, to analyze quantified incorporation of nucleotides (Click-iT EdU Alexa Fluor 488 Flow cytometry Assay Kit (Life Technologies)). Mice were analyzed 4 hours after injection by flow cytometry as recommended by the manufacturer.

5.6 Epigenetics

5.6.1 Purification and bisulfite conversion of genomic DNA

CG methylation analysis with the 454 pyrosequencing technology was performed in the Division of Epigenetics of the DKFZ in Heidelberg by Dr. Achim Breiling.

To analyze specific demethylation of the T_{reg}-specific demethylated region (TSDR), we isolated T_{reg} cells and T_{conv} cells from Foxp3-DTReGFP mice via FACS. DNA of indicated sorted cell populations was purified according to manufacturer's guidelines using the DNEasy Blood and Tissue kit (Quiagen). DNA purity and concentration was measured via a NanoDrop® photometer and DNA concentration was adjusted to 2000 ng DNA. Bisulfite-conversion was performed using the EpiTect Bisulfite Conversion Kit (Quiagen). The Bisulfite Primer Seeker Software (http://www.zymoresearch.com/tools/bisulfite-primer-seeker) was used to calculate primer sequences based on manufacturers recommendations. To generate PCR amplicons from bisulfite-converted DNA we used barcode-labeled primers. PCR amplicons were separated from primer dimers on a 1 - 2% agarose gel. The amplicons were purified using a Quick Gel Extraction Kit (Life Technologies) and afterwards processes on a GS Junior Sequencer (Roche). Sequence reads were aligned to the BS-converted mouse genome. The methylation levels were visualized in heat maps.

5.7 Proteomics

Quantitative differential proteomics experiments were performed in the Genome Biology Unit of the EMBL in Heidelberg by Sophia Föhr and Dr. Jeroen Krijgsveld.

5.7.1 Protein digestion, labeling of peptides with stable isotopes (TMT) and fractionation

Tissues from 10 day-old and 6 week-old livers were isolated 48 hours after T_{reg} cell depletion with DT or PBS treatment. Mouse liver tissue (around 20 mg) was dissected, washed three times with ice cold PBS and subsequently grounded in a 1 ml douncer. The slurry was washed again with ice cold PBS. The supernatant was sonicated in a Covaris S220 (430s, 17W). Extracted proteins were reduced and alkylated with 5 mM DTT and 10 mM iodoacetamide. Subsequently around 10 mg portions were digested with LysC according to SP3 protocol (Hughes et al. 2014). Resulting peptides of replicates were pooled and labeled with TMT 10plex according to the manufacturer's protocol. The labels 126, 127N, 127C, 128N, 128C, 129N, 129C, 130N, 130C and 131 were mixed 1:1:1:1:1:1:1:1:1:1 based on peptide ratio and fractionated into 10 peptide fractions by high-pH reversed-phase chromatography (Sieber et al. 2016).

5.7.2 LC-ESI-MS/MS analysis

Peptides were separated using a nanoACQUITY UPLC system (Waters) fitted with a trapping column (nanoAcquity Symmetry C18; 5 µm (average particle diameter); 180 µm (inner diameter) × 20 mm (length)) and an analytical column (nanoAcquity BEH C18; 1.7 µm (average particle diameter); 75 µm (inner diameter) × 200 mm (length)). Peptides were separated on a 120-minute gradient and were analyzed by electrospray ionization–tandem mass spectrometry using an Orbitrap Fusion (Thermo Fisher Scientific). Using a multi-notch approach (McAlister et al. 2014) the 10 most-abundant ions from each MS1 scan were fragmented by collision-induced dissociation to generate an MS2 spectrum. Following each MS2 spectrum, an MS3 spectrum was acquired as described (McAlister et al. 2014), in which multiple MS2 fragment ions were selected in the MS3 precursor population using isolation

waveforms with multiple frequency notches, using high energy collision-induced dissociation (HCD) and analysis in the Orbitrap.

5.7.3 Protein identification and quantification

MS raw data files were processed with ProteomeDiscoverer (version 1.4.) using Mascot (version 2.2.07) as the search engine against the Uniprot mouse database. Cysteine carbamidomethylation and methionine oxidation were set as fixed and variable modifications, respectively, and specifying digestion with LysC and quantification with TMT 10plex. A 1% false-discovery rate was required both at the peptide and protein level.

5.8 PCR techniques

5.8.1 RNA isolation and cDNA synthesis

RNA was extracted using the RNeasy Microarray Tissue Mini Kit (Qiagen) or the innuPREP RNA Mini Kit (analytic jena). For the RNeasy Microarray Tissue Mini Kit liver and lung tissues (10 mg) were mechanically dispersed in 1 ml of TRIzol or QIAzol Lysis Reagent according to manufacturer's instructions and frozen at -80°C until further processing

For total RNA extraction of livers from Mdr2$^{-/-}$ mice peqGOLD RNAPure (Peqlab Biotechnologie, Erlangen, Germany) was used according to the manufacturer's instructions.

Sorted hepatic Foxp3^{+}CD25^{+}TCRb^{+}CD4^{+} Treg cells, NK1.1^{+} NK cells, F4/80^{+} Kupffer cells and Ly6C^{high} monocytes were FACS purified and RNA was extracted using the RNeasy Plus Micro Kit (Qiagen).

For cDNA synthesis, the SuperScript reverse transcriptase (Invitrogen) and oligo(dT) primers were used according to manufacturer's instructions.

5.8.2 Quantitative real-time PCR

For transcript quantification cDNA samples were analyzed by quantitative real-time PCR using the Power SYBR Green master mix (Life technologies) and the ViiA7 instrument (Life technologies). Primer sequences are listed below. All qPCR primers were tested by serial dilutions, melting curve analysis and efficiency testing. Transcripts levels of target genes ('gene X') were quantified relative to the abundance of *Hprt* by the change-in-threshold (C_T) method:

relative expression = 2^ - (CT (gene X) - CT(Hprt))

5.8.3 RNA expression profiling

The DKFZ Genomics and Proteomics Core Facility amplified and hybridized material to the Illumina MouseWG-6 v2.0 Expression BeadChip containing a total of 46,238 probes. Microarray scanning was done using an iScan array scanner. Data extraction was done for all beads individually, and outliers were removed when the absolute difference to the median was greater than 2.5 times MAD (2.5 Hampelís method). All remaining bead level data points were than quantile normalized.

5.9 Bioinformatic and statistical analysis

5.9.1 Bioinformatic and statistical analysis of proteomic data

Quantitative differential proteomics experiments were performed in the Genome Biology Unit of the EMBL in Heidelberg by Sophia Föhr and Dr. Jeroen Krijgsveld.

For the protein quantification only peptides were considered with summed reporter ion intensity greater than 10000 and with a value in at least two of four replicates, used as an input for the limma package in R/Bioconductor to calculate the adjusted P value. Proteins with an adjusted P value lower than 0.05 were considered to be differentially expressed between the treatment and age of the mouse liver.

5.9.2 Bioinformatics and statistical analysis of microarray data

Bioinformatic analysis of microarray data were performed in the Division of Biostatistics of the DKFZ in Heidelberg by Thomas Hielscher.

Gene expression data sets of DT and PBS treated livers and lungs of 10 day-old and 6 week-old Foxp3-DTReGFP mice were analyzed. Unspecific filtering was applied keeping only probes with at least one normalized expression value exceeding 100 in any of the samples. Normalized expression values were log2 transformed. Circadian probes in PBS samples were identified with the JTK_CYCLE algorithm (Hughes, Hogenesch, and Kornacker 2010) using false discovery rates (FDR) of 5% and 20% as cut-offs. Phase and amplitude estimates were used to fit a sinusoidal model for illustration. In a second approach, the RAIN algorithm (Thaben and Westermark 2014) was applied with a FDR cut-off of 1%. Unlike JTK, RAIN is able to additionally detect non-symmetrical wave pattern such as saw-tooth type rhythms.

Differentially expressed probes between PBS and DT groups were identified using the empirical Bayes approach based on moderated t/F-statistics as implemented in the Bioconductor package limma (Ritchie et al. 2015). All P values in limma were adjusted for multiple testing using Benjamini-Hochberg correction in order to control the FDR. Probes with an FDR <5% were considered statistically significant. A model with factors group and time point was fitted and the group factor was tested for all probes. Fisher's exact test was used to test for enrichment of circadian probes among probes being differentially expressed in DT samples. For the final list of regulated circadian probes, an interaction term between group and time was added to allow for detecting time-dependent differences/shifts between groups and an F-test on group and group-time interaction coefficients was performed.

Samples from different organs (liver and lung) and mice of different age (6 week-old and 10 day-old) were assessed at a single time point for regulation due to T_{reg} cell depletion (DT). In each subgroup a model with only group effect was fitted. The number of differentially expressed probes was subsequently compared between subgroups using a Chi2-test for proportions. Kolmogorov-Smirnov test was used to compare distribution of phase estimates between significantly and non-significantly regulated circadian probes.

Pearson's correlation coefficient was used to find probes showing a similar DT-PBS regulation pattern over time as *Per1* and *Rev-Erb-*α. Here, the mean log2 expression was calculated at each measured time point for DT and PBS samples separately, and the difference between group means at each time point was used as time-series of regulation. Goeman's global test was used to compare expression of CYP family genes between age conditions.
All analyses were performed using statistical software. RAIN was used as implemented in Bioconductor package rain. R v3.2. JTK_CYCLE software was downloaded from http://openwetware.org/wiki/HughesLab:JTK_Cycle.

5.9.3 General statistical analysis

Prism software (GraphPad) was used for statistical analysis of experimental data. Results were considered statistically significant with P values less than 0.05 and statistical tests and corresponding parameters are mentioned in the respective figure legends.

6 Materials

6.1 Mice

Mice were obtained from Charles River Breeding Laboratories (Wilmington, MA) or the Jackson Laboratory (Bar Harbor, ME) and housed under specific pathogen-free conditions in the German Cancer Research Center animal facility:

- Wild-type C57BL/6 mice
- Nr4a1-eGFP (B6-Tg(Nr4a1-eGFP/cre)820Khog/J; Jackson stock no.: 016617)
- Csf1r-DTR mice (B6-Tg(Csf1r-HBEGF/mCherry)1Mnz x Lyz2tm1(cre)Ifo) (Schreiber et al. 2013)

Mice bred and housed under specific pathogen-free conditions in the German Cancer Research Center animal facility:

- Foxp3-DTReGFP mice (B6N.129(Cg)-Foxp3tm3Ayr; Jackson stock no.: 016958)
- Rag2-deficient mice (B6-Rag2tm1Fwa) (Shinkai et al. 1992)
- Tlr4-deficient mice (B6.Tlr4lps-del/JthJ) (Poltorak et al. 1998)
- Trif-deficient mice (B6.CgTicam1tm1Aki) (Ermolaeva et al. 2008)
- MyD88-deficient mice (B6.Cg Myd88tm1Aki) (Adachi et al. 1998)
- Mdr2-deficient mice (129-Abcb4tm1Bor) (Mauad et al. 1994)

All animal experiments were approved by the Regierungspräsidium (Karlsruhe, Germany).

6.2 Antibodies

Table 1: List of antibodies

Antigen	Clone	Isotype	Company
CD11a	M17/4	Rat IgG2a k	BioLegend
CD11b	M1/70	Rat IgG2a k	BioLegend
CD11c	N418	Arm. Hamster IgG	BioLegend
CD19	145-2C11	Rat IgG2a k	BioLegend
CD25	PC61	Rat IgG1l	BioLegend
CD3	145-2C11	Arm. Hamster IgG	BioLegend
CD4	RM4-5	Rat IgG2a k	BioLegend
CD43	1b11	Rat IgG2a k	BioLegend
CD44	IM7	Rat IgG2a k	BioLegend
CD45	30-F11	Rat IgG2a k	BioLegend
F4/80	BM8	Rat IgG2a k	BioLegend
Foxp3	FJK-16s	Rat IgG2a k	eBioscience
Foxp3	MF-14	Rat IgG2a k	BioLegend
Helios	22F6	Arm. Hamster IgG	BioLegend

Ly6C	HK1.4	Rat IgG2a k	BioLegend
Ly6G	1A8	Rat IgG2a k	BioLegend
NK1.1	PK136	Mouse IgG2 k	BioLegend
Nrp1	N43-7	Rat IgG2a k	BioLegend
Pcbd1	#PA5-26121	Rabbit / IgG	Thermo Fisher Scientific
TCRb	H57-597	Arm. Hamster IgG	BioLegend

6.3 Cytokines

Table 2: List of cytokines

Stimuli	Company
IL-6 recombinant murine	Pepro Tech
IL-10 recombinant murine	Pepro Tech
TGFβ recombinant human	Pepro Tech
TNFα recombinant murine	Pepro Tech
IFNγ recombinant murine	Pepro Tech

6.4 Kits

Table 3: List of Kits

Kit	Company
RNeasy Microarray Tissue Mini Kit	Qiagen
innuPREP RNA Mini Kit	Analytic Jena
peqGOLD RNAPure	Peqlab Biotechnologie
RNeasy Plus Micro Kit	Qiagen
SuperScript reverse transcriptase	Invitrogen
DNEasy Blood and Tissue kit	Quiagen
EpiTect Bisulfite Conversion Kit	Quiagen
Quick Gel Extraction Kit	Life Technologies
intracellular Foxp3 staining buffer set	eBioscience
Click-iT EdU Alexa Fluor 488 Flow cytometry Assay Kit	Life Technologies

6.5 Bisulfite Primer

Table 4: List of Bisulfite Primer

Sample		Primer sequence
Liver Treg 10d	**ForP**	CGTATCGCCTCCCTCGCGCCATCAGTATATCTGGGTTTTTTTGGTATTTAAGAAAG
	RevP	CTATGCGCCTTGCCAGCCCGCTCAGTATATCAAAAAACAAATAATCTACCCCACAA
Liver Tconv 10d	**ForP**	CGTATCGCCTCCCTCGCGCCATCAGCCACGCTGGGTTTTTTTGGTATTTAAGAAAG
	RevP	CTATGCGCCTTGCCAGCCCGCTCAGCCACGCAAAAAACAAATAATCTACCCCACAA
Spleen Treg 10d	**ForP**	CGTATCGCCTCCCTCGCGCCATCAGATTATATGGGTTTTTTTGGTATTTAAGAAAG
	RevP	CTATGCGCCTTGCCAGCCCGCTCAGATTATAAAAAACAAATAATCTACCCCACAA
Spleen Tconv 10d	**ForP**	CGTATCGCCTCCCTCGCGCCATCAGTCCGTCTGGGTTTTTTTGGTATTTAAGAAAG
	RevP	CTATGCGCCTTGCCAGCCCGCTCAGTCCGTCAAAAAACAAATAATCTACCCCACAA
Liver Treg 6w	**ForP**	CGTATCGCCTCCCTCGCGCCATCAGATGTCATGGGTTTTTTTGGTATTTAAGAAAG
	RevP	CTATGCGCCTTGCCAGCCCGCTCAGATGTCAAAAAACAAATAATCTACCCCACAA
Liver Tconv 6w	**ForP**	CGTATCGCCTCCCTCGCGCCATCAGGCTACCTGGGTTTTTTTGGTATTTAAGAAAG
	RevP	CTATGCGCCTTGCCAGCCCGCTCAGGCTACCAAAAAACAAATAATCTACCCCACAA
Spleen Treg 6w	**ForP**	CGTATCGCCTCCCTCGCGCCATCAGACTCTCTGGGTTTTTTTGGTATTTAAGAAAG
	RevP	CTATGCGCCTTGCCAGCCCGCTCAGACTCTCAAAAAACAAATAATCTACCCCACAA
Spleen Tconv 6w	**ForP**	CGTATCGCCTCCCTCGCGCCATCAGCGTACGTGGGTTTTTTTGGTATTTAAGAAAG
	RevP	CTATGCGCCTTGCCAGCCCGCTCAGCGTACGAAAAAACAAATAATCTACCCCACAA

6.6 Quantitative real-time PCR primer

Table 5: List of Sybr Primer

Gene	For Primer	Rev Primer
Atf3	GAGGATTTTGCTAACCTGACACC	TTGACGGTAACTGACTCCAGC
Bhlhb2	ACGGAGACCTGTCAGGGATG	GGCAGTTTGTAAGTTTCCTTGC
Ccl2	AGGTCCCTGTCATGCTTCTG	GCTGCTGGTGATCCTCTTGT
Ccl4	ATGAAGCTCTGCGTGTCTG	GAAACAGCAGGAAGTGGGAG
Ccl5	CTGCTGCTTTGCCTACCTCT	CCCACTTCTTCTCTGGGTTG
Ccr2	CCTTGGGAATGAGTAACTGTGTGAT	ATGGAGAGATACCTTCGGAACTTCT
Ciart	CCCTTCTGATAACGAGAGGGA	TGAGGTGCTGTATGTTGGTTACT
Cxcl10	CTCATCCTGCTGGGTCTGAG	TCTTTTTCATCGTGGCAATG
Dbp	CATTCCAGGCCATGAGACTT	TGGCTGCTTCATTGTTCTTG
Foxo3	CTGGGGGAACCTGTCCTATG	TCATTCTGAACGCGCATGAAG
Hprt	CTTTGCTGACCTGCTGGATT	TATGTCCCCCGTTGACTGAT
Ifng	CAGCAACAGCAAGGCGAAA	CTGGACCTGTGGGTTGTTGAC
Il10	ATCGATTTCTCCCCTGTGAA	TGTCAAATTCATTCATGGCCT
Il15	TGCAATGAACTGCTTTCTCC	TCTCCTCCAGCTCCTCACAT
Il18	ACAACTTTGGCCGACTTCAC	AGAGAGGGTCACAGCCAGTC
Il1b	AGTTGACGGACCCCAAAAG	CTTCTCCACAGCCACAATGA
Mki67	ATCATTGACCGCTCCTTTAGGT	GCTCGCCTTGATGGTTCCT
Per1	TGAAGCAAGACCGGGAGAG	CACACACGCCGTCACATCA
Per2	GAAAGCTGTCACCACCATAGAA	AACTCGCACTTCCTTTTCAGG
Rev-Erb-a	TACATTGGCTCTAGTGGCTCC	CAGTAGGTGATGGTGGGAAGTA
Rev-Erb-b	TGAACGCAGGAGGTGTGATTG	TGAACGCAGGAGGTGTGATTG
Tfgb	GGAGAGCCCTGGATACCAA	AGGGTCCCAGACAGAAGTTG
Tnfa	CCACCACGCTCTTCTGTCTAC	AGGGTCTGGGCCATAGAACT

6.7 Reagents

Table 6: List of Reagents

Reagent/Kit	Company
ACK lysis buffer	Lonza
Albumin Fraction V	Roth
autoMACS Running Buffer	Miltenyi Biotec
Anti-Biotin Micro-Beads	Miltenyi Biotec
Bovine Serum Albumin	Sigma
Chloroform	Carl Roth
Collagenase IV	Sigma
Deoxyribonucleotide Triphosphates (dNTPs)	Life Technologies
Dexamethasone	Sigma
Diphtheria Toxin From Corynebacterium	Sigma
DMSO	Genaxxon Bioscience
DNase I	Roche
Dulbecco's Phosphate Buffered Saline (PBS)	Sigma-Aldrich
Ethanol 99,8%	Roth
Fetal Calf Serum (FCS) (Cat. No. A15-101, Lot No. A10109-2802)	PAA Laboratories

Foxp3 / Transcription Factor Staining Buffer Set	eBioscience
GlycoBlue	Life Technologies
Heparin 5000U/ml	Biochrom
HEPES Solution	PAA Laboratories
Hoechst 33342 trihydrochlorid trihydrate	Life Technologies
L-glutamine	Invitrogen
Nuclease free sterile water	Biomol
Oligo(dT) primers	Life Technologies
Penicillin	Invitrogen
Percoll	GE Healthcare
RNAse Inhibitor	Genaxxon Bioscience
streptomycin	Invitrogen
Superscript 2	Life Technologies
Sybr Green Power Master Mix	Life Technologies
TRIzol	Life Technologies
Trypan Blue	Biochrom

6.8 Plastic ware and consumables

Table 7: List of Plastic ware and consumables

Product	Company
Cell culture plates flat bottom 6, 24, 96 well	PAA
Cell culture plates round bottom 96 well	PAA
Cell strainer 40µm	BD Falcon
Conical tubes 15 ml	Nerbe Plus
collagen type I-coated culture dishes 6 well	Becton Dickinson
Conical tubes 50 ml	Greiner GBO
Nitex nylon filter	SEFAR
Pipette filter tips 1-200, 100-1000 µl	StarLab
Pipette tips 0.1-10, 1-200, 100-1000 µl	StarLab
Reaction tubes 1.5 ml	Steinbrenner Laborsysteme
Reaction tube safe-lock	Eppendorf
Syringe Luer-Lok 3 ml	BD

6.9 Buffers and solutions

Table 8: List of buffers and solutions

Buffer/Solution	Composition
ACK Lysis Buffer	PBS, 0.15 M NH_4Cl, 10 mM $KHCO_3$, 0.1 mM Na_2-EDTA *stored at RT, pH 7.3, sterile filtrated*
Adhesion medium	Williams E medium phenol red-free 10% FCS 100 nM Dexamethasone 1% penicillin/streptomycin 2 mM L-glutamine *Fresh prepared*
Complete Medium	DMEM, 10% (v/v) FCS, 10 mM HEPES,100 U/ml Penicillin, 100 µg/ml Streptomycin, 1 mM Pyruvate *stored at 4°C*
EGTA Buffer	475 mg EGTA Add ddH_20 to 10 ml add NaOH for dissolving adjust pH 7.6 (HCL) *sterile filter and stored at 4°C*
FACS buffer	PBS, 0.1% (w/v) NaN_3, 1% (v/v) FCS *stored at 4°C, pH 7.4*
PBS	Water, 0.27 mM KCl, 13.7 mM NaCl, 10 mM Na_2HPO_4, 0.2 mM KH_2PO_4 *stored at RT, pH 7.4, autoclaved*
Primary Hepatocyte culture medium	Williams E medium phenol red-free 1% penicillin/streptomycin 2 mM L-glutamine *stored at 4°C*

6.10 Equipment

Table 9: List of equipment

Equipment	Manufacturer
AutoMACS Pro Separator	Miltenyi Biotec
Cell Culture Hood Safe 2020	Thermo fisher scientific
Cell Culture Incubator, Galaxy 170 S	Eppendorf
Centrifuge 5415 R, 5424 and 5810 R	Eppendorf
FACSAria I, II and III	BD Biosciences
FACSCanto II, LSR II, LSRFortessa	BD Biosciences
Freezer (-20°C, -80°C)	Liebherr and Thermo Fisher Scientific
Fridge (4°C)	Liebherr
Mastercycler Pro S	Eppendorf
Nanodrop 2000	Thermo Fisher Scientific
Neubauer Counting Chamber	Karl Hecht
pH Meter	Sartorius
Thermoblock Neoblock 1	Neolab
UV gel documentation system	Herolab
ViiA 7 Real-Time PCR System	Life Technologies

6.11 Software

Table 10: List of software used for analysis

Software	Company
Adobe Illustrator	Adobe System
EndNote	Thomson Reuters
FACS DIVA	BD Biosciences
FlowJo	Treestar / Thermo Fisher
ImageJ 64	ImageJ freeware
Microsoft Office	Microsoft
Graphpad Prism	Graphpad
Viia 7 software	Applied Biosystems

7 Results

7.1 Hepatic regulatory T cells

Increased T_{reg} cell frequency in neonatal liver tissue

T_{reg} cell development is well described for the thymus of neonatal mice (Dujardin et al. 2004; Fontenot et al. 2005). Hepatic T_{reg} cells have been extensively studied under disease conditions such as autoimmune hepatitis or primary biliary cirrhosis, though less is known about the physiological function of T_{reg} cells in the liver, especially during neonatal development.

To study neonatal T_{reg} cells in the liver and lung tissue via flow cytometry, we used Foxp3eGFP reporter mice and co-stained for intracellular Foxp3 expression after careful exclusion of circulating T_{reg} cells from liver and lung of 10 day-old and 6 week-old mice (Fig. 6). Around 10 days after birth neonatal mice showed an increase in T_{reg} cell frequency as well as total number of T_{reg} cells per gram of liver tissue as compared to 6 week-old mice (Fig. 6a; Fig. 7a, b). Interestingly, this difference was not observed in the spleen and only slightly seen in the lung of the same mice (Fig. 6; Fig. 7a). The percentage of $CD4^+$ T cells was lower in the liver and spleen of neonatal mice as compared to adult mice, which was not observed in the neonatal lung (Fig. 6).

A Foxp3 expression kinetic revealed that the hepatic T_{reg} cell frequency peaked with around 30% of $CD4^+$ T cells at day 10 and declined to less than 10% of $CD4^+$ T cells during maturation of the mice which was not observed in the spleen or lung of the same mice (Fig. 7c, d).

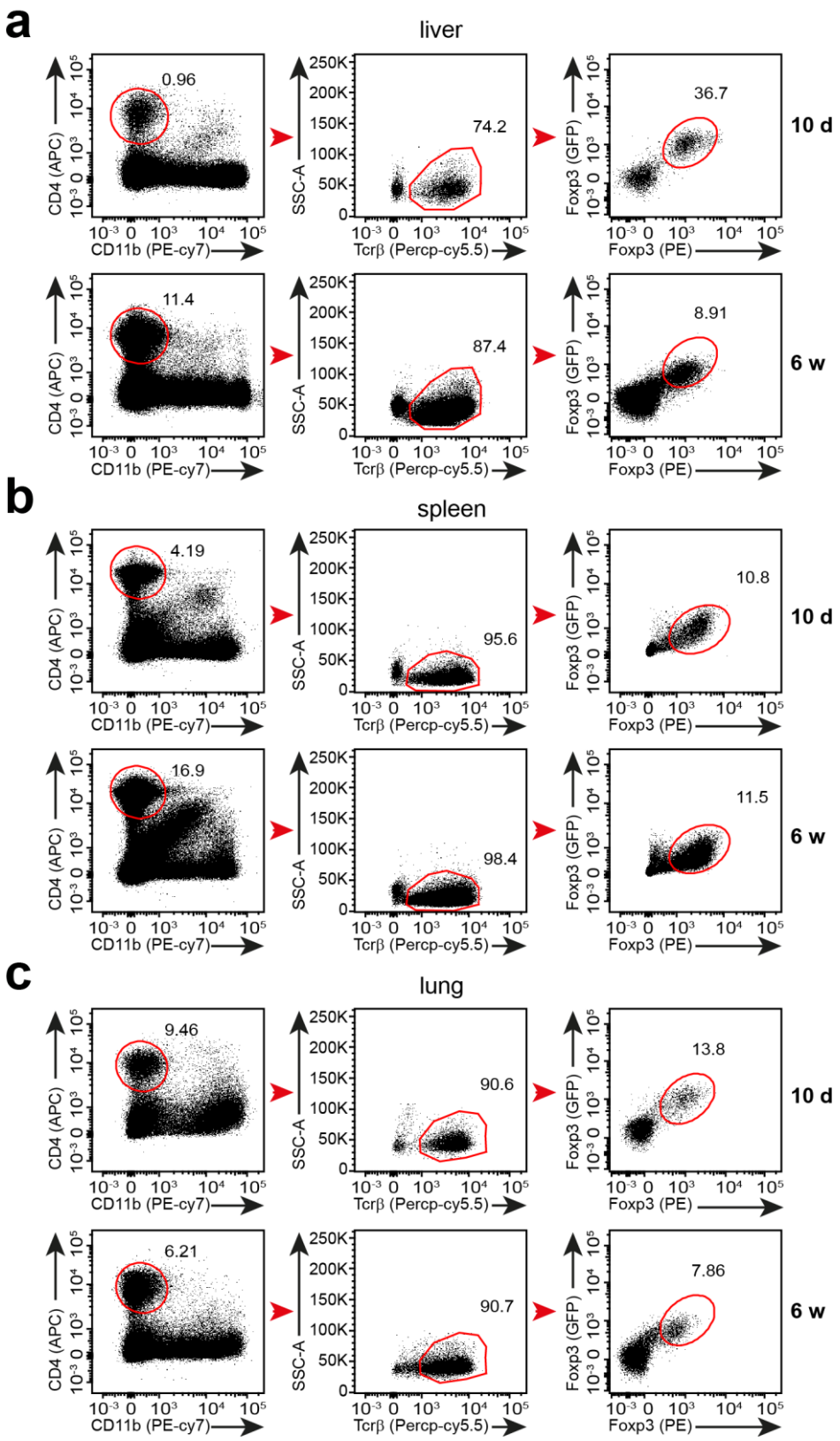

Figure 6: T_{reg} cell gating strategy in liver, spleen and lung. Flow cytometry analysis of Foxp3GFP$^+$Foxp3$^+$CD4$^+$TCRb$^+$ T_{reg} cells from (**a**) liver, (**b**) spleen or (**c**) lung of about 10 day-old (10 d) and 6 week-old (6 w) Foxp3eGFP mice.

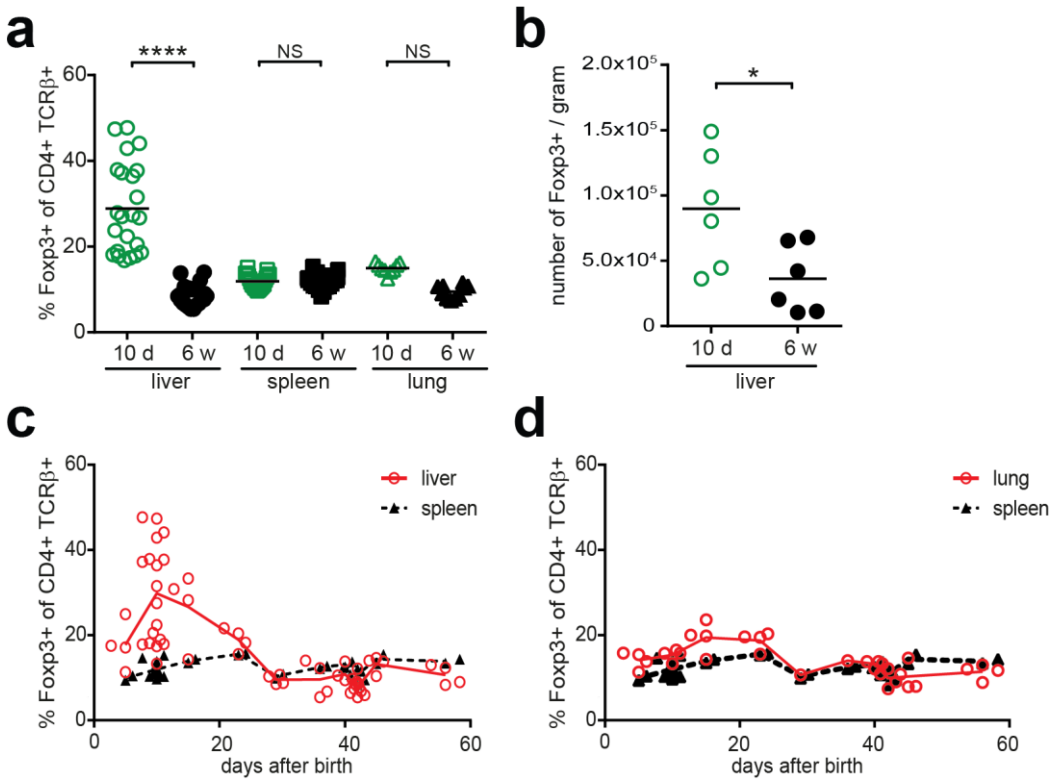

Figure 7: T_{reg} cells in liver, spleen and lung of neonatal mice. T_{reg} cells from about 10 day-old (10 d) Foxp3eGFP mice were compared to 6 week-old (6 w) Foxp3eGFP mice. (**a**) Quantification of Foxp3⁺ T_{reg} cells in liver, spleen and lung. (**b**) Total numbers of Foxp3⁺ T_{reg} cells per gram liver. (**c**) Kinetic of Foxp3⁺ T_{reg} cell accumulation in liver and spleen. (**d**) Kinetic of Foxp3⁺ T_{reg} cell accumulation in lung and spleen. Symbols represent individual animals and *P* values represent comparisons between 10 d and 6 w mice using ordinary two-way ANOVA with Sidak´s multiple comparison test (**a**) or Wilcoxon Test (**b**). NS, not significant; $^{*}P < 0.05$ and $^{****}P < 0.00005$.

To further characterize the origin of these T_{reg} cells in the neonatal liver, we stained for the transcription factor Helios and the cell surface transmembrane glycoprotein Nrp1, both markers for thymus-derived T_{reg} cells. T_{reg} cells in the neonatal liver expressed Helios as well as Nrp1 (Fig. 8a - d). However, a slight increase in Helios expression as well as a decrease in Nrp1 expression was observed in hepatic T_{reg} cells at the neonatal stage as compared to 6 week-old mice (Fig. 8b, d). Another way to identify stable Foxp3 expressing T_{reg} cells is to analyze the DNA CpG methylation status of the T_{reg}-specific demethylation region (TSDR) located in the conserved non-coding region 2 (CNS2) of the *Foxp3* gene (Floess et al. 2007) (Fig. 8e). The epigenetic analysis revealed a demethylated TSDR in T_{reg} cells from the neonatal and adult liver as well as the spleen (Fig. 8f). Therefore, Helios and Nrp1 expression as well as the DNA methylation status confirmed that hepatic T_{reg} cells from neonatal mice were bona-fide thymus-derived T_{reg} cells (Fig. 8f).

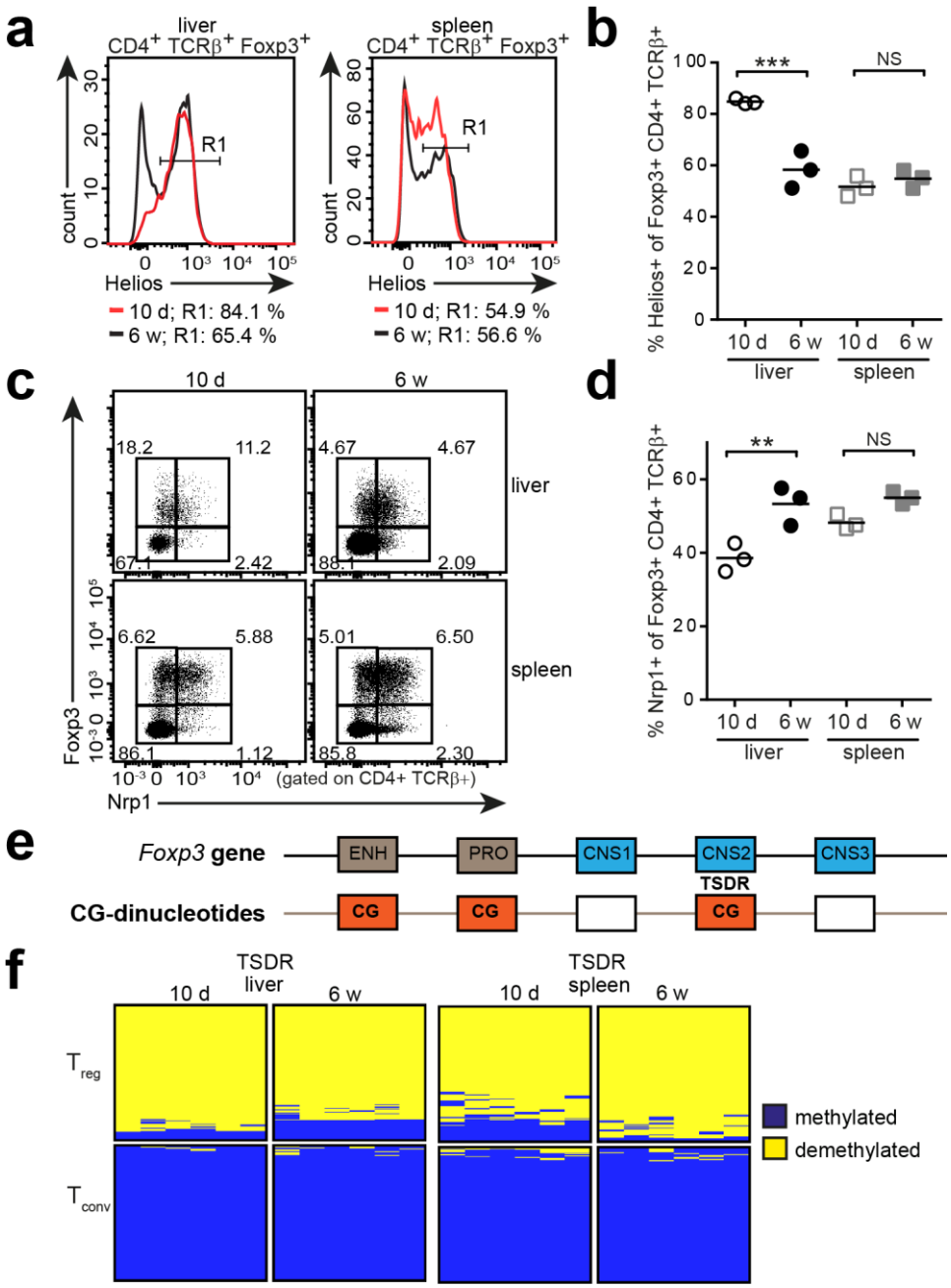

Figure 8: Hepatic T_{reg} cells in neonatal mice are thymus-derived. T_{reg} cells from about 10 day-old (10 d) Foxp3eGFP mice were compared to 6 week-old (6 w) Foxp3eGFP mice. (**a**) Representative flow cytometry gating and (**b**) quantification of Helios$^+$Foxp3$^+$CD4$^+$TCRb$^+$ T_{reg} cells in liver and spleen. (**c**) Representative flow cytometry gating and (**d**) quantification of Nrp1$^+$Foxp3$^+$CD4$^+$TCRb$^+$ T_{reg} cells in liver and spleen. (**e**) Schematic figure of the *Foxp3* gene with high CG-dinucleotide content highlighted in orange in the enhancer (ENH), promoter (PRO) and the T_{reg}-specific demethylated region (TSDR) in the conserved-non-coding sequences 2 (CNS2). (**f**) Bisulfite sequencing of 6 CpGs in the TSDR region of the CNS2 in the *Foxp3* gene of sorted Foxp3$^+$CD4$^+$ T_{reg} cells and Foxp3$^-$CD4$^+$ T_{conv} cells from liver and spleen; yellow: demethylated CpG; blue: methylated CpG. Symbols represent individual animals and *P* values represent comparisons between 10 d and 6 w mice using ordinary two-way ANOVA with Sidak´s multiple comparison test (**b, d**); NS, not significant; $^{**}P < 0.005$, $^{***}P < 0.0005$.

To exclude the possibility that the increased accumulation of T_{reg} cells in the liver of neonatal mice was C57BL/6 background-specific, we analyzed Foxp3$^+$ T cells in mice carrying the non-obese diabetic (NOD) background (Fig. 9). NOD mice spontaneously develop Type 1 diabetes at the age of around 10 weeks. We analyzed the mice before the development of the disease to test whether the T_{reg} cell frequencies were different in neonatal NOD mice. As seen previously in the liver of Foxp3eGFP C57BL/6 mice (Fig. 6; Fig. 7), the T_{reg} cell frequency in the neonatal liver of NOD mice was significantly increased as compared to 6 week-old NOD mice (Fig. 9a, b). This difference was not observed in the spleen of the same mice (Fig. 9a, b). Based on our findings, we suggest that accumulation of Foxp3$^+$ T cells in neonatal mice is mouse strain-independent.

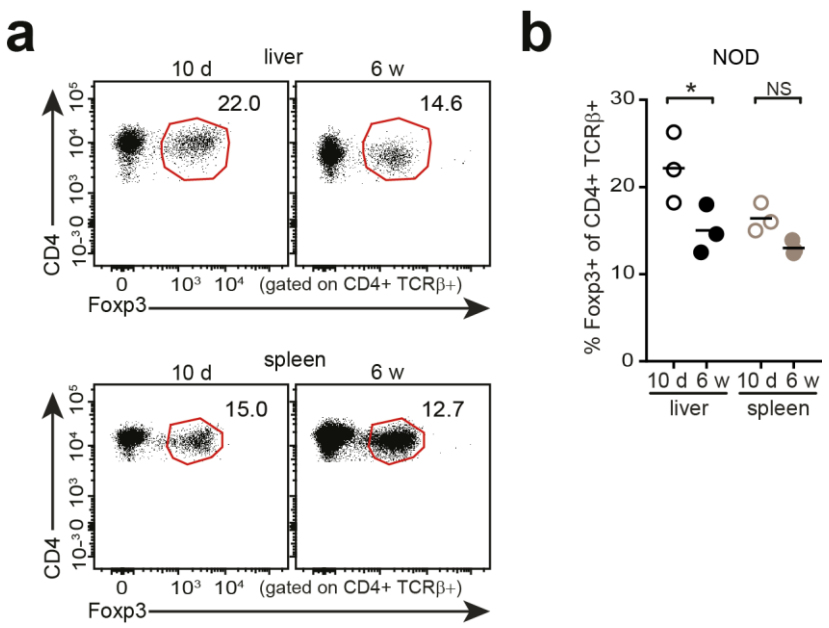

Figure 9: Hepatic T_{reg} cells in neonatal NOD mice. T_{reg} cells from about 10 day-old (10 d) NOD mice were compared to 6 week-old (6 w) NOD mice. (**a**) Representative flow cytometry gating of Foxp3$^+$CD4$^+$TCRb$^+$ T_{reg} cells in liver and spleen. (**b**) Quantification of Foxp3$^+$CD4$^+$TCRb$^+$ T_{reg} cells in liver and spleen. Symbols represent individual animals and *P* values represent comparisons between 10 d and 6 w mice using ordinary two-way ANOVA with Sidak´s multiple comparison test. NS, not significant; *$P < 0.05$.

For further characterization of the hepatic T_{reg} cells in the liver of neonatal mice we studied CD44 and CD11a expression. CD44 is a transmembrane glycoprotein involved in T cell activation and memory (Dutton, Bradley, and Swain 1998; Baaten et al. 2010). We observed that generally around 70 - 80% of Foxp3$^+$ T_{reg} cells in the liver and around 40 - 60% of Foxp3$^+$ T_{reg} cells in the lung and spleen expressed CD44 (Fig. 10a - c). At the neonatal stage, the liver, lung and spleen showed an increase of activated CD44$^+$Foxp3$^+$ T_{reg} cells as compared to the same organs in adult mice. The neonatal liver contained with around 80% of CD44$^+$ T_{reg} cells a larger antigen-experienced and activated T_{reg} cell population as the lung and the spleen of the same mice (Fig. 10a, c).

The lymphocyte function-associated antigen 1 (CD11a; LFAT) is expressed on activated T cells and has been implicated in mediating the homing of T cells to lymphoid and non-lymphoid tissue (Koboziev et al. 2012), as well as function as a co-stimulatory molecule for T cell activation (Kandula and Abraham 2004; Koboziev et al. 2012). In general, we observed a higher CD11a expression on hepatic T cells in comparison to splenic T cells (Fig. 11a, b). Around 70% of T_{reg} cells in the neonatal liver and 40% of T_{reg} cells in the adult liver expressed CD11a (Fig. 11a).

Taken together, our findings indicate that the accumulation of thymus-derived T_{reg} cells in 10 day-old mice is liver-specific and that these cells show characteristic high expression levels of the activation marker CD44 and the adhesion molecule CD11a.

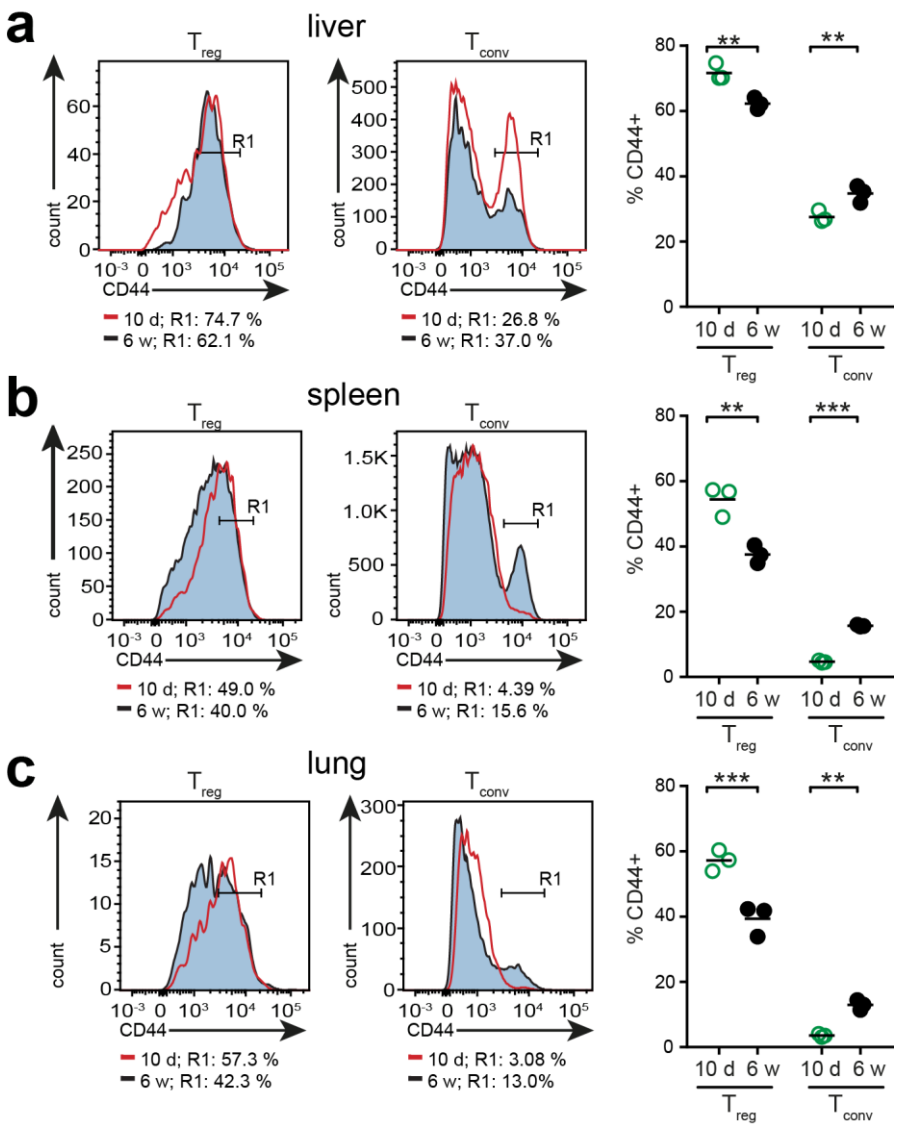

Figure 10: CD44 surface expression of T_{reg} and T_{conv} cells in liver, spleen and lung. Representative histograms of $CD44^+Foxp3^+CD4^+TCRb^+$ T_{reg} cells (R1, right panel) and $CD44^+Foxp3^-CD4^+TCRb^+$ T_{conv} cells (R1, middle panel) from (**a**) liver, (**b**) spleen or (**c**) lung of 10 day-old (10 d; red line) and 6 week-old (6 w, black line) Foxp3eGFP mice. (**a** - **c**; left panel) Quantification of $CD44^+Foxp3^+CD4^+TCRb^+$ T_{reg} cells and $CD44^+Foxp3^-CD4^+TCRb^+$ T_{conv} cells in liver, spleen and lung. Symbols represent individual animals and *P* values represent comparisons between 10 d and 6 w mice using ordinary two-way ANOVA with Sidak´s multiple comparison test (**a** - **c**). $^{**}P < 0.005$, $^{***}P < 0.0005$.

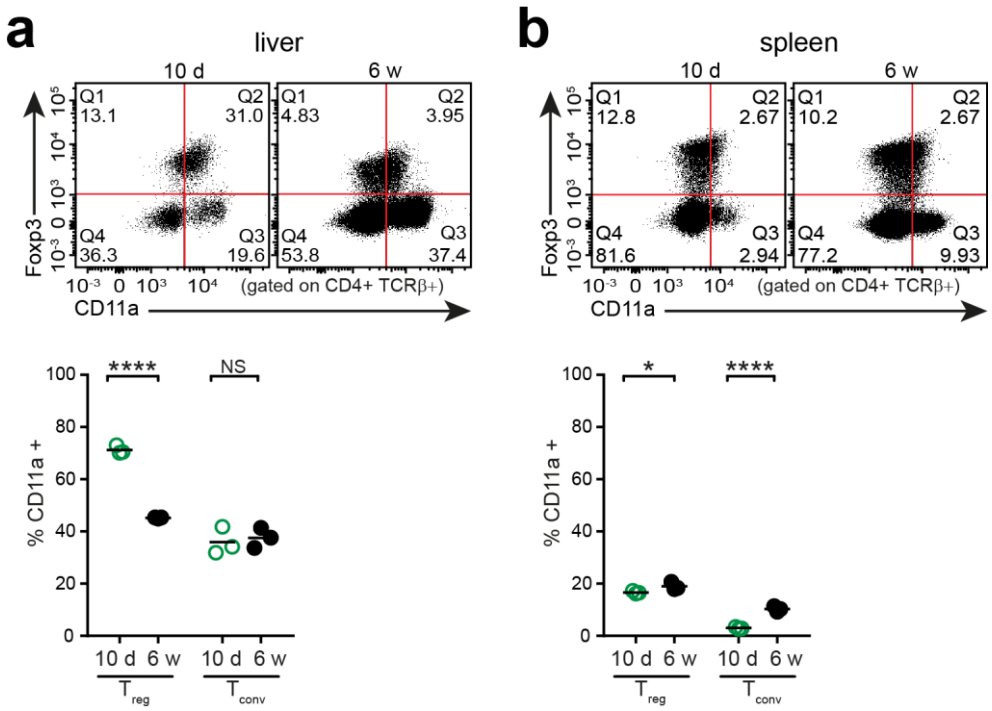

Figure 11: CD11a$^+$ T_{reg} and T_{conv} cells in liver and spleen. (**a** - **b**) T_{reg} cells from about 10 day-old (10 d) C57BL/6 mice were compared to 6 week-old (6 w) C57BL/6 mice. Representative dot plots (upper panel) and quantification (lower panel) of CD11a$^+$Foxp3$^+$CD4$^+$TCRb$^+$ T_{reg} cells and CD11a$^+$Foxp3$^-$CD4$^+$TCRb$^+$ T_{conv} cells in (**a**) liver and (**b**) spleen. Symbols represent individual animals and *P* values represent comparisons between 10 d and 6 w mice using ordinary two-way ANOVA with Sidak´s multiple comparison test. NS, not significant; *$P < 0.05$, ****$P < 0.00005$.

Proliferation activity of hepatic T_{reg} cells

To test whether the hepatic T_{reg} cell accumulation in neonatal liver tissue is based on local proliferation, we measured the proliferative activity of T cell populations in neonatal and adult mice. We observed that T_{reg} cells in tissues of neonatal mice seemed to be generally more proliferative than T_{conv} cells or T_{reg} cells in the adult liver based on two different assays: a cell-cycle state assessment using the DNA-intercalating dye Hoechst 33342 (Fig. 12) and a rapid nucleotide-incorporation assay using the thymidine analog EdU (Fig. 13a, b). In addition, hepatic T_{reg} cells from neonatal mice were also more proliferative than their counterparts in spleen and lung (Fig. 12d, Fig. 13b). EdU incorporation assay revealed that about 16% of the T_{reg} cells in the neonatal liver were in cycle which was substantially higher than the 8% of proliferating T_{reg} cells found in the neonatal spleen (Fig. 13b).
Next, we determined whether the *in situ* proliferation of T_{reg} cells from the neonatal liver was induced by antigen-specific TCR activation. *Nur77*-eGFP reporter mice have been described to highlight TCR activation by *Nr4a1* (*Nur77*)-induced GFP expression without detecting cytokine-driven activation of T cells (Moran et al. 2011). Analyzing these reporter mice, we observed a significantly higher percentage of Nr4a1^{+} T_{reg} cells in 10 day-old livers as compared to 6 week-old livers. Consequently, the T_{reg} cell proliferation in the liver tissue of neonatal mice seems to be due to an antigen-specific TCR-driven proliferation (Fig. 13c, d).

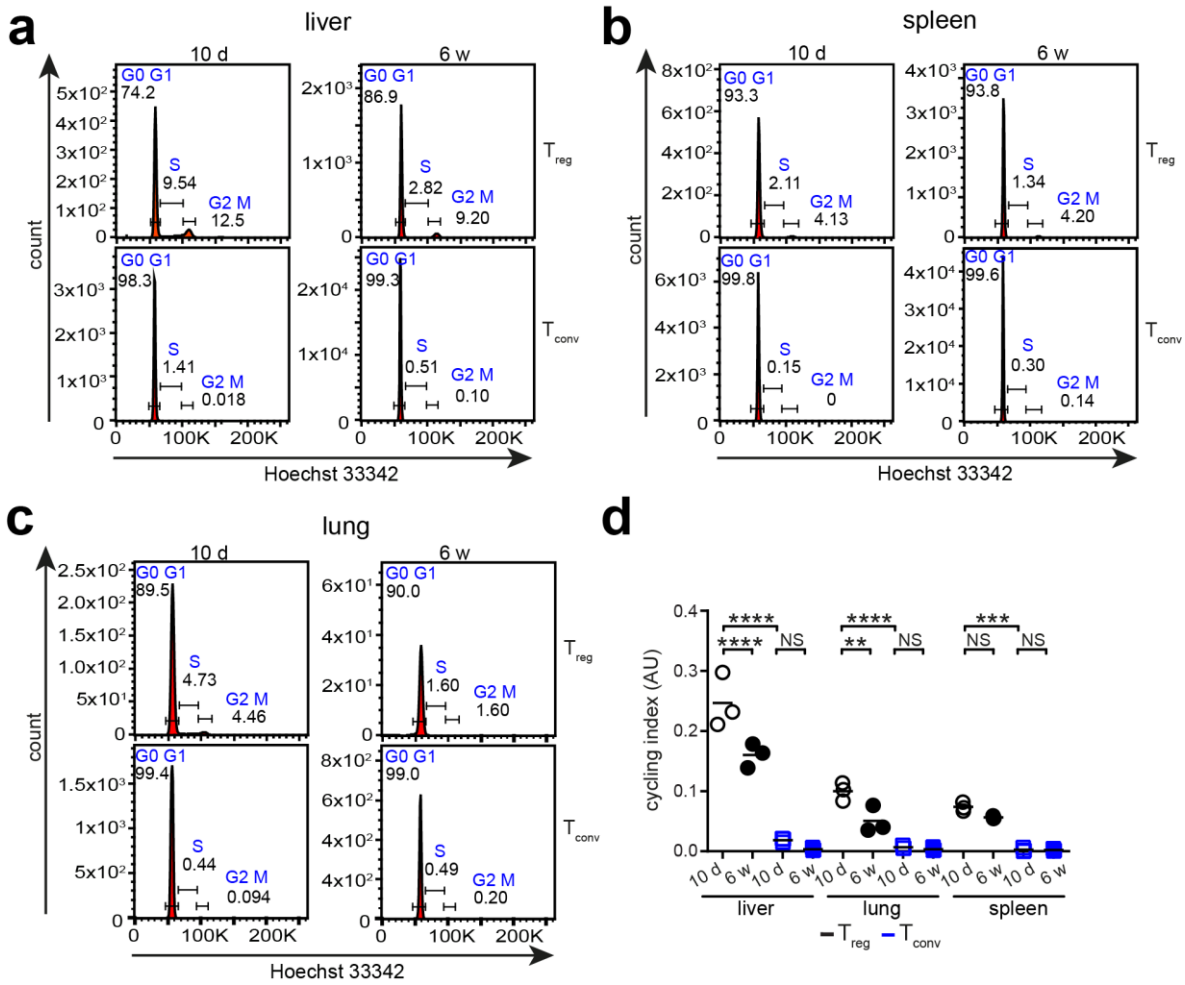

Figure 12: Proliferative activity of T cell populations in liver, lung and spleen measured by flow cytometry staining with Hoechst 33342-A. (**a** - **c**) Representative histograms of Foxp3^{+}CD4^{+}TCRb^{+} T_{reg} cells and Foxp3^{-}CD4^{+}TCRb^{+} T_{conv} cells showing percent cells in the G1-G0 (left), S (middle) and G2-M (right) phases of the cell cycle from about 10 day-old (10 d) and 6 week-old (6 w) Foxp3eGFP mice. (**d**) Quantification of cell-cycle indices calculated as ((S + G2-M) / G1-G0) and presented in arbitrary units (AU). Symbols represent individual animals and *P* values represent comparisons between 10 d and 6 w mice using ordinary two-way ANOVA with Sidak´s multiple comparison test (**d**). NS, not significant; $^{**}P < 0.005$, $^{***}P < 0.0005$, $^{****}P < 0.00005$.

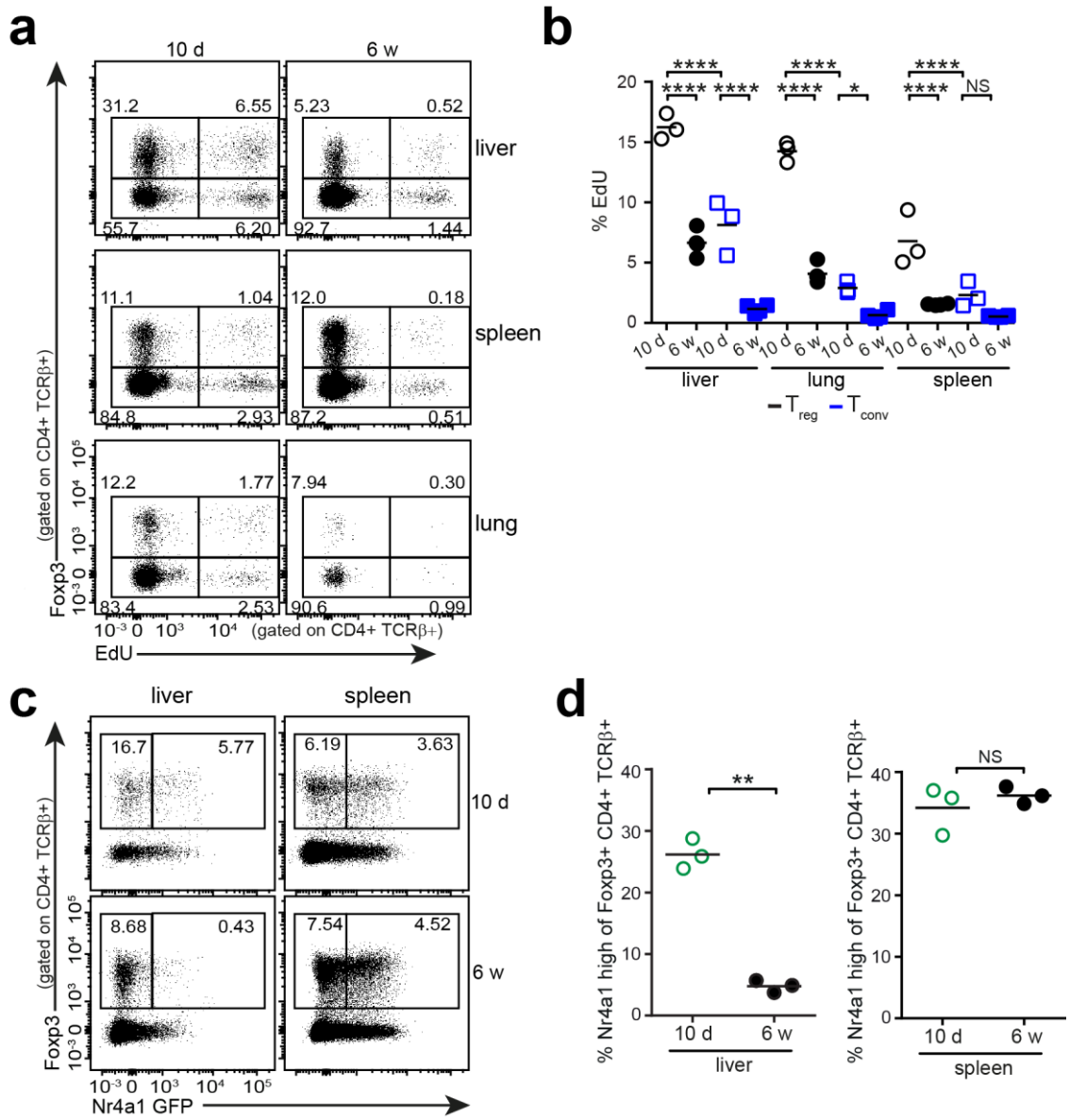

Figure 13: Proliferative activity and TCR stimulation of hepatic T_{reg} cells. (**a**) Representative dot plots and (**b**) quantification of EdU⁺ cells of Foxp3⁺ T_{reg} cells (black) and Foxp3⁻ T_{conv} cells (blue) from liver, lung and spleen of about 10 day-old (10 d) and 6 week-old (6 w) Foxp3eGFP mice. (**c**) Flow cytometry gating and (**d**) quantification of Nr4a1^{high}Foxp3⁺ T_{reg} cells from the liver of 10 day-old (10 d) and 6 week-old (6 w) Nur77-eGFP mice. Symbols represent individual animals and *P* values represent comparisons between 10 d and 6 w old mice using ordinary two-way ANOVA with Sidak´s multiple comparison test (**b**) or unpaired *t* test with Welch-correction (**d**). NS, not significant; **P* < 0.05, ***P* < 0.005, and *****P* < 0.00005.

Gene expression analysis of hepatic T_{reg} cells

Gene expression studies using a RNA-based microarray platform helped us to further characterize the proliferating neonatal wave of hepatic T_{reg} cells. We detected about 100 two-fold differentially expressed genes in hepatic T_{reg} cells from 10 day-old mice in comparison to their counterparts in adult livers (Fig. 14a). While expression of the T_{reg} cell characteristic transcription factor *Foxp3* was similar in 10 day-old and 6 week-old hepatic T_{reg} cells, one of the strongest differentially expressed genes was *Interleukin 10* (*Il10)* (Fig. 14a). In comparison to T_{reg} cells from the adult liver or the neonatal spleen, *Il10* was highly over-expressed in T_{reg} cells from the neonatal liver (Fig. 14a, b, c). More differences were found in the expression of survival- (*Birc5 (Survivin); Ier3*), co-stimulation- (*Tnfrsf9*) or chemotactic migration- (*Cxcr3*) related genes (Fig. 14a). Additionally, the serum glycoprotein *Alpha2-HS* (*Ahsg*), synthesized by hepatocytes, and the *natural killer cell protein 7 (Nkg7*), which has been described to be under control of *Foxp3* (Sugimoto et al. 2006), were highly up-regulated in T_{reg} cells from the neonatal liver in comparison to T_{reg} cells from the adult liver or the neonatal spleen (Fig. 14a, b). The over-expression of these genes was specific for T_{reg} cells from the neonatal liver, since neither the comparison to T_{reg} cells from the adult liver nor the comparison to T_{reg} cells from the neonatal spleen revealed the same expression level (Fig. 14a, b, c).

Analysis using the Gene Ontology (GO) platform showed that several clusters of over-expressed genes in the 10 day-old hepatic T_{reg} cells were involved in metabolic processes as well as DNA replication (Fig. 14d). The significantly increased expression pattern of ligase *Lig1*, several members of the DNA helicase complex (*Mcm2, 5, 7*), endonuclease *Fen1* and DNA topoisomerase *Top2a* in 10 day-old hepatic T_{reg} cells, further supported the increased proliferative potential of these cells (Fig. 14e).

Collectively, our results reveal a distinct phase during the neonatal liver development with an elevated accumulation of proliferating thymus-derived T_{reg} cells over-expressing distinct genes such as *Il10*.

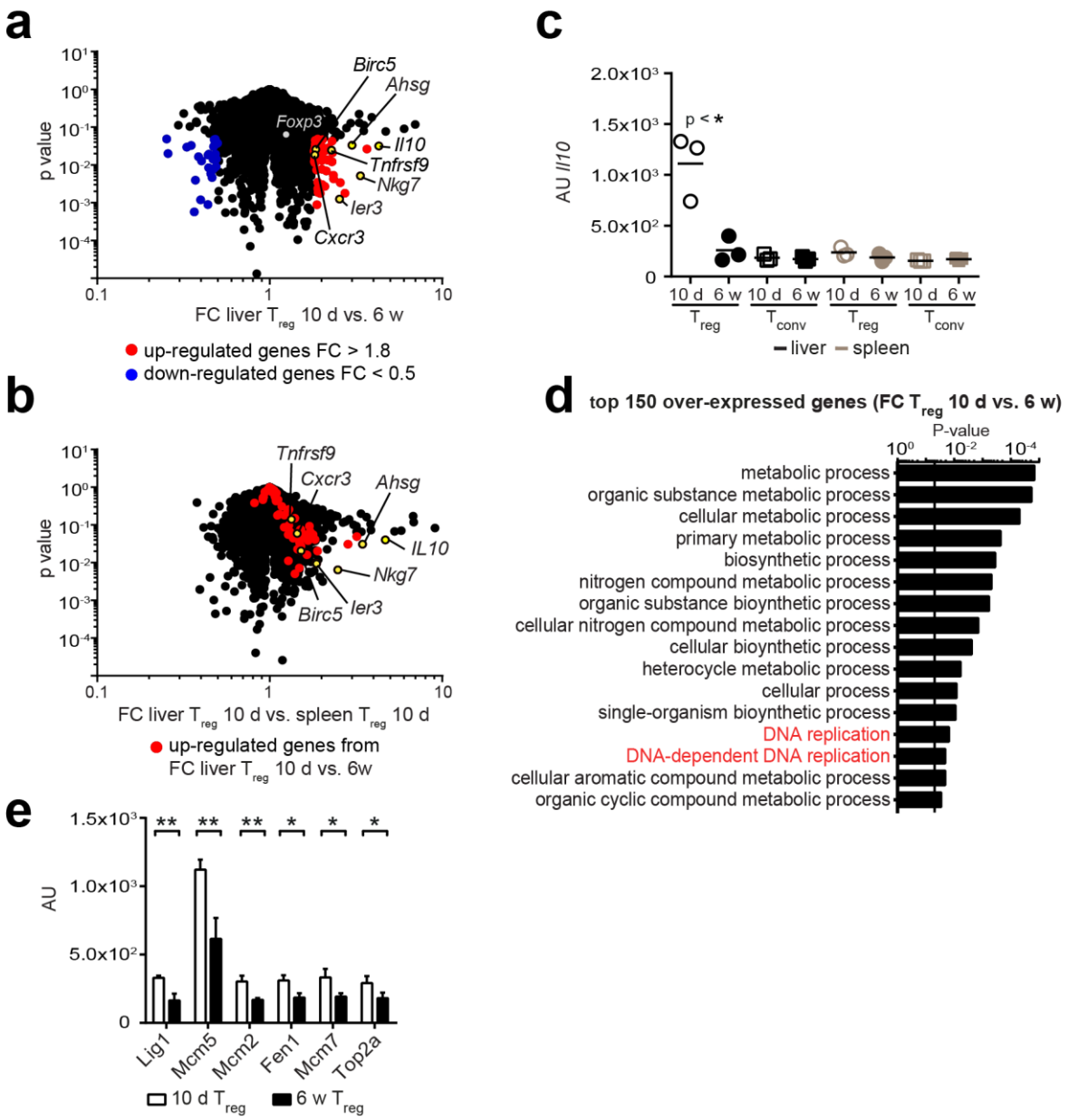

Figure 14: Gene expression analysis of hepatic T_{reg} cells. RNA microarray analysis of sorted T cells from 10 day-old (10 d) and 6 week-old mice. (**a**) Fold change (FC) to *P* value plot of hepatic Foxp3⁺CD4⁺ T_{reg} cells from 10 d and 6 w mice. (**b**) Fold change to *P* value plot of hepatic versus splenic Foxp3⁺CD4⁺ T_{reg} cells from 10 d mice. Significantly up-regulated genes of the comparison hepatic 10 d versus 6 w T_{reg} cells from (**a**) are highlighted in red in both (a) and (b). (**c**) *Il10* gene expression in Foxp3⁺ T_{reg} cells and Foxp3⁻ T_{conv} cells from liver (black) and spleen (grey) in 10 d and 6 w mice, presented in arbitrary units (AU). (**d**) Gene ontology analysis of the top 150 significantly up-regulated genes of the comparison of 10 d versus 6 w hepatic T_{reg} cells represented with their *P* values per process. (**e**) Gene expression of *Lig1*, *Mcm5*, *Mcm2*, *Fen1*, *Mcm7*, *Top2a* in Foxp3⁺ T_{reg} cells of 10 d and 6 w mice, presented in AU. Symbols represent individual animals (**c**) and *P* values represent comparisons between 10 d versus 6 w mice using paired *t* test (**c**), PANTHER over-representation test (**d**) or unpaired *t* test with Welch-correction (**e**). *$P < 0.05$ and **$P < 0.005$.

7.2 The neonatal liver

The liver microenvironment in neonatal mice

Since high T_{reg} cell frequencies are usually associated with some kind of inflammation, we decided to explore the liver microenvironment during the time the neonatal wave of proliferating hepatic T_{reg} cells occurred using quantitative real-time PCR. We detected an around two-fold increase in the expression levels of pro- and anti-inflammatory cytokines such as *Tnfa*, *Tgfb* and *Il1b* in the neonatal liver (Fig. 15a). Additionally, elevated expression levels of distinct chemokine ligands (Ccl) such as *Ccl2*, C*cl4* and *Ccl5* were observed (Fig. 15b, c).

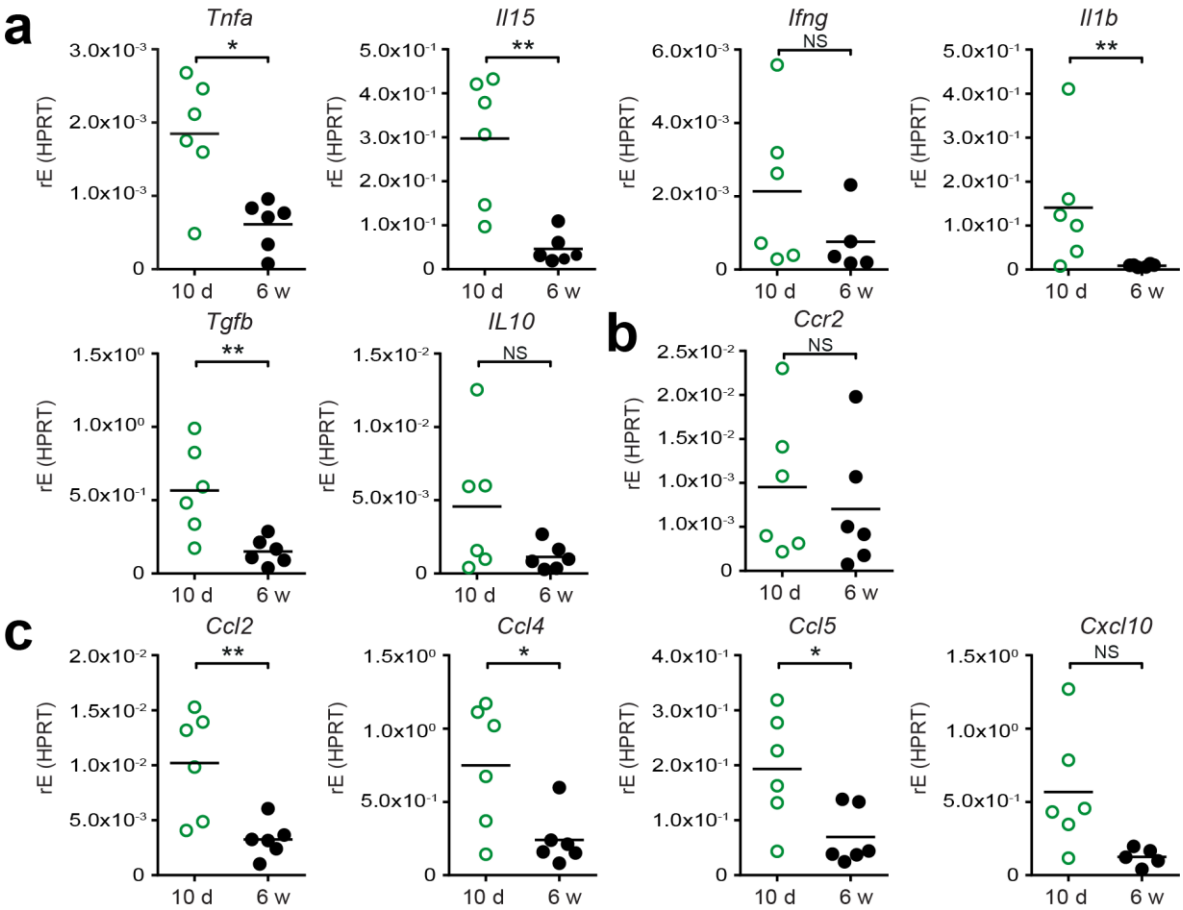

Figure 15: Gene expression in neonatal and adult livers. Quantitative real-time PCR analysis of whole liver mRNA for (**a**) cytokines (*Tnfa*, *Tgfb*, *Ifng*, *Il1b*, *Il15, Il10*), (**b**) the chemokine receptor *Ccr2* and (**c**) chemokines (*Ccl2, Ccl4, Ccl5, Cxcl10)* in 10 day-old (10 d) and 6 week-old (6 w) Foxp3eGFP mice. Symbols represent individual animals and *P* values represent comparisons between 10 d and 6 w mice using unpaired *t* test with Welch-correction calculated with log2 values. NS, not significant, *$P < 0.05$ and **$P < 0.005$.

To determine whether immune cells other than T_{reg} cells also accumulate in the neonatal liver compartment, we analyzed the frequency of hepatic macrophages, monocytes and NK cells (Fig. 16, left and middle panels). Neonatal mice showed no increased accumulation of hepatic NK cells, macrophages or monocytes (Fig. 16 left and middle panels). Instead, we detected a significantly higher percentage of F4/80$^+$ Kupffer cells and Ly6C^{low} monocytes in the liver of 6 week-old mice compared to 10 day-old mice (Fig. 16b, c; middle panels). Interestingly, the neonatal liver revealed a F4/80$^-$CD11b$^+$ population which was not detectable in the adult liver (Fig. 16b, left panel, black gate). After sorting of NK1.1$^+$ NK cells, F4/80$^+$ Kupffer cells and Ly6C^{high} monocytes we analyzed once the expression levels of *Ifng* or *Tnfa* (Fig. 16, right panels). Hepatic NK1.1$^+$ NK cells from neonatal mice seemed to express a slightly increased level of *Ifng* compared to 6 week-old mice. Moreover, we observed an up-regulated level of *Tnfa* in F4/80$^+$ Kupffer cells as well as hepatic Ly6C^{high} monocytes in these neonatal mice (Fig. 16b, c, right panels).

Overall, by analyzing the frequencies of different, but not all, immune cell subsets, T_{reg} cells appear to be the only cells that accumulate in the neonatal liver. However, the up-regulated expression of *Ifng* and *Tnfa* by NK and myeloid cells may correlate with the measured increased expression levels of these cytokines in the liver of neonatal mice (Fig. 15).

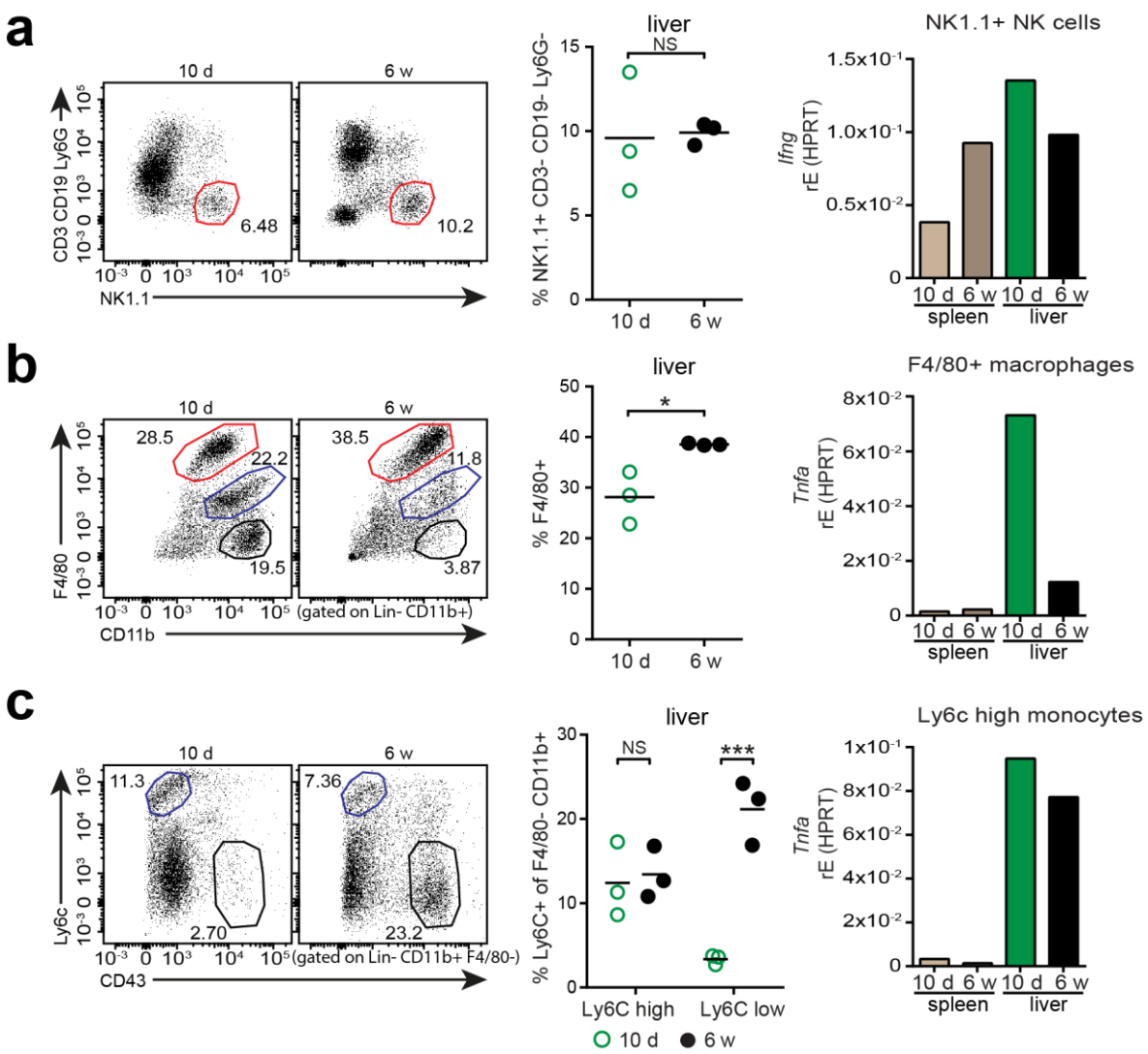

Figure 16: NK cells, macrophages and monocytes in the neonatal liver. Analysis of hepatic NK cells, F4/80⁺ macrophages and monocytes in 10 day-old (10 d) and 6 week-old (6 w) mice. (**a**) Representative dot plot (left panel) and quantification (middle panel) of sorted hepatic NK1.1⁺ cells. Quantitative real-time PCR analysis (right panel) for *Ifng* of sorted hepatic and splenic NK1.1⁺ cells. (**b**) Representative dot plot (left panel) and quantification (middle panel) of sorted hepatic F4/80⁺ macrophages (red gate) and monocytes (blue and black gates). Quantitative real-time PCR analysis (right panel) for *Tnfa* of sorted hepatic or splenic F4/80⁺ macrophages (red gate). (**c**) Representative dot plot (left panel) and quantification (middle panel) of Ly6c^{high} (blue gate) and Ly6c^{low} monocytes (black gate), pre-gated on F4/80^{low}CD11b⁺ cells (blue gate in **b**, left panel). Quantitative real-time PCR analysis (right panel) for *Tnfa* of sorted hepatic or splenic Ly6c^{high} monocytes (blue gate). For quantitative real-time PCR analysis, RNA was isolated from pooled cells out of about 5 - 8 mice. Symbols represent individual animals and *P* values represent comparisons between 10 d and 6 w mice using unpaired *t* test with Welch-correction (**a**, **b**) and ordinary two-way ANOVA with Sidak´s multiple comparison test (**c**). NS, not significant, $^{*}P < 0.05$ and $^{***}P < 0.0005$.

To determine whether hepatocytes are the main producer of the increased cytokine and chemokine levels in the neonatal liver, we performed quantitative real-time PCR analysis with primary hepatocytes isolated from neonatal and adult livers. The expression levels of the cytokines *Tnfa* and *Il1b* were significantly increased in primary hepatocytes from neonatal mice (Fig. 17), as seen before in the quantitative real-time PCR analysis of whole liver RNA (Fig. 15a). These findings support the assumption that mainly hepatocytes are responsible for the increased secretion of cytokines and chemokines in the neonatal liver.

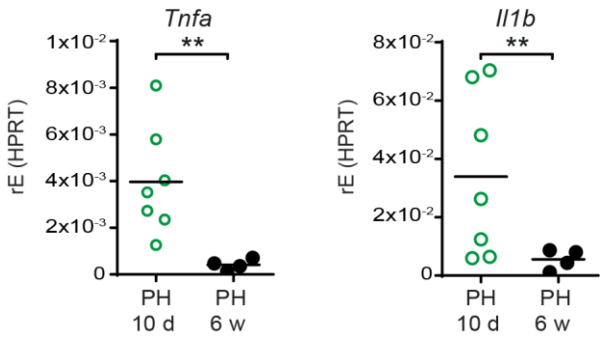

Figure 17: Gene expression in neonatal and adult primary hepatocytes. Quantitative real-time PCR analysis of *Il1b* and *Tnfa* in isolated primary hepatocytes (PH) of 10 day-old (10 d) and 6 week-old (6 w) mice. Symbols represent individual animals and *P* values represent comparisons between 10 d versus 6 w mice using unpaired *t* test with Welch-correction calculated with log2 values.**$P < 0.005$.

It is known that the gut-liver axis plays a critical role in modulating the hepatic immune system since the liver receives blood via the portal vein from the gut (Crispe 2003). We determined whether bacterial antigen could trigger the accumulation of hepatic T_{reg} cells and the characteristic inflammatory liver gene-signature by analyzing neonatal mice deficient for receptor molecules or adapter molecules of the Toll-like-receptor (TLR) pathways (Fig. 18a, b, c, d). Interestingly, neonatal mice deficient for *Tlr4* or the TLR adapter molecules *Trif* and *MyD88* showed the same accumulation of hepatic T_{reg} cells as previously observed in 10 day-old Foxp3eGFP mice (Fig. 18a; Fig. 7a). Therefore, our results indicate a limited effect of bacterial antigens or bacterial products on the T_{reg} cell accumulation in the neonatal liver. Furthermore, the increased gene expression levels of the cellular proliferation marker *Mki67* (Fig. 18b) as well as *Ccl2* and *Tgfb* (Fig. 18c, d) in the neonatal liver of $Tlr4^{-/-}$ and $Trif^{-/-}$ mice indicated the same inflammatory milieu and a high proliferative activity of liver cells as observed before in Foxp3eGFP mice.

Another reason for the increased level of hepatic cytokines and chemokines in the 10 day-old mice could be the first settlement of lymphocytes in the neonatal liver tissue, since T cell seeding of peripheral organs continues during the neonatal period (Garcia et al. 2000). However, analysis of liver tissue isolated from neonatal Rag2-deficient mice, which lack mature B and T cells, showed the same characteristic inflammatory liver gene-signature detected before in Foxp3eGFP mice (Fig. 18e). Therefore, we assume that neonatal tissue seeding by T cells and B cells is not the cause for the characteristic low-grade inflammatory signature in the neonatal liver.

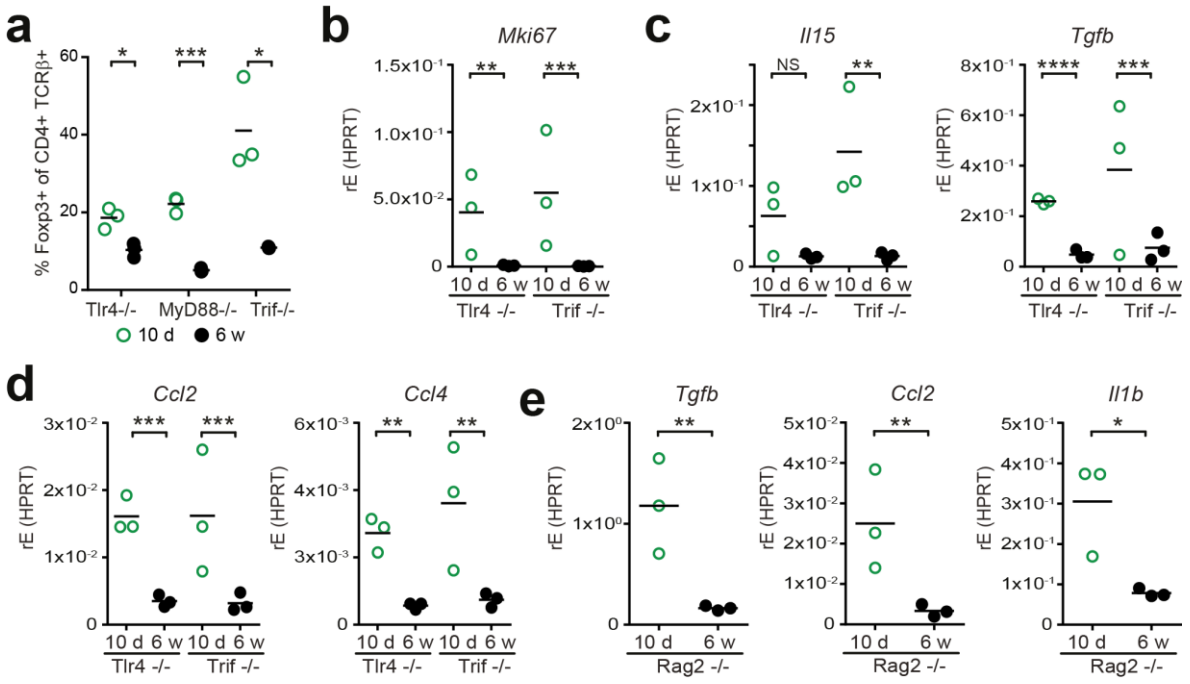

Figure 18: Hepatic gene expression in MyD88$^{-/-}$, Trif$^{-/-}$, Tlr4$^{-/-}$ and Rag2$^{-/-}$ mice. (**a**) Quantification of Foxp3^{+} T_{reg} cells in 10 day-old (10 d) and 6 week-old (6 w) Tlr4$^{-/-}$, MyD88$^{-/-}$ and Trif$^{-/-}$ mice assessed by flow cytometry. (**b** - **d**) Quantitative real-time PCR analysis of whole liver mRNA for (**b**) *Mki67*, (**c**) cytokines and (**d**) chemokines in 10 d and 6 w Tlr4$^{-/-}$, MyD88$^{-/-}$ and Trif$^{-/-}$ mice. (**e**) Quantitative real-time PCR analysis of whole liver mRNA for cytokines and chemokines in 10 d and 6 w Rag2$^{-/-}$ mice. Symbols represent individual animals and *P* values represent comparisons between 10 d and 6 w mice using ordinary two-way ANOVA with Sidak´s multiple comparison test (**a**) calculated with log2 values (**b** - **d**) and unpaired *t* test with Welch-correction calculated with log2 values (**e**). NS, not significant, **P* < 0.05, ***P* < 0.005, ****P* < 0.0005 and *****P* < 0.00005.

Assuming liver-intrinsic reasons for the accumulation of T_{reg} cells and the characteristic low-grade inflammatory signature in the neonatal liver, we performed microarray analysis to study differences between neonatal and adult livers. We identified about 1700 differentially expressed gene probes. Among those, we detected some expected differences such as *alpha-fetoprotein* (*Afp*), produced in the liver during fetal development (Fig. 19a). Other differences, such as the increased expression of genes from the S100 family indicated tissue-stress and inflammation in the liver of 10 day-old mice, whereas the reduced gene expression of members of the aldehyde dehydrogenase (Aldh) family, the cytochrome P450 (Cyp) family and the major urinary family (Mup) family demonstrated the functional immaturity of the neonatal liver (Fig. 19a). Interestingly, almost all genes from the Cyp family were under-represented in the neonatal liver (Fig. 19b), which was not observed in other peripheral organs such as the lung (Fig. 19c). Quantitative proteomic analysis by mass spectrometry revealed the same decreased protein expression of Cyp family members in the neonatal liver in comparison to the adult liver (Fig. 19d, Appendix Table 11). Additionally, the neonatal liver showed under-represented gene expression of members of the Mup family, which was not observed in the lung of the same mice, as Mup proteins are known to be primarily made in the liver and secreted through the kidneys into the urine (Fig.19e, f).

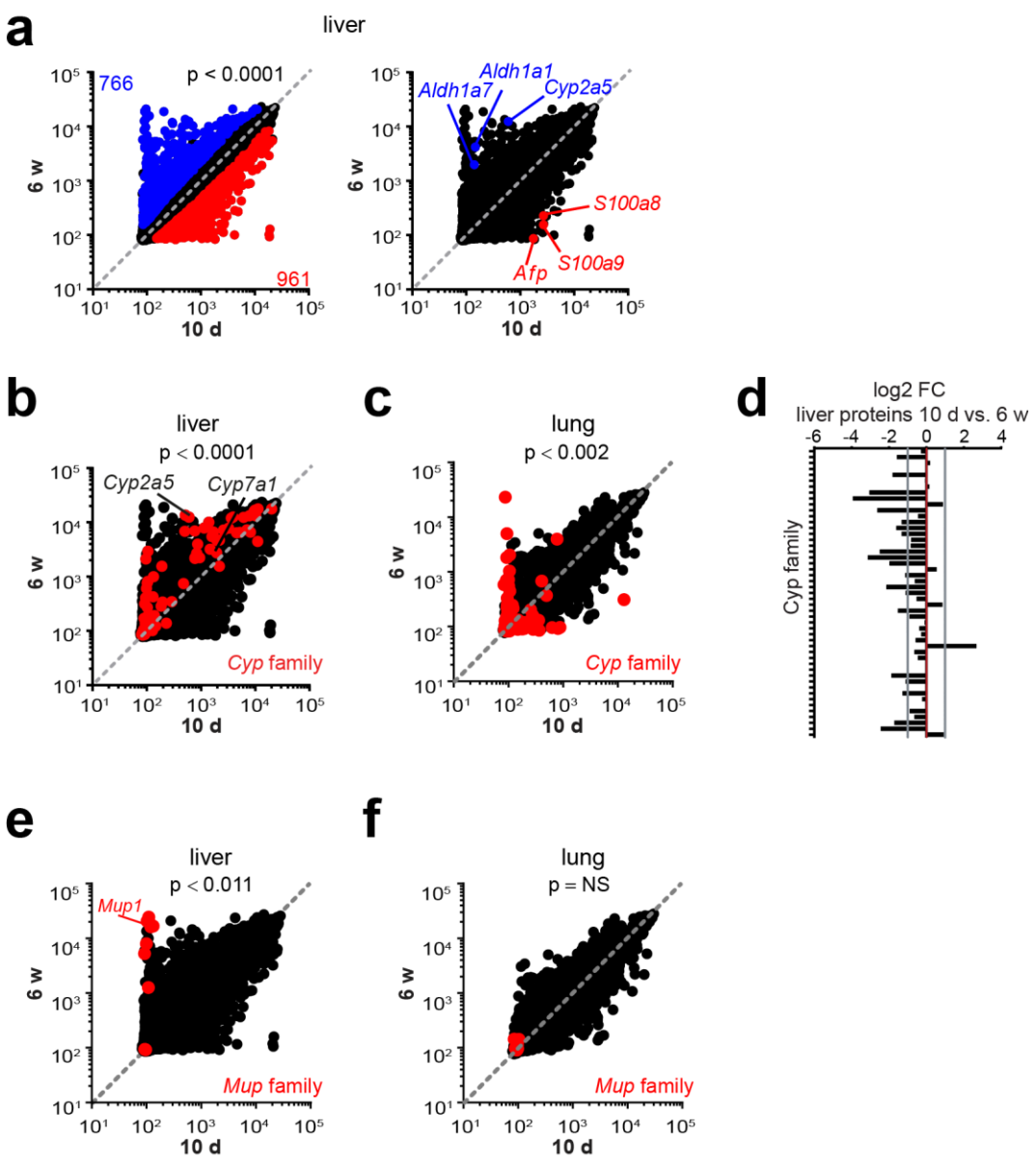

Figure 19: The neonatal liver. (**a**) Hepatic RNA-based microarray analysis: significantly >2-fold differentially expressed genes are highlighted in 6 week-old (6 w) mice (right panel, blue) and 10 day-old (10 d) mice (right panel, red) with indicated genes (left panel). (**b**) Hepatic RNA-based microarray analysis of 10 d and 6 w mice with highlighted gene expression of the Cyp family. (**c**) Lung RNA-based microarray analysis of 10 d and 6 w mice with highlighted gene expression of the Cyp family. (**d**) Quantitative mass spectrometry analysis of Cyp protein expression in 10 d mice compared to 6 w mice presented in log2 ratios. (**e** - **f**) RNA-based microarray analysis of (**e**) liver and (**f**) lung in 10 d and 6 w mice with highlighted gene expression of the Mup family. *P* values represent comparisons between 10 d versus 6 w mice using the Goemans Global Test (**a**) and the Chi-squared test (**b**, **d**, **e**, **f**), NS = not significant.

Analysis using the Gene Ontology (GO) platform revealed that many of the two-fold up-regulated genes in the liver of 10 day-old mice were involved in processes of cell cycle and cell division regulation (Fig. 20a). We therefore tested the proliferative activity of primary hepatocytes from neonatal livers. Staining with Hoechst 33342 and quantitative real-time PCR for the proliferation marker *Mki67* revealed increased proliferation by primary hepatocytes in the neonatal mice compared to the adult mice (Fig. 20b, c).

In summary, we detected a proliferating and expanding liver environment in addition to the functional immaturity of the neonatal liver, the elevated inflammatory liver microenvironment and the high number of proliferating T_{reg} cells.

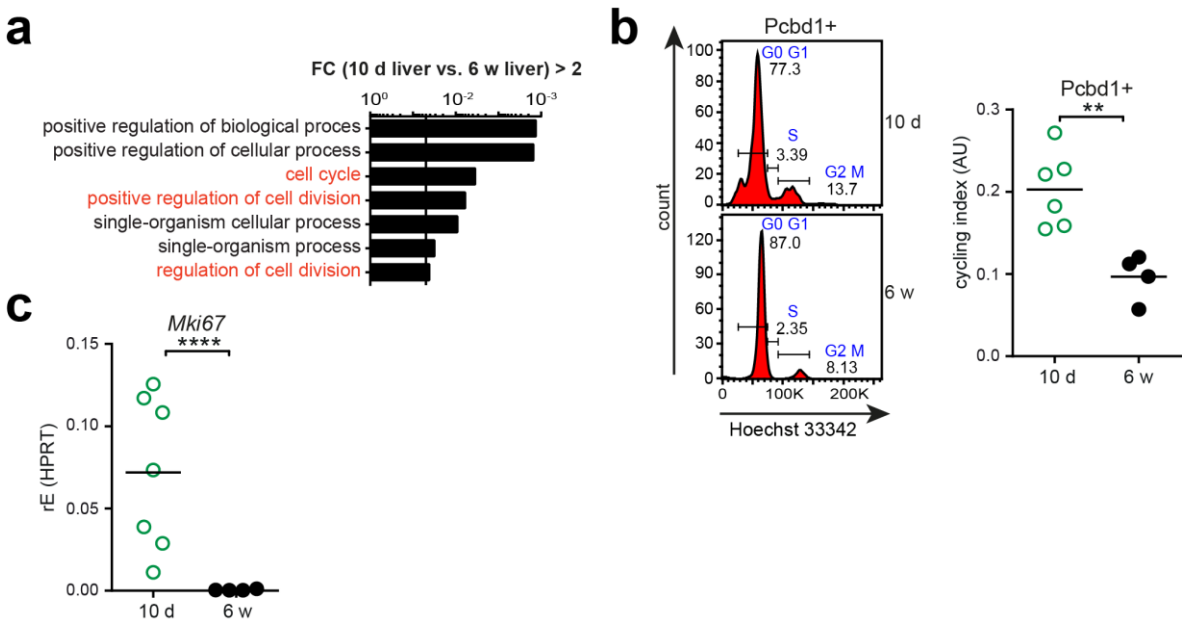

Figure 20: Proliferative activity in neonatal primary hepatocytes. (**a**) Gene ontology (GO) analysis of the > 2-fold significantly up-regulated genes in neonatal livers, detected by RNA-based microarray analysis of 10 d versus 6 w livers and represented with their *P* values per process. (**b**) Proliferative activity of Pcbd1⁺ primary hepatocytes measured by flow cytometry staining with Hoechst 33342-A. Representative histograms of Pcbd1⁺ hepatocytes showing percent cells in the G1-G0 (left), S (middle) and G2-M (right) phases of the cell cycle (left panel) from about 10 day-old (10 d) and 6 week-old (6 w) Foxp3eGFP mice (left panel); quantification of cell-cycle indices calculated as ((S + G2-M) / G1-G0) and presented in arbitrary units (AU) (right panel). (**c**) Quantitative real-time PCR analysis of *Mki67* in primary hepatocytes. Symbols represent individual animals and *P* values represent comparisons between 10 d versus 6 w mice using PANTHER over-representation test (**a**) and unpaired *t* test with Welch-correction (**b**) calculated with log2 values (**c**). $^{**}P < 0.005$ and $^{****}P < 0.00005$.

7.3 T_{reg} cells in the neonatal liver protect liver homeostasis and metabolic liver function

To analyze the function of T_{reg} cells in the liver, a mouse model of Diphtheria toxin receptor (DTR)-mediated T_{reg} cell depletion was used. T_{reg} cells were depleted by injecting Diphtheria toxin (DT) in Foxp3-DTReGFP mice expressing the *DTR* as well as *GFP* under control elements of the *Foxp3* promoter (Kim, Rasmussen, and Rudensky 2007). Flow cytometry analysis revealed that around 95% of Foxp3GFP$^+$ T_{reg} cells were depleted in the spleen and the liver 48 hours after DT injection in 10 day-old as well as 6 week-old mice (Fig. 21a).

In order to determine whether T_{reg} cell ablation resulted in liver damage we measured the concentrations of the enzymes alanine-aminotransferase (ALT/GPT) and aspartate transaminase (AST/GOT) in the blood of neonatal mice (Fig. 21b). Whereas T_{reg} cell depletion led to no differences in the AST presence in the blood, we detected a slight increase in the ALT concentration in the blood of DT-treated 10 day-old mice. Additionally, T_{reg} cell depletion in neonatal as well as adult mice resulted in a significant increase of cytokine and chemokine expression levels assessed by quantitative real-time PCR as well as microarray analysis (Fig. 21c, d). Analysis of DT-injected DTR negative control mice alongside the Foxp3-DTReGFP animals showed no elevated gene expression levels, indicating that DT injection itself had no effect on the hepatic gene expression (Fig. 21c).

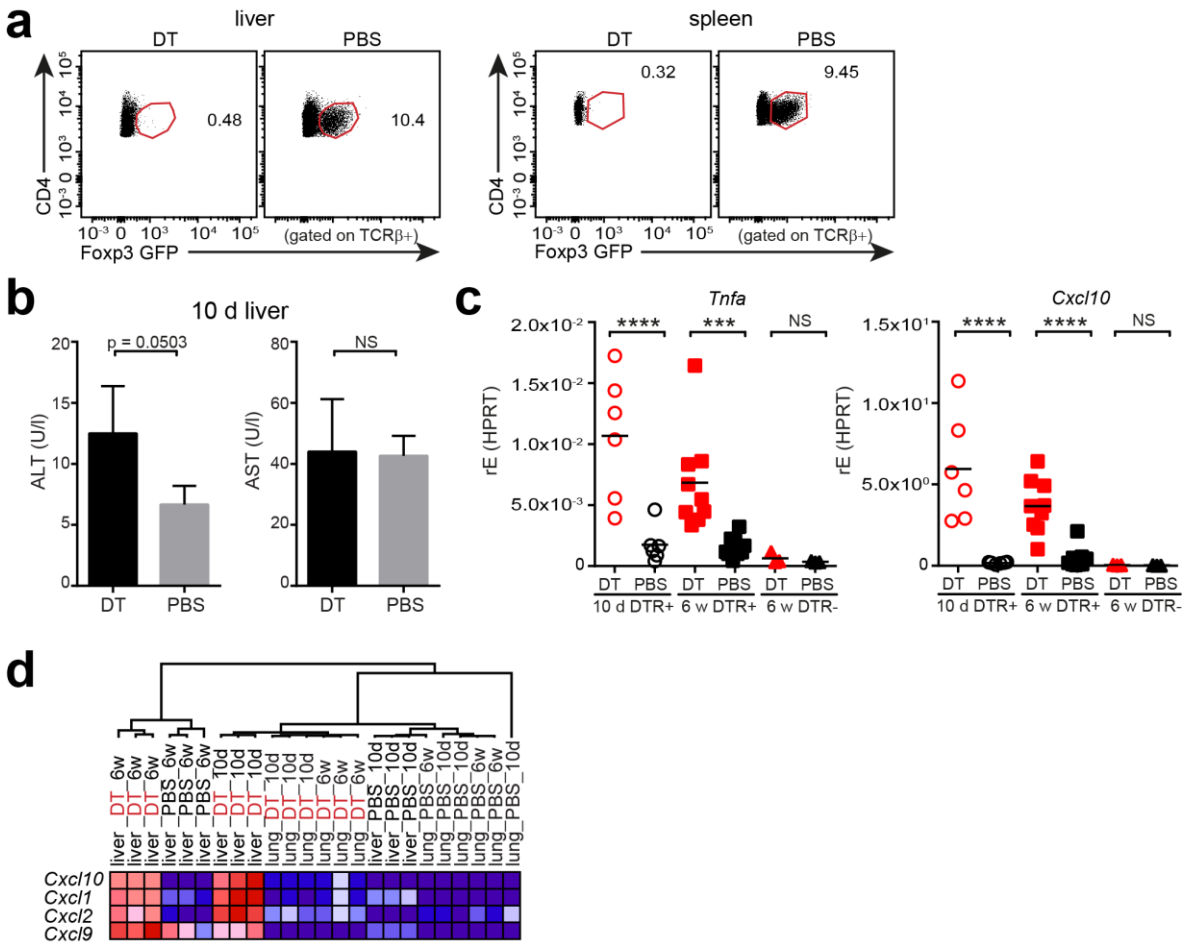

Figure 21: T_{reg} cell depletion in neonatal and adult livers. T_{reg} cells were depleted by injecting Diphtheria Toxin (DT) into 10 day-old (10 d) and 6 week-old Foxp3-DTReGFP mice (DTR+) or C57BL/6 mice (DTR-) and analyzed after 48 h. PBS injected mice served as control mice. (**a**) T_{reg} cell depletion efficiency measured via flow cytometry by the presence of Foxp3$^+$ T_{reg} cells in the liver and spleen of DT-treated mice. (**b**) Photometric analysis of alanine-aminotransferase (ALT/GPT) and aspartate transaminase (AST/GOT) in blood plasma of 10 d mice. (**c**) Quantitative real-time PCR analysis of *Tnfa* and *Cxcl10* in livers of DT or PBS treated mice. (**d**) Heat map of chemokine expression assessed by RNA-based microarray analysis in liver and lung from 10 d and 6 w DT or PBS treated mice. Genes with greatest (red) or least (blue) transcript abundance in each group, presented as Pearson's correlation (row normalized; n = 3). *P* values represent comparisons between DT and PBS treated livers of 10 d or 6 w mice using unpaired *t* test with Welch-correction (**b**) and ordinary two-way ANOVA with Sidak´s multiple comparison test calculated with log2 values (**c**). NS, not significant; ***$P < 0.0005$ and ****$P < 0.00005$.

With the help of RNA-based microarray analysis we measured the effect of T_{reg} cell depletion on hepatic gene expression. More than 5000 gene probes were differentially expressed in the neonatal liver in comparison to the significantly altered 80 gene probes in the liver of 6 week-old mice (Fig. 22a). Interestingly, the loss of T_{reg}-mediated control had little effect on the gene expression in the lung of the same mice (Fig. 21d; Fig. 22b). In comparison to the liver, no differences in cytokine and chemokine gene expression were detected in the lung after loss of T_{reg}-mediated control (Fig, 21d) and significantly less genes were differentially expressed in the T_{reg}-depleted lung (Fig. 22b). These findings suggest that T_{reg} cells have a critical role in the liver.

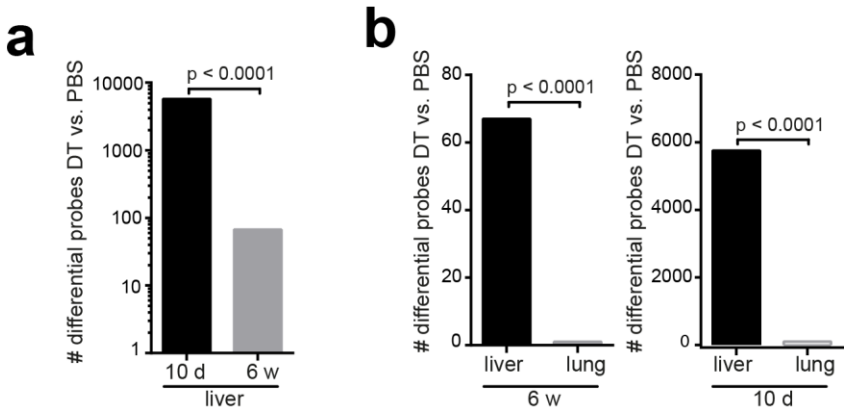

Figure 22: Gene expression in neonatal livers was strongly affected after T_{reg} cell depletion. T_{reg} cells were depleted by injecting Diphtheria Toxin (DT) into 10 day-old (10 d) and 6 week-old Foxp3-DTReGFP mice. PBS injected mice served as control mice. The livers of theses mice were analyzed after 48 h. (**a**) Differentially expressed hepatic gene probes of DT versus PBS treated 10 d or 6 w mice. (**b**) Differentially expressed gene probes of DT versus PBS treated mice in liver and lung of 6 w or 10 d mice. *P* values represent comparisons between DT and PBS treated livers or lungs of 10 d or 6 w mice using Chi2-test for proportions.

Among the 5000 differentially expressed genes in the neonatal T_{reg}-depleted liver, we observed a significantly increased expression of transcriptions factors (Fig. 23a, b). Interestingly, the increased gene expression of transcription factors (Fig. 23a, b) as well as chemokines (Fig. 21d) in the T_{reg}-depleted liver was more specific for the neonatal state than for the adult state.

Therefore, we suggest that the effect of removing T_{reg}-mediated control is more pronounced in the 10 day-old liver as compared to the adult liver.

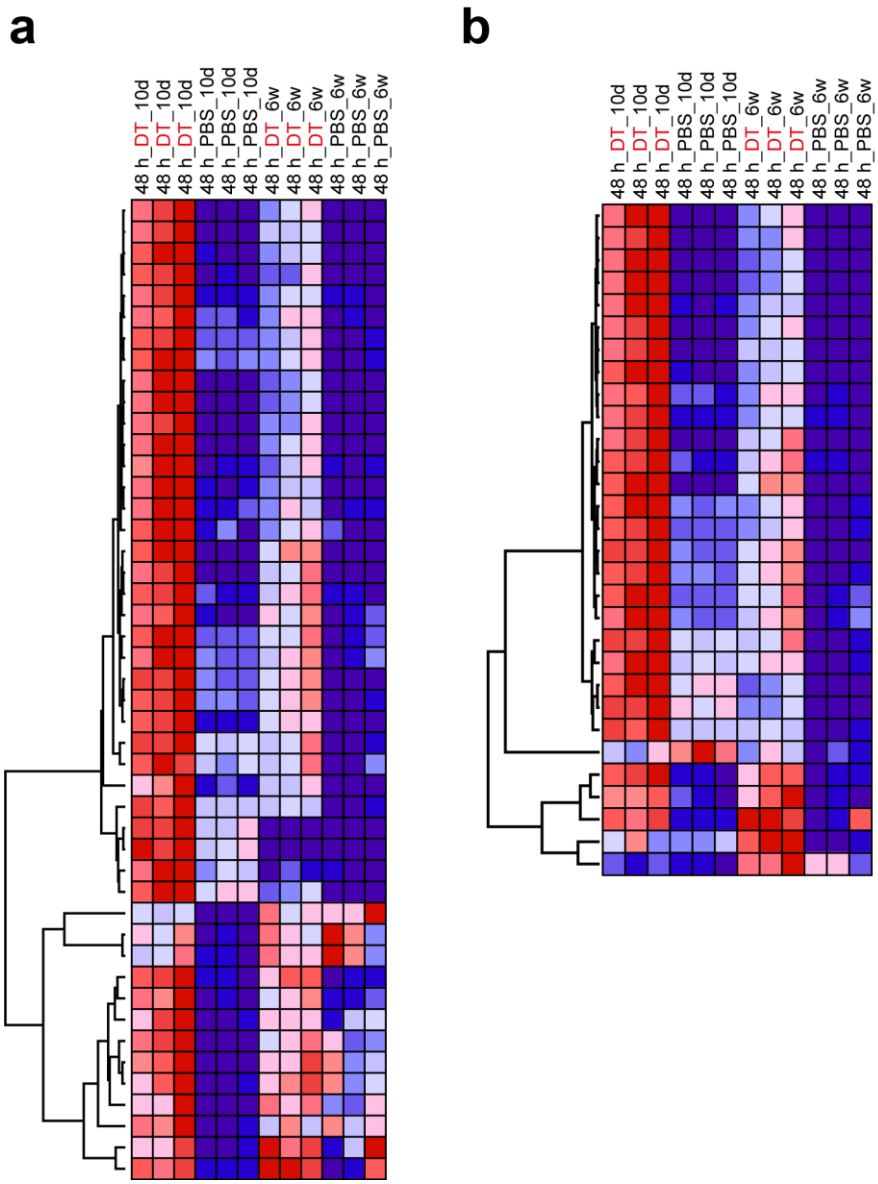

Figure 23: Expression of transcriptions factors in the livers of T_{reg}-depleted mice. T_{reg} cells were depleted by injecting Diphtheria Toxin (DT) into 10 day-old (10 d) and 6 week-old (6 w) Foxp3-DTReGFP mice. PBS injected mice served as control mice. The livers of these mice were analyzed after 48 h. Heat maps of transcriptions factor gene expression: genes with greatest (red) or least (blue) transcript abundance in each group, presented as Pearson's correlation (row normalized; n = 3) and assessed by RNA-based microarray analysis. (**a**) Significantly 2-fold up-regulated gene expression in T_{reg}-depleted livers of 10 d mice in comparison to livers of 10 d control mice. (**b**) Significantly 2-fold up-regulated gene expression in T_{reg}-depleted livers of 6 w mice in comparison to livers of 6 w control mice.

To determine whether we could detect the same changes on protein level, we performed an unbiased quantitative proteome analysis of DT-injected and PBS-injected neonatal and adult livers. In total we identified 4440 proteins in all groups. Through the direct comparison of significantly down-regulated proteins with their mRNA expression, we showed that in most cases protein followed mRNA expression (Fig. 24a).

Since microarray array analysis demonstrated elevated hepatic gene expression in T_{reg}-depleted neonatal mice, including cytokines, chemokines and several transcription factors (Fig. 21-23), we were interested in the protein and gene expression that were down-regulated after loss of T_{reg} cells in the neonatal liver. Using the Gene Ontology (GO) platform, we detected that most under-represented hepatic proteins as well as genes at the neonatal stage were involved in metabolic processes such as organic acid or fatty acid metabolism (Fig. 24b, c).

Two pathways were of particular interest. First, genes encoding proteins involved in the alpha amino acid metabolic pathway such as the enzymes cysteine sulfinic acid decarboxylase (Csad), the D-aspartate oxidase (Ddo) or arylformamidase (Afmid) were significantly down-regulated in the liver of 10 day-old mice without T_{reg}-mediated control (Fig. 24d). The same pattern could be observed in a second group of genes interacting in the acyl-CoA metabolism, such as acetyl-coenzyme A synthetase (*Acss2*), different members of acyl-CoA thioesterase (*Acot 3, 12, 14*) and acyl-CoA dehydrogenase (*Acadsb*) (Fig. 24e).

Taken together, these results suggest that the presence of T_{reg} cells in the liver at the neonatal stage is necessary to establish liver homeostasis and proper metabolic liver function since T_{reg} cell ablation in neonatal mice resulted in altered expression of genes involved in metabolic processes in the liver.

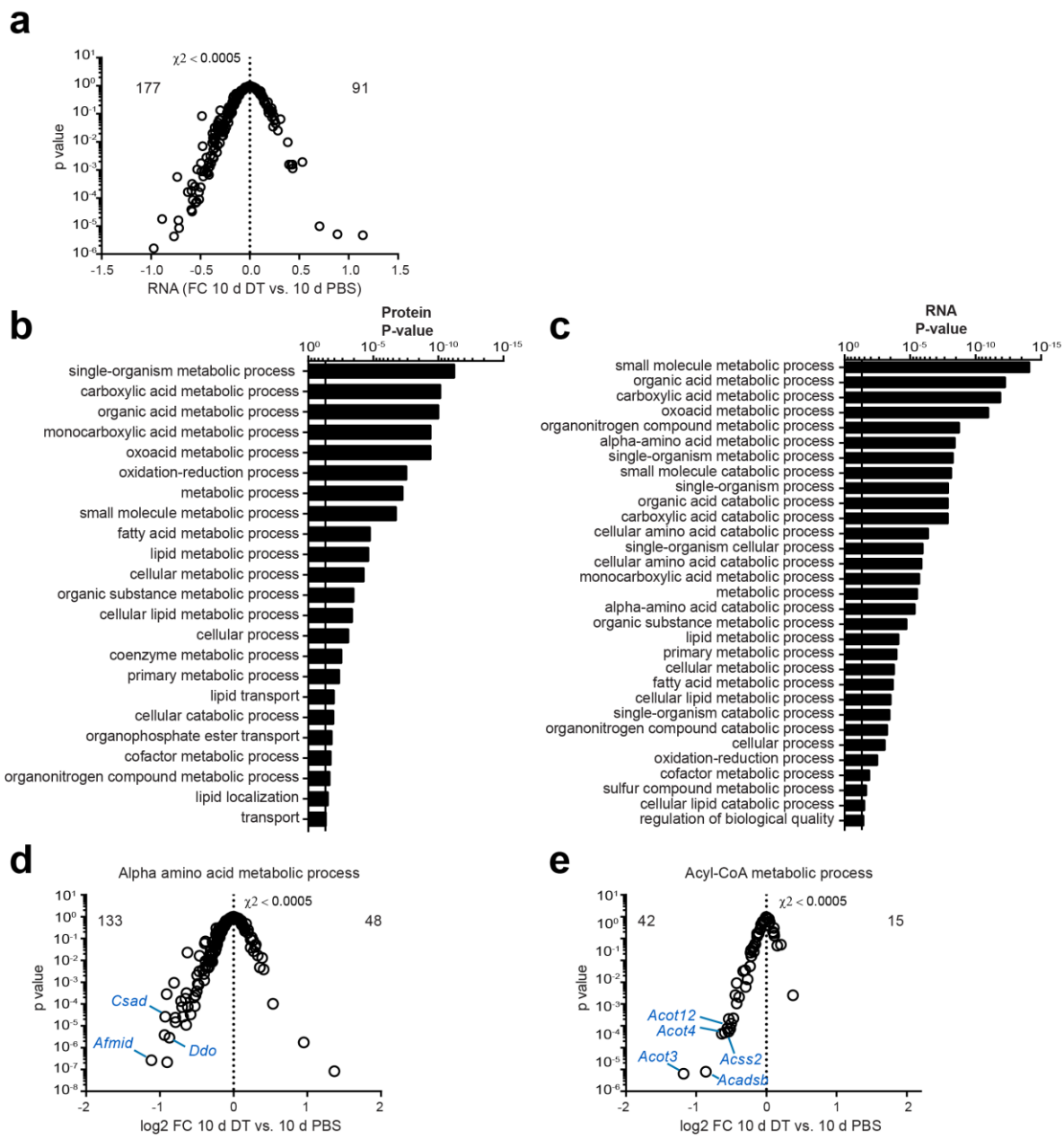

Figure 24: T_{reg} cell depletion in neonatal livers induced changes in expression of genes involved in metabolic liver function. T_{reg} cells were depleted by injecting Diphtheria Toxin (DT) into 10 day-old (10 d) and 6 week-old Foxp3-DTReGFP mice. The livers of the mice were analyzed after 48 h with microarray analysis and quantitative proteomics. PBS injected mice served as control mice. (**a**) Fold-change by *P* value plot of hepatic 268 gene probes identified to be significantly down-regulated on protein level after T_{reg} cell depletion in 10 d mice. (**b** - **c**) Gene ontology (GO) analysis of (**b**) proteins and (**c**) genes significantly down-regulated in livers from DT versus PBS treated 10 d mice. (**d** - **e**) Fold-change by *P* value plot of hepatic genes with (**d**) the GO 1901605 coding for the alpha amino acid metabolic process or (**e**) GO 0006637 coding for the acyl-CoA metabolic process in DT versus PBS treated 10 d mice. Individual genes are highlighted. *P* values represent comparisons between DT and PBS treated 10 d mice using ordinary two-way Chi2-test for proportions (**a**, **d, e**) or PANTHER over-representation test (**b**, **c**).

7.4 T_{reg} cells influence the circadian rhythm

T_{reg} cell depletion affected core-clock gene expression in the liver

As described in the previous section, loss of T_{reg}-mediated immune control by depletion of T_{reg} cells induced strong alterations in the gene as well as protein expression levels in the liver (Fig. 21-24). A fold-change to fold-change comparison showed up-regulation of transcription factors involved in regulation of the circadian rhythm in both T_{reg}-depleted livers of neonatal as well as adult mice (Fig. 25a). For example, the negative feedback regulators of the clock *Rev-Erb-*α, *Rev-Erb-*β, *Per1, Per2*, *Bhlhb2* and the circadian associated repressor of transcription (*Ciart)*, as well as the clock-controlled gene *Dbp* (albumin D-box binding protein) and *Jun B proto-oncogene* (*Junb*) were highly up-regulated at both ages (Fig. 25a, b and c). Quantitative real-time PCR analysis confirmed our microarray results (Fig. 25a, d). As seen before for the gene expression of cytokines and chemokines (Fig. 21c), analysis of DT-injected DTR negative control mice alongside the Foxp3-DTReGFP mice demonstrated that DT injection itself had no effect on the elevated hepatic expression of core-clock genes and clock-controlled genes (Fig. 25d). The liver seemed to be in a stressed state due to the elevated expression levels of cytokines and chemokines (Fig. 21) and genes involved in the complex process of the cellular stress response such as the *activating transcription factor 3* (*Atf3*) (Fig. 25b, c, d). Interestingly, the lung, another peripheral organ for which gene expression is known to be partly regulated by the circadian clock, did not show these differences in neonatal or adult mice (Fig. 25b, c).

Taken together, our findings demonstrate that the loss of T_{reg}-mediated immune control lead to an age-independent up-regulation of genes involved in regulation of the hepatic circadian clock.

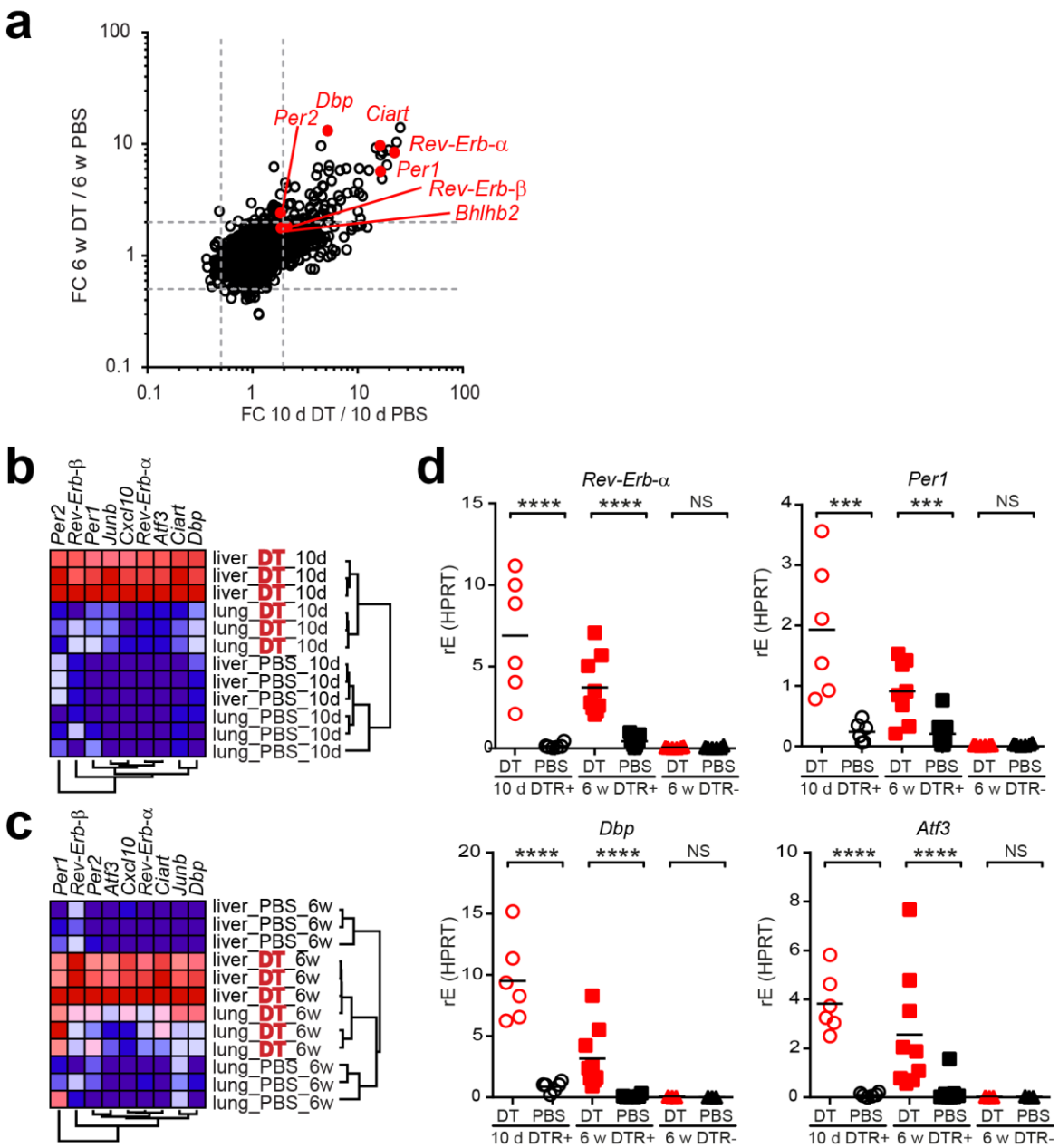

Figure 25: Loss of T_{reg}-mediated control induced elevated levels of core-clock gene expression in the liver. T_{reg} cells were depleted by injecting Diphtheria Toxin (DT) into 10 day-old (10 d) and 6 week-old (6 w) Foxp3-DTReGFP mice. PBS injected mice served as control mice. The liver and lung of these mice were analyzed after 48 h. (**a**) Fold-change by fold-change plot of hepatic gene expression of DT versus PBS treated 10 d and 6 w mice. (**b** - **c**) Heat maps of hepatic gene expression in livers and lungs from DT and PBS treated 10 d and 6 w mice. Genes with greatest (red) or least (blue) transcript abundance in each group, presented as Pearson's correlation, row normalized (n=3). (**d**) Quantitative real-time PCR analysis of *Atf3,* the core-clock genes *Rev-Erb-α* and *Per1* and the clock-controlled gene *Dbp* in livers of DT and PBS treated Foxp3-DTReGFP mice (DTR+) and C57BL/6 mice (DTR-) of both age groups. Symbols represent individual animals and *P* values represent comparisons between DT versus PBS treated 10 d or 6 w mice using ordinary two-way ANOVA with Sidak´s multiple comparison test calculated with log2 values (**d**). NS, not significant; ***$P < 0.0005$ and ****$P < 0.00005$.

Modified hepatic circadian rhythm in T_{reg}-depleted livers

Circadian rhythms are known to occur with a repeating period close to 24 hours (Scheiermann, Kunisaki, and Frenette 2013). As described in the previous section we observed elevated gene expression levels of circadian core-clock genes and clock-controlled genes in the liver 48 hours after the loss of T_{reg}-mediated control. To analyze the changes in the hepatic circadian rhythm before and after the 48 hour time point, we depleted T_{reg} cells in 6 week-old mice over a period of 54 hours and harvested the organs every 6 hours to cover different night and day periods. During this depletion kinetic we detected a constant over-expression of chemokines initially found to be differentially expressed at the 48 hour time point after T_{reg} cell depletion (Fig 21d). Chemokines such as *Cxcl10* were reproducibly up-regulated at every time point of the kinetic measured by RNA-based microarray analysis (Fig. 26a). The changes in T_{reg}-depleted livers occurred extremely rapidly, as we detected an elevated chemokine expression level already after 24 hour DT treatment in the liver (Fig. 26a). With the help of RNA-based microarray analysis we were able to measure oscillation patterns of core-clock genes (Fig. 26b) and clock-controlled genes (Fig. 26c). The expression of the negative feedback regulators of the clock *Rev-Erb-α*, *Rev-Erb-β*, *Per1*, *Per2*, *Ciart* and *Bhlhb2* as well as the clock-controlled genes *Dbp* and *Foxo3* (*insulin-phosphatidylinositol 3-kinase-Forkhead box class O3a*) were all significantly altered in T_{reg}-depleted livers and showed a complete loss of rhythmicity or a change of the oscillation phase (Fig. 26b, c). The core-clock genes *Clock* and *Bmal1* showed slight changes in T_{reg}-depleted livers, but overall the oscillation pattern of *Clock* and *Bmal1* were less affected as compared to the negative feedback regulators of the hepatic clock and the clock-controlled genes, whose circadian rhythms were partly or completely abrogated (Fig. 26b, c). To understand the impact of the changes in the hepatic clock, we statistically analyzed the oscillation patterns of genes with a circadian and non-circadian expression in T_{reg}-deficient and T_{reg}-sufficient livers. Therefore we used the established JTK_CYCLE algorithm (Hughes, Hogenesch, and Kornacker 2010) with false discovery rates (FDR) of 5% or 20% (Fig. 26d). We detected that about 25 to 30% of the genes with a circadian expression showed an altered oscillation pattern when T_{reg}-mediated control was absent in the liver, whereas the expression pattern of genes without circadian regulation were less affected (around 10%) by T_{reg} cell depletion (Fig. 26d).

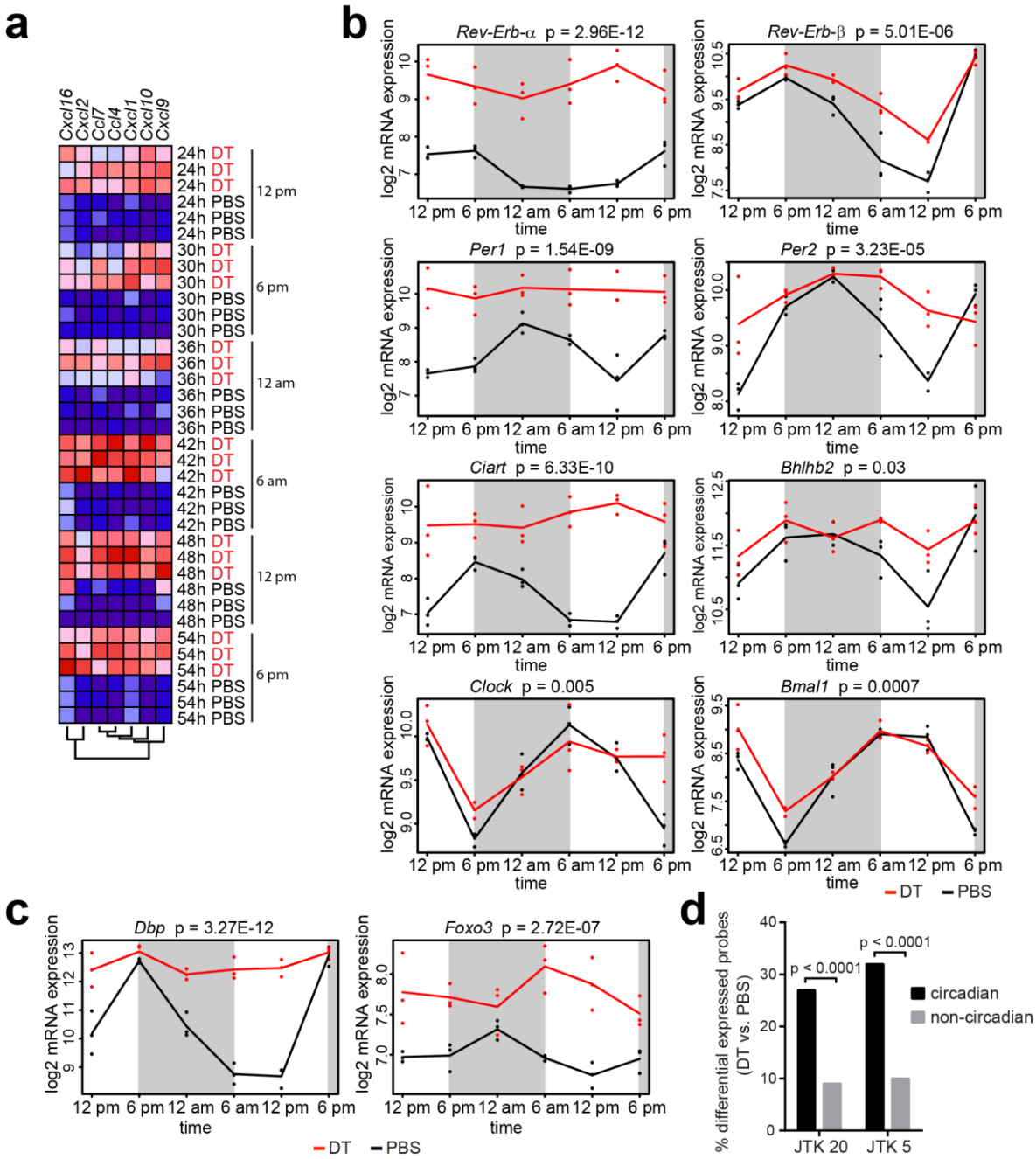

Figure 26: Disturbed circadian gene expression in T_{reg}-depleted livers. T_{reg} cells were depleted by injecting Diphtheria Toxin (DT) in 6 week-old Foxp3-DTReGFP mice. PBS injected mice served as control mice. Livers were harvested 24 h (12 pm), 30 h (6 pm), 36 h (12 am), 42 h (6 am), 48 h (12 pm) and 54 h (6 pm) after the first DT injection and the hepatic gene expression were assessed by RNA-based microarray analysis. (**a**) Heat map of chemokine expression. Genes with greatest (red) or least (blue) transcript abundance in each group, presented as Pearson's correlation, row normalized (n=3 per group and time point). (**b** - **c**) Circadian expression kinetic of (**b**) core-clock genes and (**c**) clock-controlled genes in T_{reg}-depleted liver (DT, red) or control livers (PBS, black). Night phase is marked in grey. (**d**) Circadian probes were identified using the JTK_CYCLE algorithm with false discovery rates (FDR) of 5% and 20%. Genes with circadian or non-circadian expression were tested whether DT treatment significantly changed their gene expression pattern.

Furthermore, gene expression appears to follow different oscillation patterns in T_{reg}-depleted livers, whereby two clusters are particularly interesting. Genes with altered oscillation patterns seemed to follow the changed circadian expression pattern of the negative feedback regulators of the circadian clock *Per1* or *Rev-Erb-α* in T_{reg}-depleted livers. Interestingly, these clusters of genes included other negative feedback regulators of the hepatic clock as well as other genes regulated by the circadian clock (Fig. 27 a, b; Appendix Table 12, 13).

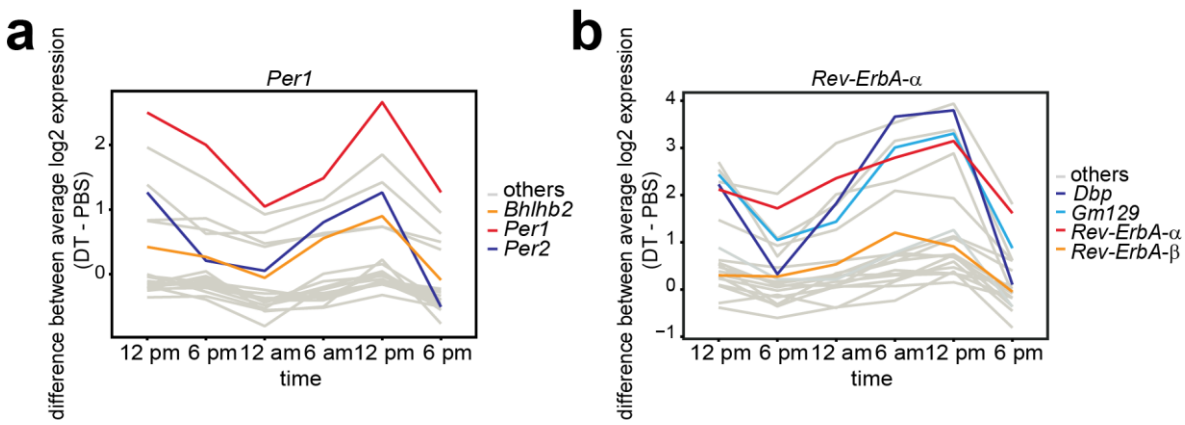

Figure 27: Different patterns of altered circadian gene expression in T_{reg}-depleted livers. T_{reg} cells were depleted by injecting Diphtheria Toxin (DT) in 6 week-old Foxp3-DTReGFP mice. PBS treated mice served as control mice. Livers were harvested 24 h (12 pm), 30 h (6 pm), 36 h (12 am), 42 h (6 am), 48 h (12 pm) and 54 h (6 pm) after first DT injection and hepatic gene expression were assessed by RNA-based microarray analysis. Gene probes showing similar DT versus PBS regulation patterns over time as (**a**) *Per1* and (**b**) *Rev-Erb-α,* which were assessed by Pearson's correlation coefficient.

In a second statistical approach, the established RAIN algorithm (Thaben and Westermark 2014) with a FDR of 1% was used to identify and verify genes with a circadian expression. In accordance with the JTK_CYCLE algorithm analysis, oscillating genes identified by the RAIN algorithm were significantly more affected by the loss of T_{reg} cells in the liver as compared to non-circadian genes (Fig. 28a). For example, the clock-controlled gene *Junb* completely lost its circadian expression pattern after DT treatment (Fig. 28b). Studies in rodents have shown that Junb expression in the SCN is induced by light and correlates with the light-mediated phase shifts in circadian rhythm of the SCN (Beaule and Amir 1999). With the help of JTK_CYCLE and RAIN algorithm we detected in total more than 400 oscillating genes showing an altered circadian expression pattern in T_{reg}-depleted livers, with an overlap of 297 genes between the two approaches (Fig. 28c).

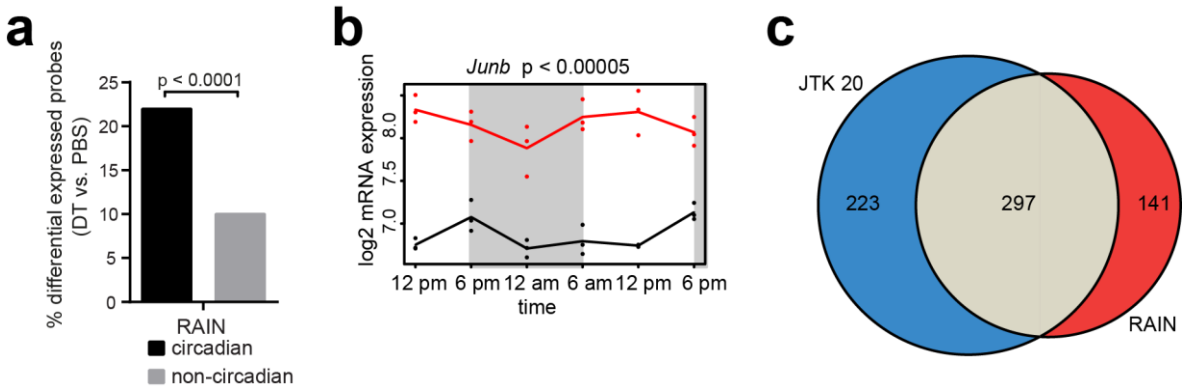

Figure 28: RAIN algorithm identified altered circadian gene expression in T_{reg}-depleted livers. T_{reg} cells were depleted by injecting Diphtheria Toxin (DT) in 6 week-old Foxp3-DTReGFP mice. PBS treated mice served as control mice. Livers were harvested 24 h (12 pm), 30 h (6 pm), 36 h (12 am), 42 h (6 am), 48 h (12 pm) and 54 h (6 pm) after first DT injection and hepatic gene expression were assessed by RNA-based microarray analysis. (**a**) Circadian probes were identified using RAIN algorithm with a FDR of 1%. Genes with circadian and non-circadian expression were tested whether DT significantly changed their gene expression pattern. (**b**) Circadian expression kinetic of the clock-controlled gene *Junb* in T_{reg}-depleted (DT, red) or control (PBS, black) livers. Dots represent individual animals. (**c**) Genes with altered circadian expression calculated with JTK_CYCLE algorithm or RAIN algorithm. Numbers indicate probes identified with the respective algorithm.

In the previous section we described that T_{reg} cell depletion resulted in down-regulation of genes involved in metabolic pathways (Fig. 24b and c). Moreover, it is known that several metabolic pathways in the liver are under control of the hepatic clock (Ferrell and Chiang 2015). To determine the relationship between the altered expression of oscillating genes in livers without T_{reg} cells and liver metabolism, we analyzed the 297 oscillating genes that show an altered oscillation pattern in T_{reg}-depleted livers identified by the RAIN- and the JTK_CYCLE algorithms using the Gene Ontology (GO) platform. Besides the expected processes of `circadian rhythm´ and `circadian regulation of gene expression´, the GO analysis revealed additional involvement of the oscillating genes in certain metabolic processes in the liver (Fig. 29a). Genes involved in the acyl-CoA metabolism or alpha amino acid metabolism showed a down-regulated circadian expression pattern in T_{reg}-depleted livers, such as the *acyl-CoA thioesterase* 12 (*Acot12)* or the *arylformamidase Afmid* (Fig. 29b, c). Interestingly, *Afmid* was completely disrupted after loss of T_{reg}-mediated control (Fig. 29c).

Collectively, our data indicates that T_{reg} cells are needed to ensure normal circadian expression of core-clock regulators and clock-controlled genes, as well as to guarantee normal regulation of metabolic processes in the liver.

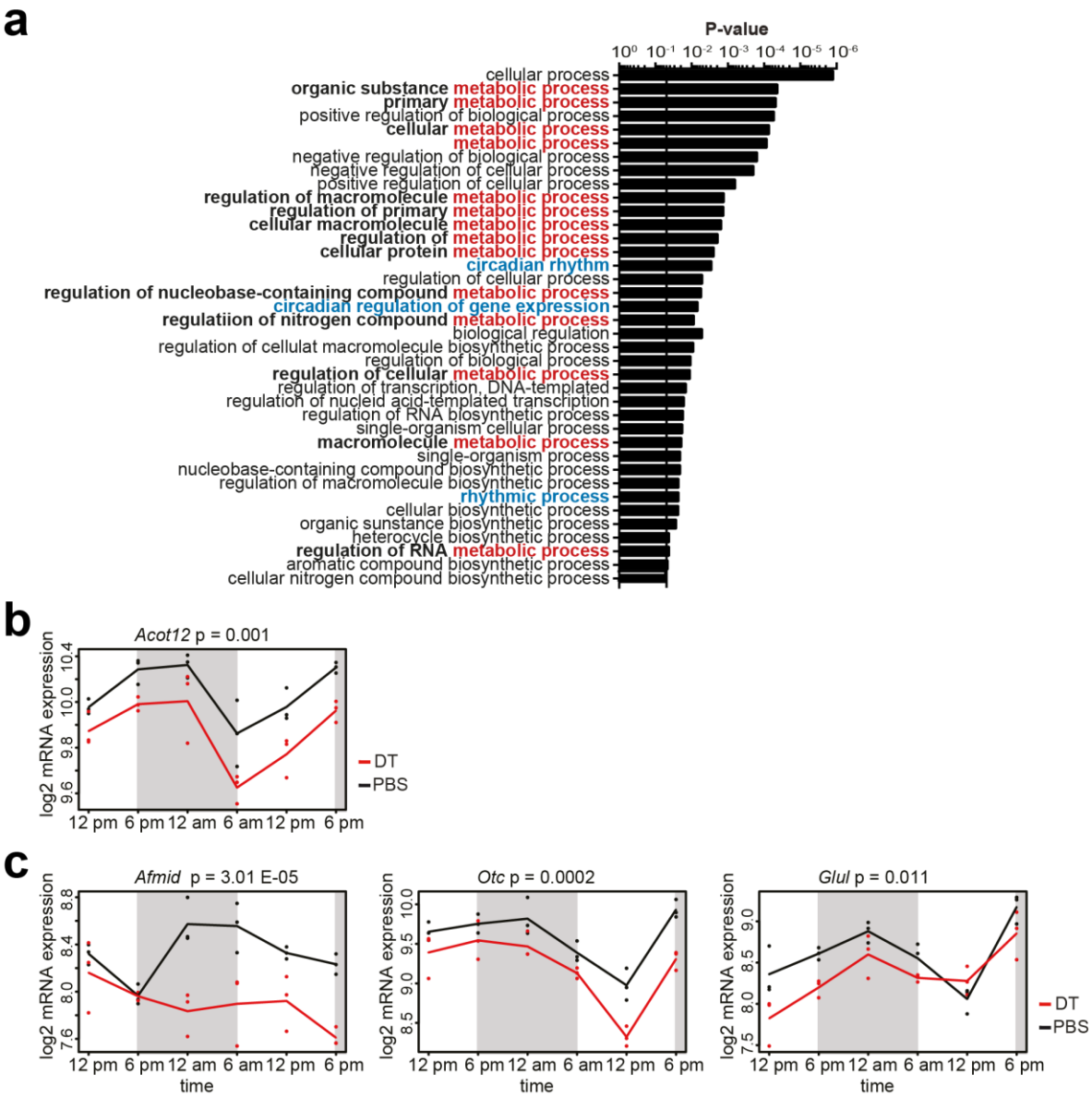

Figure 29: T_{reg} cell depletion induced altered expression of circadian genes involved in metabolic processes. (a) Gene ontology (GO) analysis of the 297 RAIN- and JTK_CYCLE-identified genes with alteration in their circadian gene expression after T_{reg} cell depletion with Diphtheria Toxin in the liver of 6 week-old Foxp3-DTReGFP. PBS treated mice served as control mice. Livers were harvested 24 h (12 pm), 30 h (6 pm), 36 h (12 am), 42 h (6 am), 48 h (12 pm) and 54 h (6 pm) after first DT injection and hepatic gene expression were assessed by RNA-based microarray analysis. (**b** - **c**) Circadian gene expression kinetic of *acyl-CoA thioesterase* 12 (*Acot12*) involved in the acyl-CoA metabolism or genes (*arylformamidase* (*Afmid*); *ornithine transcarbamylase* (*Otc*); *glutamine synthetase* (*Glul*)) involved in the alpha amino acid metabolism in T_{reg}-depleted livers (DT, red) or control livers (PBS, black). Night phase is marked in grey.

Hepatic circadian expression in Rag2$^{-/-}$ and macrophage depleted mice

To determine the specificity of the disturbed rhythmicity and phase shift in gene expression of hepatic core-clock genes and clock-controlled genes to T_{reg} cell depletion, we analyzed the oscillation pattern of the same genes in liver of Rag2-deficient mice. The complete developmental block of mature B and T cells in Rag2-deficient mice did not cause the same changes in circadian gene expression pattern of the negative feedback regulators *Rev-Erb-α* as measured before in T_{reg}-depleted livers (Fig. 30 a, b, c). The same was found for the other negative feedback regulators *Rev-Erb-β*, *Per1* and *2*, *Ciart, Bhlhb2* and the clock-controlled genes *Dbp* and *Cxcl10* (Fig. 30 b, c).

Since the permanent deficiency for mature B and T cells in Rag2-deficient mice did not mimic the altered oscillation pattern of livers without T_{reg} cells (Fig. 30), we wanted to test another acute depletion model. DT treatment of Csfr1-DTR mice results in ablation of myeloid cells, including liver-resident Kupffer cells and monocytes, and is based on the colony stimulating factor 1 receptor (*Csf1r*)-mediated expression of the DTR, which has to be first licensed by the myeloid cell specific LysM Cre-mediated excision of a loxP flanked Stop cassette (Schreiber et al. 2013). We observed an efficient depletion of F4/80^{+} Kupffer cells and Ly6C^{high} monocytes in the liver after 48 hours DT injections (Fig. 31a). The same DT concentration as in the T_{reg} cell depletion study was used. However, depletion of hepatic Kupffer cells and monocytes did not lead to significant changes in gene expression of the clock regulators *Rev-Erb-α* and *Per1*, or clock-controlled genes *Dbp* and *Cxcl10* (Fig. 31b, c). Stress-induced expression of hepatic *Atf3* was affected by T_{reg} cell depletion but not by ablation of hepatic macrophages and monocytes (Fig. 31d). The elevated expression levels of chemokines and cytokines induced by T_{reg} cell depletion (Fig. 21d) was not observed in Csfr1-DTR mice after DT injection (Fig. 31e, f). Interestingly, in contrast to the elevated hepatic chemokine expression in T_{reg}-depleted mice, we measured a slight down-regulated expression of cytokines and chemokines such as *Il15* or *Ccl5* in DT-treated Csfr1-DTR mice (Fig. 31e, f).

Taken together, these findings suggest that the detected changes in hepatic core-clock and clock-controlled gene expression are T_{reg} cell depletion specific. Neither the elimination of macrophages, the DT itself nor the apoptotic cell death induced by DT injection in the DTR-positive cells were able to alter the circadian rhythm in the liver.

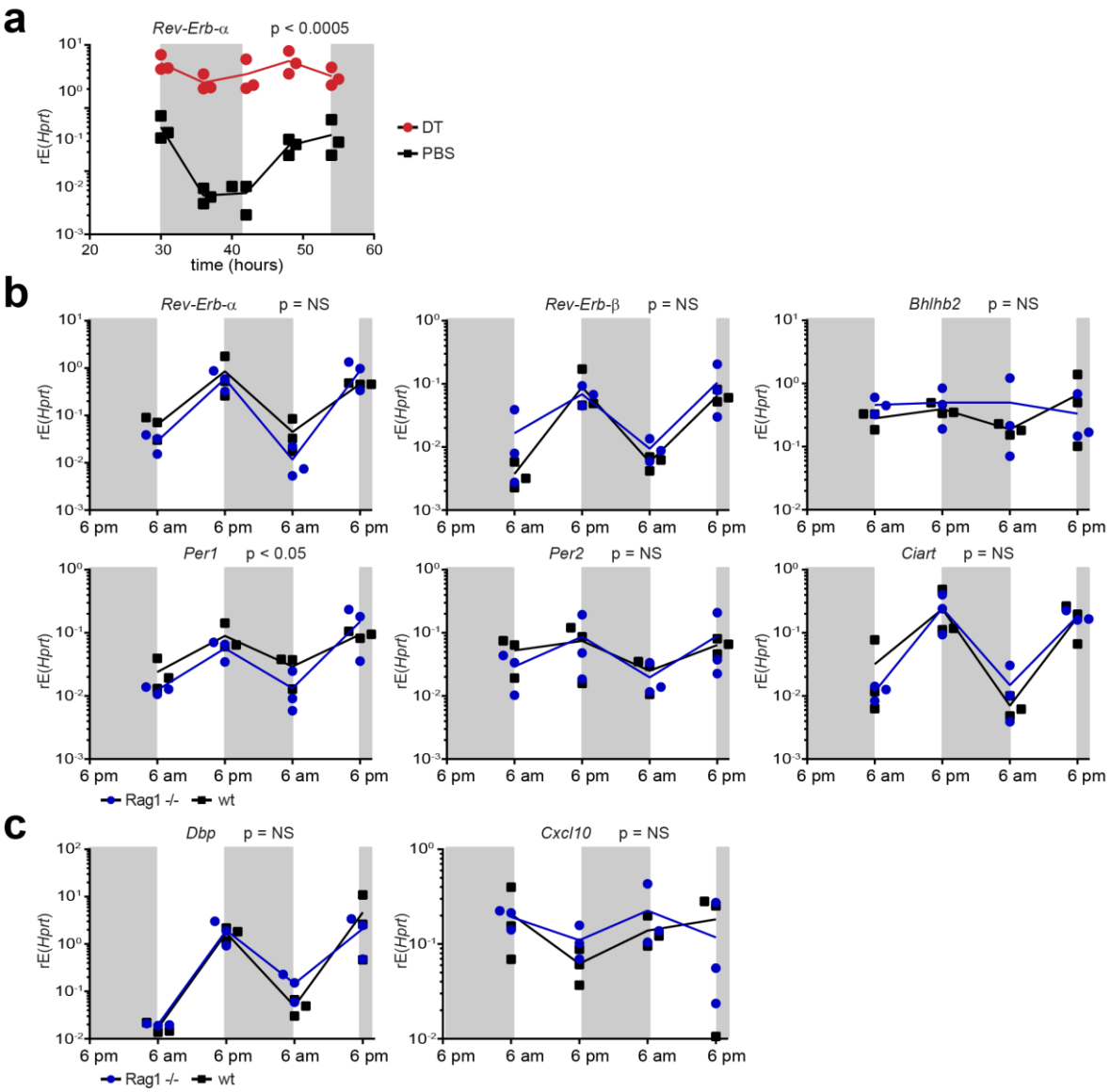

Figure 30: Development block of mature B and T cells had no influence on the hepatic circadian gene expression. Quantitative real-time PCR analysis of negative feedback regulators of the hepatic clock or clock-controlled genes. (**a**) *Rev-Erb-α* expression in livers of T_{reg}-depleted mice. (**b** - **c**) Circadian gene expression of (**b**) negative feedback regulators of the hepatic clock and (**c**) clock-controlled genes in livers of Rag2-deficient mice. Symbols represent individual animals and *P* values represent comparisons between DT versus PBS using Two-way RM ANOVA for over time analysis, NS, not significant.

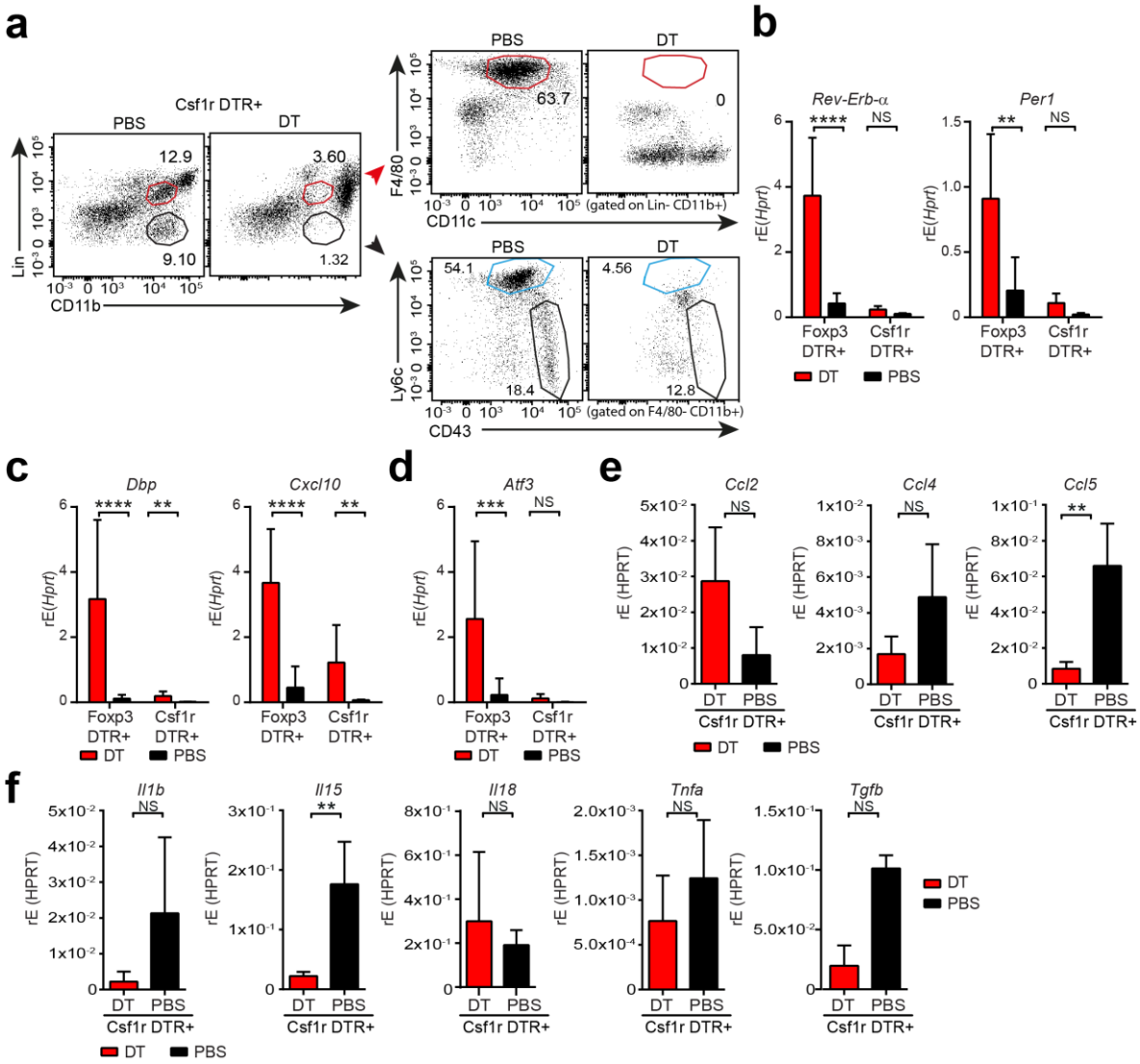

Figure 31: Loss of macrophages did not mimic T_{reg} cell depletion induced changes in circadian gene expression. Csf1r DTR mice were injected with Diphtheria Toxin (DT) to deplete macrophages and monocytes. PBS injected mice served as control mice. (**a**) Flow cytometry gating of F4/80^{+} Kupffer cells (red gate) and Ly6C^{high} monocytes (blue gate) in DT or PBS injected mice. Ly6C^{low} monocytes are gated in black. (**b - c**) Quantitative real-time PCR analysis of (**b**) core-clock genes, (**c**) controlled genes and (**d**) *Atf3* in myeloid cell-depleted livers (Csf1r DTR+) and T_{reg}-depleted livers (Foxp3 DTR+). (**e - f**) Quantitative real-time PCR analysis of (**e**) chemokines and (**f**) cytokines in Csf1r-DTR mice. *P* values represent comparisons between DT versus PBS using ordinary two-way ANOVA with Sidak´s multiple comparison test calculated with log2 values (**b** - **d**) and unpaired *t* test with Welch-correction calculated with log2 values (**e**, **f**). NS, not significant; $^{**}P < 0.005$, $^{***}P < 0.0005$ and $^{****}P < 0.00005$.

Liver inflammation and the circadian rhythm

Since previous findings showed that T_{reg} cell depletion resulted in elevated levels of hepatic chemokines and cytokines (Fig. 21), we analyzed whether inflammatory mediators could induce the loss of circadian rhythmicity. We isolated primary hepatocytes from 6 week-old livers and cultured them for 48 hours *in vitro* with different stimuli such as TNF-α, IFN-γ, IL-6, IL-10, TGF-β or the glucocorticoid dexamethasone, a hormone known to be a circadian time cue for the hepatic clock (Scheiermann, Kunisaki, and Frenette 2013). The clock regulator *Rev-Erb-α* was one of the genes whose circadian expression was strongly disturbed in the liver of T_{reg}-depleted mice (Fig. 25, Fig. 26b, Fig. 30a). However, in the culture system of primary hepatocytes neither dexamethasone nor any of the cytokines could mimic any of the changes in *Rev-Erb-α* expression pattern detected in T_{reg}-depleted livers (Fig. 32).

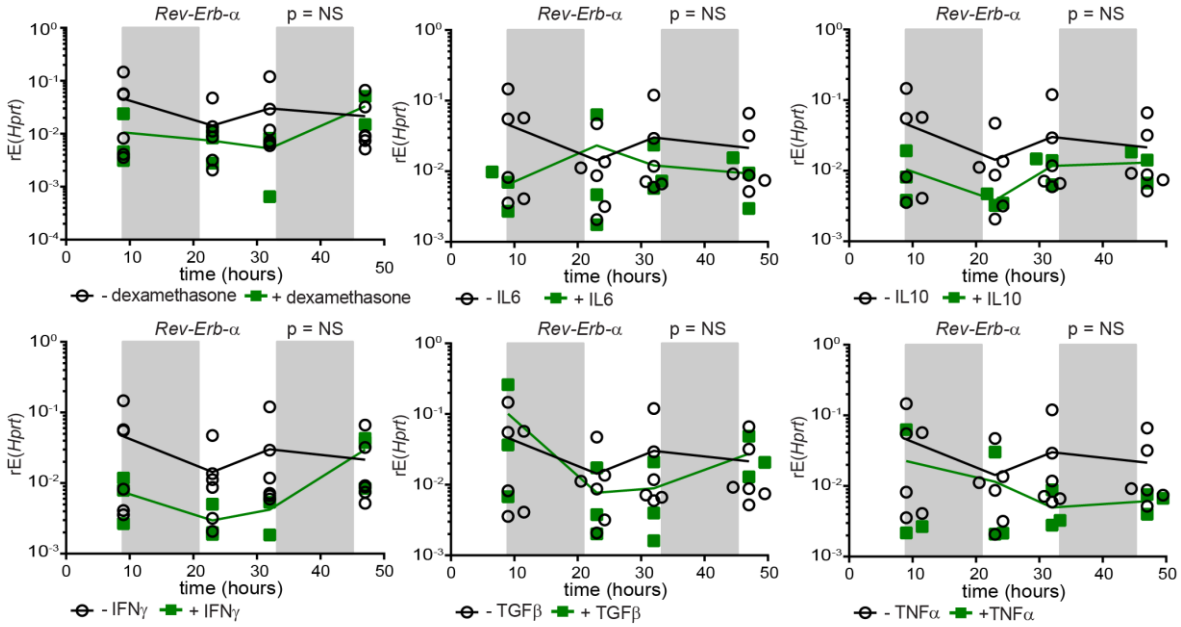

Figure 32: Cytokine or dexamethasone treatment did not result in alteration of *Rev-Erb-α* gene expression. Quantitative real-time PCR analysis of *Rev-Erb-α* expression in primary hepatocytes cultured in Williams E medium (black) and supplemented with either Dexamethasone, TNF-α, IFN-γ, TGF-β, IL-6 or IL-10 (green). Cells were harvested every 12 hours. Symbols represent individual animals and *P* values represent comparisons between different *in vitro* treatments using Two-way RM ANOVA for over time analysis, NS, not significant.

Furthermore, expression of genes showing a changed expression pattern in the liver of T_{reg}-depleted mice (Fig. 25, Fig. 26), such as *Atf3* and several core-clock and clock-controlled genes, were generally not altered in the primary hepatocytes (Fig. 33). However, we could observe changes of individual parameters. For example, IFN-γ treatment led to significantly increased expression of *Atf3* and *Cxcl10,* as well as TGF-β could efficiently induce the expression of *Bhlhb2* in primary hepatocytes (Fig. 33b, c, e). In contrast to the observed *in vivo* data, we saw that the expression of some parameters were even reduced. For example, the expression levels of *Dbp* and *Atf3* were significantly down-regulated after treatment with TGF-β (Fig. 33c, e). Additionally, treatment with TNF-α or dexamethasone led to a down-regulated gene expression of the clock-controlled gene *Dbp* (Fig. 33a, d, e).

Therefore we conclude that treatment with individual effector molecules might not accurately mirror the complex situation observed in the *in vivo* model.

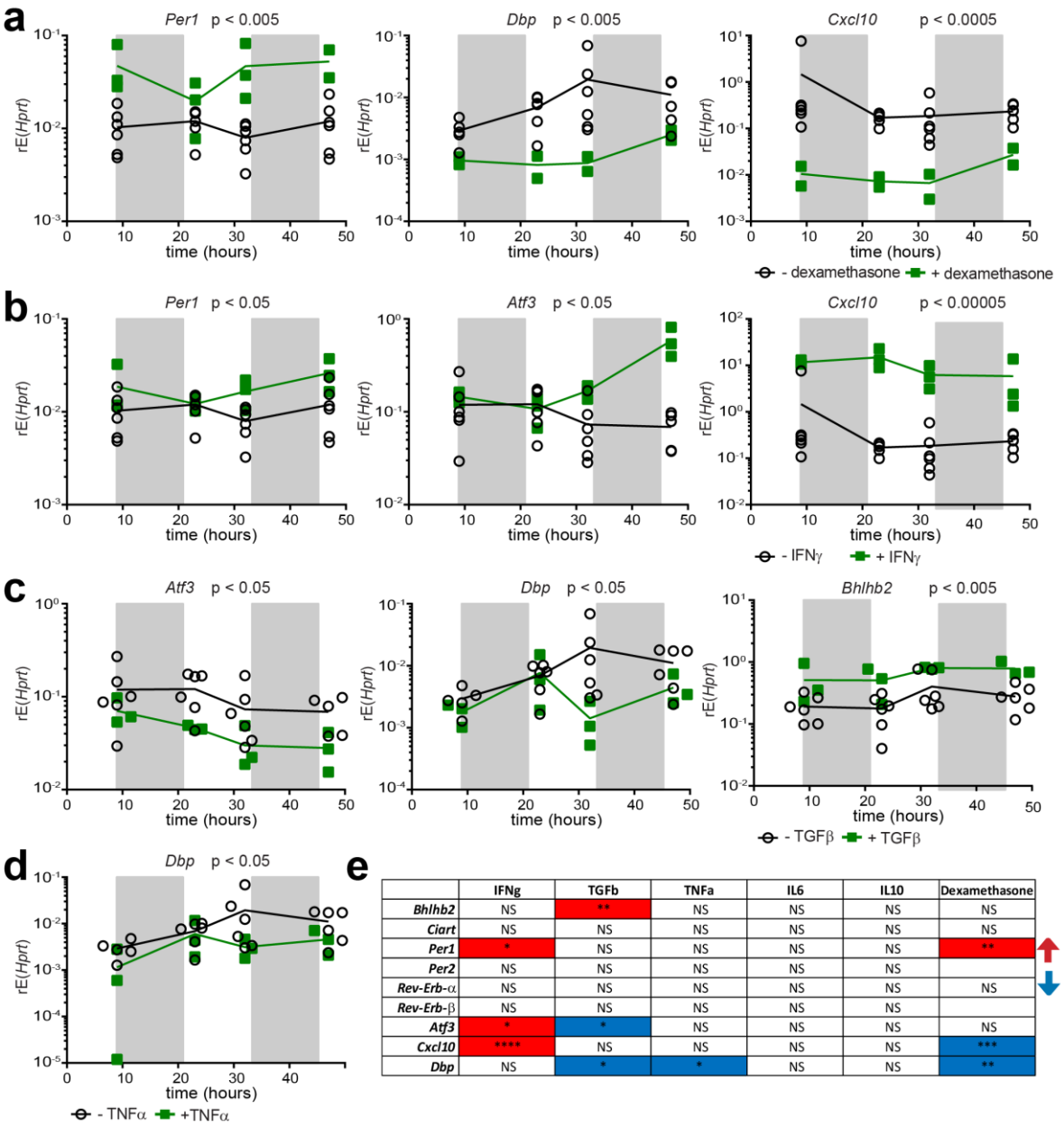

	IFNg	TGFb	TNFa	IL6	IL10	Dexamethasone
Bhlhb2	NS	**	NS	NS	NS	NS
Ciart	NS	NS	NS	NS	NS	NS
Per1	*	NS	NS	NS	NS	**
Per2	NS	NS	NS	NS	NS	
Rev-Erb-α	NS	NS	NS	NS	NS	NS
Rev-Erb-β	NS	NS	NS	NS	NS	
Atf3	*	*	NS	NS	NS	NS
Cxcl10	****	NS	NS	NS	NS	***
Dbp	NS	*	*	NS	NS	**

Figure 33: Gene expression of *in vitro* cultured primary hepatocytes. Quantitative real-time PCR analysis of gene expression in cultured primary hepatocytes (black line), which were stimulated (green line) with (**a**) dexamethasone, (**b**) IFN-γ, (**c**) TGF-β or (**d**) TNF-α. Cells were harvested every 12 hours. Night phase (6 pm to 6 am) is marked in grey. (**e**) Summary table of stimuli induced differences in gene expression of primary hepatocytes represented with their *P* values. Red and blue indicate significant increased or decreased gene expression. *P* values represent comparisons between stimulated versus unstimulated primary hepatocytes using Two-way RM ANOVA for over time analysis. NS, not significant; **P* < 0.05, ***P* < 0.005, ****P* < 0.0005 and *****P* < 0.00005.

To determine in a mouse model whether liver inflammation triggered the observed alteration in the circadian rhythm, we analyzed the inflammatory liver model of Mdr2-deficient mice which develop chronic liver inflammation (Mauad et al. 1994; Pusterla et al. 2013). We analyzed the liver of six month-old Mdr2-deficient mice and observed clear signs of inflammation as detected by the increased expression levels of cytokines and chemokines (Fig. 34a). *Atf3* expression was slightly up-regulated in Mdr2-deficient mice (Fig. 34b). However, we could not measure elevated gene expression levels of the clock-controlled genes *Dbp*, *Foxo3* and *Junb* as well as the negative feedback regulators *Rev-Erb-*α and β, *Per1* and *2*, *Ciart* and *Bhlhb2* (Fig. 34c, d). These findings indicate that the oscillation of hepatic genes was not modified by chronic inflammation.

Together, these results suggest that the induction of changes in the hepatic circadian rhythm are T_{reg}-specific and could not be mimicked by treatment with dexamethasone and individual cytokines or by chronic liver inflammation.

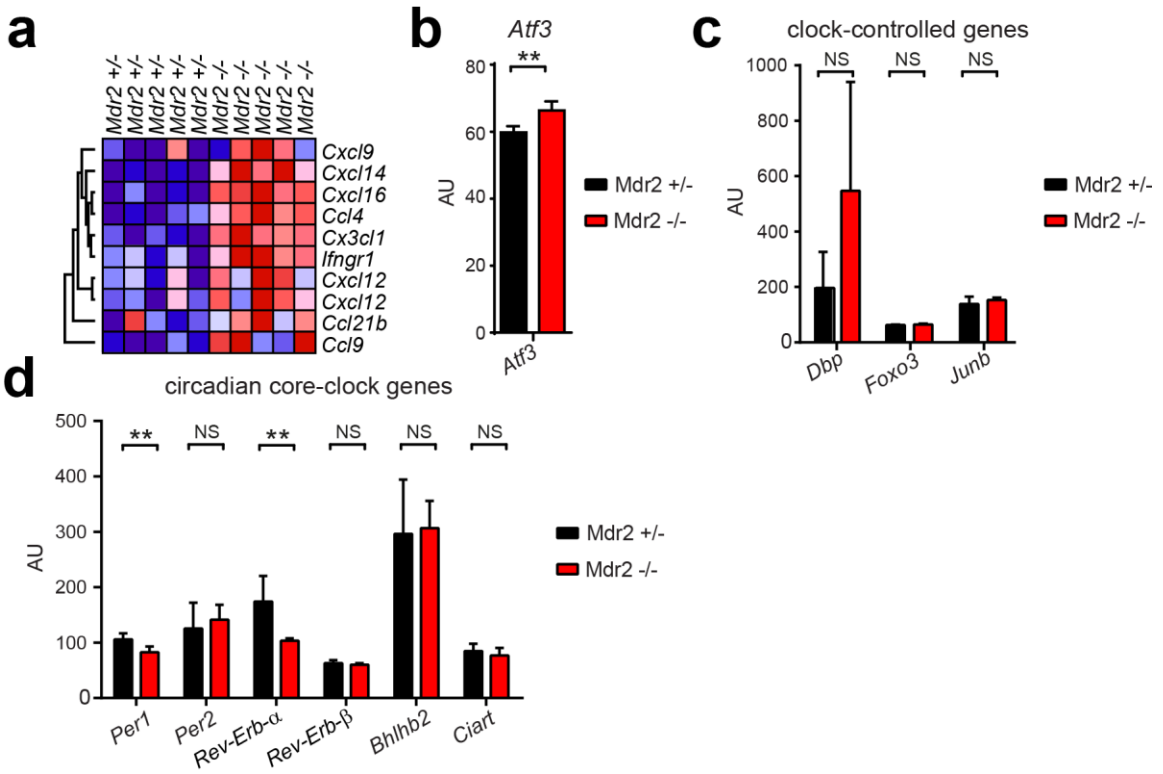

Figure 34: Circadian gene expression in livers of Mdr2$^{-/-}$ mice. RNA-based microarray analysis of hepatic genes in 6 month-old Mdr2$^{+/-}$ or Mdr2$^{-/-}$ mice. (**a**) Heat-map and hierarchical clustering of hepatic chemokine expression. Genes with greatest (red) or least (blue) transcript abundance in each group, presented as Pearson's correlation (row normalized). (**b** - **d**) Gene expression of (**b**) *Atf3,* (**c**) clock-controlled genes and (**d**) core-clock genes represented as arbitrary units (AU). *P* values represent comparisons between Mdr2$^{+/-}$ and Mdr2$^{-/-}$ mice using unpaired *t* test with Welch-correction. NS, not significant; $^{**}P < 0.005$.

Hepatic T_{reg} cells safeguard the hepatic circadian rhythm

Next, we wanted to analyze whether T_{reg} cells could normalize the hepatic circadian rhythm. In the used T_{reg} cell depletion model, T_{reg} cells reappear after a week (Kim, Rasmussen, and Rudensky 2007). Seven days after T_{reg} cell depletion, we detected that about 3% of the hepatic as well as splenic $CD4^+$ T cell pool were $Foxp3^+$ T_{reg} cells (Fig. 35a). Therefore, about 40% of the normal hepatic T_{reg} cell percentage reappeared (Fig. 35b).

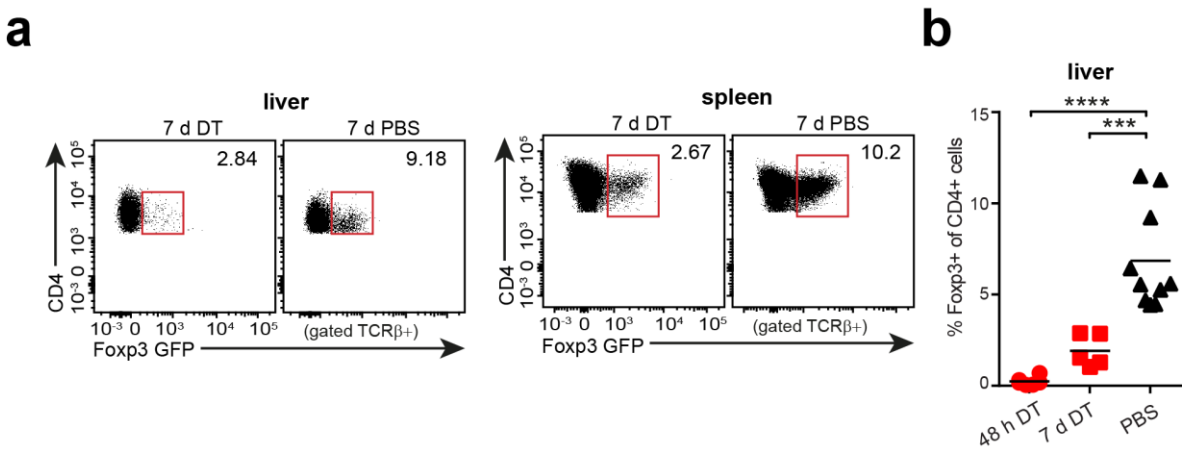

Figure 35: Hepatic T_{reg} cell frequency 7 days after T_{reg} cell depletion. T_{reg} cells were depleted by injecting Diphtheria Toxin (DT) into 6 week-old Foxp3-DTReGFP mice and analyzed after 7 days (7 d). PBS injected mice served as control mice. (**a**) T_{reg} cell depletion efficacy measured via flow cytometry by the presence of $Foxp3^+$ T_{reg} cells in the liver and spleen of DT-treated mice. (**b**) Quantification of T_{reg} cell frequencies after 48 h and 7 d DT treatment. Symbols represent individual animals and *P* values represent comparisons between DT versus PBS treated mice using Wilcoxon Test. ***$P < 0.0005$and ****$P < 0.00005$.

Interestingly, we could not detect elevated expression levels of the clock regulators *Rev-Erb-α* and *Per1,* the clock-controlled genes *Dbp* and *Foxo3* or the stress-induced gene *Atf3* seven days after T_{reg} cell depletion. The expression of these genes that initially showed a significant increase 48 hours after T_{reg} cell depletion (Fig. 25) went back to normal 7 days after DT treatment (Fig. 36a, b, c). Interestingly, signs of liver damage could be observed 7 days after T_{reg} cell depletion as measured by the significant increased concentration of ALT in the blood of the mice (Fig. 37a). In addition, the liver still showed clear signs of inflammation as measured by up-regulated levels of pro-inflammatory mediators such as *Tnfa*, *Ifng*, *Il1b*, *Ccl5* and *Ccl2* (Fig. 37b, c).

Taken together, our data support the idea that T_{reg} cells function as safeguards of the circadian rhythm in the liver. Hepatic T_{reg} cells are able to regain control over the disturbed and imbalanced circadian rhythm. Moreover, these findings suggest that protection of the hepatic circadian rhythm and the anti-inflammatory properties of hepatic T_{reg} cells may not necessarily be performed in a simultaneous manner.

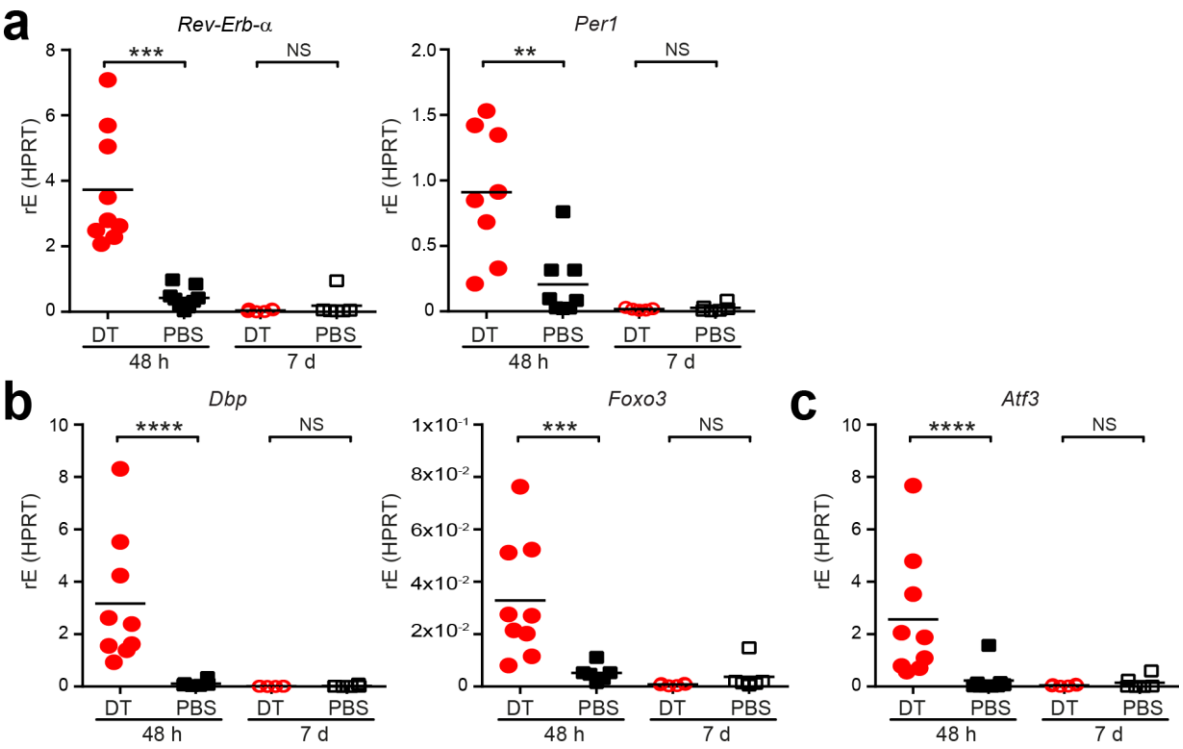

Figure 36: Normalized circadian gene expression after return of T_{reg} cells in the liver. T_{reg} cells were depleted by injecting Diphtheria Toxin (DT) into 6 week-old Foxp3-DTReGFP mice and analyzed after 7 days (7 d). PBS injected mice served as control mice. (**a** - **c**) Quantitative real-time PCR analysis of (**a**) core-clock genes, (**b**) clock-controlled genes and (**c**) *Atf3.* Symbols represent individual animals and *P* values represent comparisons between DT versus PBS treated mice using unpaired ordinary two-way ANOVA with Sidak´s multiple comparison test calculated with log2 values. NS, not significant; $^{**}P < 0.005$, $^{***}P < 0.0005$ and $^{****}P < 0.00005$.

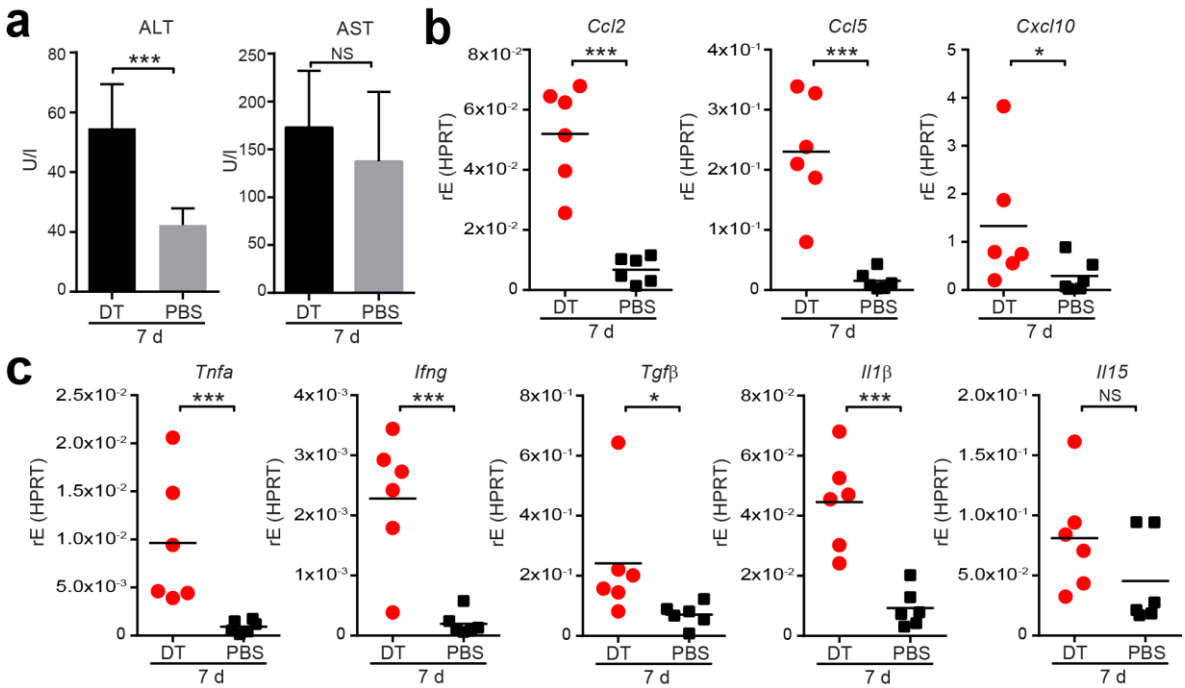

Figure 37: Liver inflammation after return of hepatic T_{reg} cells. T_{reg} cells were depleted by injecting Diphtheria Toxin (DT) into 6 week-old Foxp3-DTReGFP mice and analyzed after 7 days (7 d). (**a**) Photometric analysis of alanine-aminotransferase (ALT/GPT) and aspartate transaminase (AST/GOT) in blood plasma. (**b** - **c**) Quantitative real-time PCR analysis of (**b**) cytokines and (**c**) chemokines. Symbols represent individual animals and *P* values represent comparisons between DT versus PBS treated mice using *t* test with Welch-correction (**a**) calculated with log2 values (**b** - **c**). NS, not significant; *$P < 0.05$ and ***$P < 0.0005$.

8 Discussion

This thesis investigated the function and phenotype of T_{reg} cells in the murine liver. We described a new function of hepatic T_{reg} cells to safeguard the hepatic circadian rhythm. At the same time, T_{reg} cells play an important role in securing the expression of genes involved in liver metabolism, which are known to be partly controlled by the circadian rhythm. Furthermore, we identified a distinct phase during neonatal liver development, which is characterized by the functional immaturity of the liver, strongly proliferating hepatocytes and a low-grade inflammatory liver environment. This phase coincided with an accumulation of proliferating T_{reg} cells in the liver of neonatal mice.

8.1 The neonatal liver

Through the strategic location at a crossroad of the systemic circulation, the liver is able to carry out its function in lipid metabolism, degradation of toxic products as well as carbohydrate and protein generation (Crispe 2003). Published studies have reported that the neonatal liver undergoes functional maturation to meet the metabolic demands previously shared with the placenta by highly expressing genes involved in metabolism, mediating lipid oxidation, sulfation and dicarboxylate transport (Kelley-Loughnane et al. 2002). We propose that the around 10 day-old liver is undergoing maturation to achieve the full metabolic and functional demands of an adult liver, since we detected a special hepatic environment with a high proliferation activity of hepatocytes in the liver of neonatal mice.

On the one hand, the neonatal liver showed an increased inflammatory hepatic environment with up-regulated expression levels of cytokines, chemokines, as well as the immune-related genes *S100a8* and *S100a9*.

On the other hand, distinct gene families involved in liver metabolism were under-represented in neonatal livers in comparison to adult livers, indicating the immature state of the liver. For example, aldehyde dehydrogenases, known to be highly concentrated in the liver and responsible for the oxidation of aldehydes to carboxylic acids, were less expressed in neonatal livers (Koppaka et al. 2012).

Additionally almost all members of the *Cyp* family were under-represented in the 10 day-old liver in comparison to the adult liver. Bilirubin, the end product of heme catabolism, has been identified as the first endogenous substrate for Cyp2a5, whose gene was significantly lower expressed in neonatal livers as compared to adult livers. Cyp2a5 is normally induced by exposure to chemical hepatoxins, nuclear receptor ligands, metals or by liver injury and has an important role in bilirubin clearance mechanisms as well as the resulting cytoprotection against bilirubin hepatotoxicity (Abu-Bakar et al. 2011; Camus-Randon et al. 1996; Kim et al. 2013). Another under-represented Cyp family member was the oxysterol 7α-hydroxylase encoded by the *Cyp7a1* gene, involved in the general bile acid synthesis pathway (Li-Hawkins et al. 2000). Furthermore, several *Mup* genes followed the described under-represented expression pattern in neonatal livers. Mups are unique members of the lipocalin superfamily and serve as chemical signals to regulate metabolic pathways. Especially the low expression of *Mup1* is interesting, since Mup1 has been described to be involved in the regulation of the hepatic gluconeogenic and lipogenic programs (Zhou, Jiang, and Rui 2009).

8.2 Neonatal hepatic T_{reg} cells

Besides its important role in the metabolism of glucose, bile, bilirubin and other nutrients, the liver can be considered as an immune-privileged organ. Less is known about the development of liver-resident T_{reg} cells, especially in the early postnatal phase. In general, the T cell populations of neonatal mice develop from very few T lymphocytes from day 1 to day 15 after birth (Garcia et al. 2000). T_{reg} cell development is slightly delayed relative to conventional T cells during ontogeny (Fontenot et al. 2005). We observed a strong proliferation and accumulation of T_{reg} cells in the liver of 10 day-old mice. It is described that hepatocytes are able to induce Foxp3$^+$ T_{reg} cells within a CD4$^+$ T cell population via the Notch signaling pathway *in vitro* (Burghardt et al. 2014). However, epigenetic analysis of the DNA methylation status of the T_{reg}-specific demethylated region, located in the CNS2 of the *Foxp3* gene, and flow-cytometry staining of the transcription factor Helios and the cell surface transmembrane glycoprotein Nrp1

revealed that the numerous T_{reg} cells observed in the liver of neonatal mice were thymus-derived and not peripheral induced T_{reg} cells.

RNA-based microarray analysis further emphasized the differences between hepatic T_{reg} cells in neonatal and adult mice. T_{reg} cells in the neonatal liver highly up-regulated the anti-inflammatory cytokine *Il-10* and the generally liver-synthesized glycoprotein *Ahsg* (*Fetuin-a*). The hepatokine Ahsg can act as an anti-inflammatory cytokine similar to IL-10, shows anti-fibrotic activity and is increased express in inflamed livers (Stefan and Haring 2013; Bilgir et al. 2012; Li et al. 2011). One could speculate that Ahsg may have the same regulatory function as IL-10 in neonatal T_{reg} cells to maintain homeostasis in the neonatal liver.

In addition, neonatal hepatic T_{reg} cells seem to be more activated than their counterparts in the adult liver, as seen by the elevated expression level of the transmembrane glycoprotein CD44, known to be involved in T cell activation and memory (Dutton, Bradley, and Swain 1998; Baaten et al. 2010), and the strongly up-regulated gene expression of *Nkg7*, which is expressed on activated T_{reg} cells under the control of *Foxp3* (Sugimoto et al. 2006; Turman et al. 1993). Two observations further underline the strong proliferation of the neonatal hepatic T_{reg} cells. First, the neonatal T_{reg} cells strongly expressed the co-stimulatory gene *Tnfrsf9*, known to be involved in regulation of T cell proliferation and IL-2 secretion (Watts 2005). Second, gene ontology analysis revealed that plenty of the up-regulated genes were involved in DNA replication.

Moreover, the activated and proliferating T_{reg} cells in the neonatal liver strongly expressed the adhesion protein CD11a (LFAT) on their surface. CD11a, expressed on activated T cells, has been shown to play a critical role in mediating the homing of T cells to lymphoid and non-lymphoid tissue by interaction with the intercellular adhesion molecule 1 (Icam-1) and additionally functions as a co-stimulatory molecule for T cell activation (Kandula and Abraham 2004; Koboziev et al. 2012). In the liver, lymphocyte recruitment is largely independent of selectins, required for lymphocyte rolling in peripheral vasculature (Wong et al. 1997). While this may still be true for neutrophils, $CD4^+$ T cells are mainly using integrins, such as CD11a and Vap-1 to adhere with the liver sinusoids (Crispe 2003; Bonder et al. 2005). Therefore, the interaction of CD11a with the numerous Icam-1 and Icam-2 molecules on LSECs may play a role in the recruitment of activated rather than resting T_{reg} cells in the liver of neonatal mice, since CD11a

additionally functions as a co-stimulatory molecule for T cell activation (Kandula and Abraham 2004; Koboziev et al. 2012). Furthermore, these neonatal T_{reg} cells up-regulated the *chemokine receptor Cxcr3*, known to be express on activated T cells and bind to the Cxc chemokines Cxcl9 (MIG) and Cxcl10 (IP-10) to recruit T cells and NK cells into tissues (Luster 2002). Therefore, we suggest that the process of T_{reg} cell recruitment may be stronger in the neonatal liver as compared to the adult liver, especially due to the increased expression of chemokines in the neonatal liver tissue, such as the T cell and other lymphocyte chemoattractants *Ccl5, Ccl4, Ccl2* and *Cxcl10*.

8.3 Where does the enlarged T_{reg} cell population in the liver of neonatal mice come from?

The accumulation of T_{reg} cells in the neonatal liver came along with an inflamed liver environment. One could speculate that this is induced by the first settlement of lymphocytes in the liver. It is described that T cell seeding of peripheral organs continues during the neonatal period (Garcia et al. 2000). However, only hepatic T_{reg} cells and no other hepatic lymphocytes including T_{conv} cells, NK cells, Kupffer cells and monocytes showed strong accumulation in the liver tissue. Furthermore, despite the block of mature B cells and T cells in neonatal livers of Rag2$^{-/-}$ mice, we still observed the same inflammatory hepatic environment as detected in neonatal wildtype mice. Therefore, the inflammatory liver tissue seems not to be induced by the first settlement of lymphocytes in the liver and is also not induced by the accumulation of T_{reg} cells in the neonatal liver.

Previously, a study described that TLR/MyD88-mediated responses to microbial colonization in the intestine enhance the production of TGF-β1, which triggers the increase of T_{reg} numbers in neonatal livers (Maria, English, and Gorham 2014). The gut-liver axis plays an important role in modulating the hepatic immune system as the liver receives blood from the portal vein from the gut. Thereby a high concentration of non-pathogen associated antigens such as food, and bacterial antigens reach the liver. To handle the high amount of these antigens, the liver uses a variety of mechanisms, involving the production of IL-10, Kupffer cells, as well as T_{reg} cells (Erhardt et al. 2007). However, we detected the same

accumulation of hepatic T_{reg} cells alongside the highly inflamed liver environment in neonatal mice deficient for Tlr4 or the Toll-like receptor pathway adapter molecules MyD88 and Trif. Therefore, bacterial antigens, such as lipopolysaccharide of Gram-negative bacteria which is recognized by the Tlr4, appear not to be responsible for the induction and expansion of the neonatal hepatic T_{reg} cell pool.

We speculate that the increased and strongly proliferating T_{reg} cell population in the neonatal liver could have two other reasons.

First, the strong proliferation and accumulation of hepatic T_{reg} cells could represent the early wave of Aire-dependent T_{reg} cells that the Mathis-Benoist group has recently described (Yang et al. 2015). This early wave of T_{reg} cells may seed the liver with long term liver-resident T_{reg} cells, which are described to be able to stably persist in adult mice and show distinct functional and phenotypic properties, such as higher activation and proliferation as compared to later in life generated T_{reg} cells (Yang et al. 2015). Indeed, besides the detection of the high proliferation capacity and activation of neonatal hepatic T_{reg} cell, we detected that the hepatic T_{reg} cell proliferation is an antigen-driven TCR-dependent process, as we saw an elevated proportion of Nr4a1 positive T_{reg} cell in neonatal livers. Nr4a1 expression is described in several studies to monitor TCR activation in T cells (Moran et al. 2011).

Second, the liver is in a stressed condition resulting from its metabolic immaturity and inflammatory environment. Therefore, the liver acutely recruits and fosters proliferation of T_{reg} cells. This T_{reg} cell wave would be transient until the liver fully matures. In general, the neonatal environment is described as functionally lymphopenic, since CD4 T cells transferred into neonatal mice undergo similar proliferation compared to cells transferred into lymphopenic environments in adult mice (Min et al. 2003; Adkins, Leclerc, and Marshall-Clarke 2004). Cytokines such as IL-15, of which we have seen elevated levels in neonatal livers, are key players in such homeostatic proliferation (Cookson and Reen 2003). Increased accumulation of highly proliferating T_{reg} cells by day 10 was only detectable in the liver and not in other peripheral organs, such as spleen and lung. Therefore, we could speculate that besides the stressed state of the liver and their immaturity, the neonatal liver has a kind of T_{reg}-specific lymphopenic environment, which results in the accumulation of strongly proliferating hepatic T_{reg} cells.

However, it is not clear whether these two hypotheses of the first wave of Aire-dependent T_{reg} cells and the stressed and immature liver condition are truly two independent events that might even respond to different antigens. The molecular mechanisms that drive T_{reg} cell accumulation in neonatal liver are not yet understood.

8.4 Hepatic T_{reg} cell depletion

Neonatal livers seem to be more dependent on a functional hepatic T_{reg} cell compartment in comparison to adult livers, as seen by the slight increase of the liver damage-indicating enzyme alanine-aminotransferase and the significant altered expression of thousands of transcripts after T_{reg} cell removal. These changes in the transcriptome translated into differences in protein expression affected many metabolic pathways. For example, the majority of genes belonging to the alpha amino acid metabolism, such as *Afmid,* were down-regulated after ablation of T_{reg} cells in the neonatal liver. This arylformamidase is crucial for the tryptophan metabolisms by hydrolyzing N-formyl-L-kynurenine to L-kynurenine (Hugill et al. 2015). A study using *Afmid* knockout mice showed that deficiency of this enzyme results in impaired glucose tolerance (Hugill et al. 2015). Most of the genes involved in the acyl-CoA metabolism, including acetyl-coenzyme A synthetase and different members of acyl-CoA thioesterases, were additionally down-regulated in the T_{reg}-deficient neonatal liver. These genes are critical for different physiological processes such as fatty acid and cholesterol synthesis or lipid biosynthesis (Loikkanen et al. 2002; Horibata et al. 2013).

Based on these data, we propose that T_{reg} cells play an important role in regulating the expression of genes involved in metabolic processes in the liver, especially during maturation in the neonatal phase. Since T_{reg} cell ablation in neonatal mice resulted in altered expression of genes involved in metabolic processes in the liver, which could severely affect the ability of the neonatal liver to perform its function, we suggest that the neonatal liver requires T_{reg} cells to establish liver homeostasis and proper metabolic liver function.

Interestingly, gene expression chances induced by T_{reg} cell depletion were significantly more pronounced in liver tissue in comparison to lung tissue of both age groups. One could speculate that the neonatal liver is more vulnerable due to the intrinsic stress of being functionally underdeveloped and immature.

8.5 Removal of T_{reg} cells affects the circadian rhythm

We detected an increased expression of core-clock genes in livers from T_{reg}-depleted mice both at 10 days and 6 weeks of age. These genes included well-known negative clock regulators such as *Per1* and *Rev-Erb-*α, as well as the newly described inhibitors of the clock machinery such *Ciart* and the basic helix-loop-helix transcription factor *Bhlhb2 (Dec1*). Ciart and Bhlhb2 contribute to the transcriptional feedback loop by modifying Clock/Bmal1 activity as transcriptional repressors in addition to the clock repressors Cry and Per (Annayev et al. 2014; Scheiermann, Kunisaki, and Frenette 2013). Furthermore, T_{reg} cell removal induced the up-regulation of clock-controlled genes such as *Dbp*, whose circadian expression is driven directly by components of the molecular clock. Therefore, Dbp is activated by the Clock/Bmal1 heterodimer and repressed by the clock repressors Cry and Per (Ripperger et al. 2000).

To further study the general impact of T_{reg} cell depletion on hepatic circadian gene expression, we analyzed the oscillation patterns of hepatic expressed genes over a distinct time period. We used 6 week-old mice due to the simpler handling compared to neonatal mice. T_{reg} cell depletion led to a differential expression of about 25 - 30% of all oscillating genes in the liver, including elevated expression or partly loss of rhythmicity of core-clock genes as well as clock-controlled genes. In total, the circadian expression of more than 400 genes was affected. An interesting example is Foxo3, one of the more strongly altered clock-controlled genes in T_{reg}-depleted livers. Foxo3 is known to play a role in regulating the hepatic clock alongside insulin and is therefore critical for the regulation of gluconeogenesis and lipid metabolism (Chaves et al. 2014; Zhou et al. 2014). In general, metabolic and circadian processes are known to be tightly linked in the liver, as high-fat diet (HFD) in mice led to widespread remodeling of the hepatic clock and thereby reorganized liver metabolic pathways (Eckel-Mahan et al. 2013). Other studies

have shown that the general repressors of the core-clock machinery and other components of the principal feedback loop drive the coordination of circadian rhythm and metabolism in peripheral tissues. For example, dual depletion of *Rev-Erb-α* and β in mice results in disrupted circadian expression of core-clock genes and lipid homeostatic gene networks in liver, skeletal muscle and adipose tissue (Solt et al. 2012; Cho et al. 2012; Zhang et al. 2015). Moreover, Rev-Erb-α and β as well as Bhlhb2 and Dbp are direct regulators of the circadian oscillation of Cyp7a, involved in generation of bile acid (Li-Hawkins et al. 2000; Noshiro et al. 2007).

Gene ontology analysis helped us to determine whether the changes in circadian expressed genes were linked to metabolic pathways. Indeed, the circadian expressed genes, showing altered hepatic gene expression after T_{reg} cell removal, were partly involved in metabolic processes. Interestingly, within these genes were members belonging to the alpha amino acid metabolism and the acyl-CoA metabolism. One of the strongest examples was the acyl-CoA thioesterase 12 (Acot 12), which was significantly down-regulated after T_{reg} cell depletion. Expression of Acot12 is under control of Dbp and other clock-controlled PAR domain basic leucine zipper (PAR bZip) proteins, resulting in cyclic release of fatty acids from thioesters (Gachon et al. 2011). Therefore, we could partly link altered circadian expression in T_{reg}-depleted mice to the modified expression of genes involved in liver metabolism, such as gluconeogenesis and lipid metabolism. Consistent with the previously described T_{reg} cell function to establish liver homeostasis and proper metabolic liver function in neonatal mice, our data suggest that T_{reg} cells have an unrecognized function to secure the regulation of the hepatic circadian rhythm and closely linked metabolic pathways (Fig. 38). However, the molecular mechanisms by which loss of T_{reg} cells affect the circadian clock in the liver are not known. Further research to clarify the complex mechanisms will provide new insights into the pathogenesis of clock-induced pathologies, such as obesity, metabolic syndrome, nonalcoholic fatty liver disease and liver cancer (Turek et al. 2005; Sookoian et al. 2007; Taniguchi et al. 2009).

Besides the liver, peripheral clocks have been identified in heart (Storch et al. 2002), pancreas (Dibner and Schibler 2015), white adipose tissue (Kohsaka et al. 2007) and lung (Gibbs et al. 2009). Circadian rhythm in the lung tissue has been described to be reorganized through inflammation provoked by lung injury or

endotoxin treatment (Haspel et al. 2014; Gibbs et al. 2009). We detected no significant changes of core-clock and clock-controlled gene expression in the lung after T_{reg} cell depletion. Therefore, our data suggest a local liver-intrinsic failure of clock regulation and a specific function of hepatic T_{reg} cells.

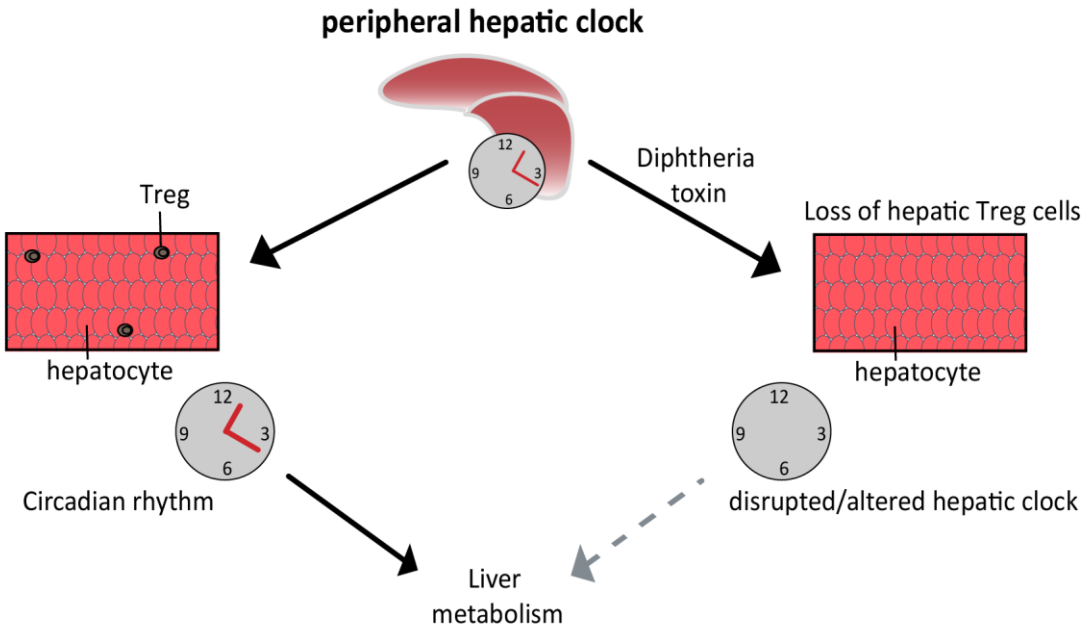

Figure 38: T_{reg} cells safeguard the circadian rhythm in the liver tissue. Loss of T_{reg}-mediating liver control leads to a disrupted circadian rhythmicity with altered expression pattern of the clock machinery in the liver of mice. Since circadian rhythm and regulation of liver metabolism pathways are closely linked, changes in the hepatic circadian rhythm induce alteration in liver metabolism.

8.6 Hepatic macrophages, liver inflammation and the circadian rhythm

To determine whether the depletion of lymphocytes other than T_{reg} cells or the increased cell death in the liver due to DT injection could induce similar changes to the hepatic circadian rhythm, we depleted Kupffer cells in the liver using Csfr1-DTR mice. In this acute depletion model, DT injection leads to ablation of macrophages and monocytes (Schreiber et al. 2013). In case the increased cell death of lymphocytes in the liver may trigger the changes of the hepatic circadian

rhythm, we should have observed the same or stronger disturbed hepatic circadian rhythm in DT-injected Csfr1-DTR mice, since Kupffer cells represent a major immune cell population in the liver and represent around 35% of the non-parenchymal cells in the liver (Crispe 2003). In contrast, only 10% of the whole hepatic CD4 T cell population are T_{reg} cells, which at least are 10-times fewer cells compared to the number of Kupffer cells. Neither the loss of Kupffer cells nor the increased apoptosis of immune cells in the liver provoke the same alteration of circadian gene expression, observed previously in T_{reg}-depleted liver. In addition, DT injection itself induced no alteration in the circadian gene expression of components of the hepatic clock machinery of DTR negative control mice. Based on these findings, we suggest a central role for T_{reg} cells in protecting the hepatic clock.

Interestingly, Kupffer cell depletion did not result in liver inflammation or induction of the stress-inducible transcription factor *Atf3* as observed before in T_{reg}-depleted mice. Atf3 belongs to the Atf/Creb family of transcription factors and is greatly increased when the cells are exposed to stress signals as injuries, toxins, serum factors or cytokines (Hai et al. 1999). In DT-injected Csfr1-DTR mice, we observed a rather down-regulation of cytokines and chemokines, including *Il-15*, *Tgfb* and *Ccl5*. In contrast, T_{reg} cell removal caused increased inflammation and stressed liver tissue as seen by the up-regulation of the stress-inducible gene *Atf3* and several cytokines and chemokines, such as the *Cxcl10* and *Tnfa*. Cxcl10 (IP-10) has been described to correlate with liver injury, but at the same time has hepatoprotective effects (Bone-Larson et al. 2001). In general, cytokines have been reported to affect the circadian clock (Lopez et al. 2014; Hashiramoto et al. 2010; Kon et al. 2008). Particularly, TNF-α and IL-1β can inhibit the ability of Bmal1/Clock to induce activation of E-box-dependent genes in the suprachiasmatic nucleus and liver (Cavadini et al. 2007).

To investigate to which extent liver inflammation plays a role in modulation of hepatic circadian expression, we used the Mdr2$^{-/-}$ mice model. The multi-drug resistance (Mdr2) protein in the canalicular membrane of the bile duct functions as an ABC transporter to transport biliary phospholipids into bile (Pikarsky et al. 2004). The lack of biliary phospholipids in the bile of Mdr2$^{-/-}$ mice results in toxic bile acid-induced bile duct damage, which finally leads to inflammation-induced hepatocellular cancer by around 12 - 16 month of age (Mauad et al. 1994;

Katzenellenbogen et al. 2007). Liver inflammation is already induced in the first weeks of life through increased levels of pro-inflammatory cytokines, such as TNF-α and IL-6, as well as NF-κB-induced chemokines and recruitment of immune cells into the liver (Fickert et al. 2004; Pikarsky et al. 2004). Despite of the high levels of chemokines and the elevated expression of *Atf3,* we could not detect a significant increase of clock inhibitors or clock-controlled genes in livers of 6 month-old Mdr2$^{-/-}$ mice, which we observed before in T_{reg}-depleted mice.

Furthermore, *in vitro* treatment of primary hepatocytes with different cytokines or the glucocorticoid dexamethasone, a key hormone known to be a circadian time cue for the hepatic clock (Oishi et al. 2005; Scheiermann, Kunisaki, and Frenette 2013), did also not induce the same changes in the circadian expression as observed before in T_{reg}-depleted mice. For example, neither dexamethasone nor any of the tested cytokines were able to modify the expression of the Bmal1 regulator *Rev-Erb-*α (Zhang et al. 2015). In T_{reg}-depleted mice, *Rev-Erb-*α expression was severely increased early on and its oscillation phase was disturbed. Some cytokines could only modify individual parameters *in vitro*. For example, TGF-β treatment led to a significantly increased expression of *Bhlhb2* in primary hepatocytes, supported by the finding that TGF-β signaling can reset the circadian clock, independently of *Per* induction, through rapid induction of *Bhlhb2* transcripts (Kon et al. 2008).

Seven days after DT treatment, T_{reg} cells were reappearing in the liver and T_{reg} cell numbers were back to about 30 - 40% of normal. At that point, the initially disturbed circadian gene expression as well as the stress-induced *Atf3* expression had normalized despite of the still existing inflammation in the liver tissue and the high level of the liver-damage enzyme ALT in the blood.

Although the inflammatory liver environment could be directly caused by the deficiency in immune regulation due to the lack of T_{reg} cells, our data suggest that T_{reg}-independent liver inflammation, assessed by elevated levels of several cytokines and chemokines, is not sufficient to induce changes in the circadian rhythm. An alternative explanation for the increased hepatic inflammation could be that some of these factors are elevated due to the dysregulated circadian rhythm in the liver of T_{reg}-depleted mice. Peripheral clocks are known to regulate several physiological processes, including immune functions in peripheral tissues (Scheiermann, Kunisaki, and Frenette 2013). For example, the core-clock

machinery controls production and release of different cytokines such as IL-1β, IL-6, IFN-γ, TGF-β and TNF-α as well as the innate immune response by NK cells, monocytes and macrophages (Arjona and Sarkar 2006; Depres-Brummer et al. 1997; Dimitrov et al. 2009; Kon et al. 2008; Keller et al. 2009; Ando et al. 2011; Bollinger et al. 2011; Hayashi, Shimba, and Tezuka 2007). Moreover, certain adaptive immune cells are dependent on the circadian clock. T_{H17} cell differentiation and proliferation has been described to be regulated by the circadian clock (Fortier et al. 2011; Yu et al. 2013). However, only cytokines have the reciprocal function to affect the circadian clock (Lopez et al. 2014; Hashiramoto et al. 2010; Kon et al. 2008). Our data now identifies T_{reg} cells as a central cellular player in safeguarding the hepatic clock by stabilizing components of the core-clock machinery, especially the negative core-clock regulators.

8.7 Conclusion and perspectives

In principle, T_{reg} cells have two functional tasks. Besides the well-studied function to establish and maintain immune tolerance and immune homeostasis, tissue-specialized T_{reg} cells have the ability to perform non-classical functions in adult tissues, such as controlling metabolic parameter in the abdominal adipose tissue (Feuerer, Herrero, et al. 2009; Cipolletta et al. 2012). The results of this thesis demonstrate that T_{reg} cells in the liver can be assigned to these tissue-specialized T_{reg} cells. The well-described T_{reg} cell population in the visceral adipose tissue (Feuerer, Herrero, et al. 2009; Cipolletta et al. 2012), injured muscle tissue (Burzyn et al. 2013) and virus-infected lung tissue (Arpaia et al. 2015) have one thing in common: they promote organismal homeostasis.

By analyzing a special T_{reg} cell population in the liver of neonatal mice, we identified a new non-classical function of T_{reg} cells, performed at a very early postnatal phase. T_{reg} cells help to establish tissue homeostasis, including for example establishment of proper metabolic function during neonatal development in still immature or stressed organs, such as demonstrated in the liver (Fig. 39).

Other tissue-specialized T_{reg} cells which are associated with controlling or regulating metabolic functions are for example the VAT-resident T_{reg} cells. These cells are able to take up fat droplets via the expression of CD36 (Feuerer et al. 2010; Cipolletta et al. 2012; Burzyn, Benoist, and Mathis 2013). It will be of great interest to further understand the exact mechanism, which underlies the neonatal tissue protection by T_{reg} cells, and examine which other organs are in need of the neonatal T_{reg} protection. One could speculate that the gastrointestinal tract or other endocrine organs than the liver, such as kidney or pancreas, could be especially sensitive for the need of T_{reg} protection in the neonatal tissue.

Furthermore, by identifying a new non-classical role of T_{reg} cells in regulating and safeguarding the hepatic clock, we show that immune cells can influence the circadian clock and partly affect the circadian clock-linked metabolism in liver tissue (Fig. 39), which was before only assigned for cytokines (Lopez et al. 2014; Hashiramoto et al. 2010; Kon et al. 2008). We are just starting to understand how the complex mechanism of the hepatic circadian clock is regulated by T_{reg} cells and how this is linked to the liver metabolism in these mice. Further research in this area may provide new insights into the specific use of T_{reg} cells or their products to interfere with circadian clock-induced diseases, such as the metabolic syndrome, nonalcoholic fatty liver, as well as liver cancer in the future.

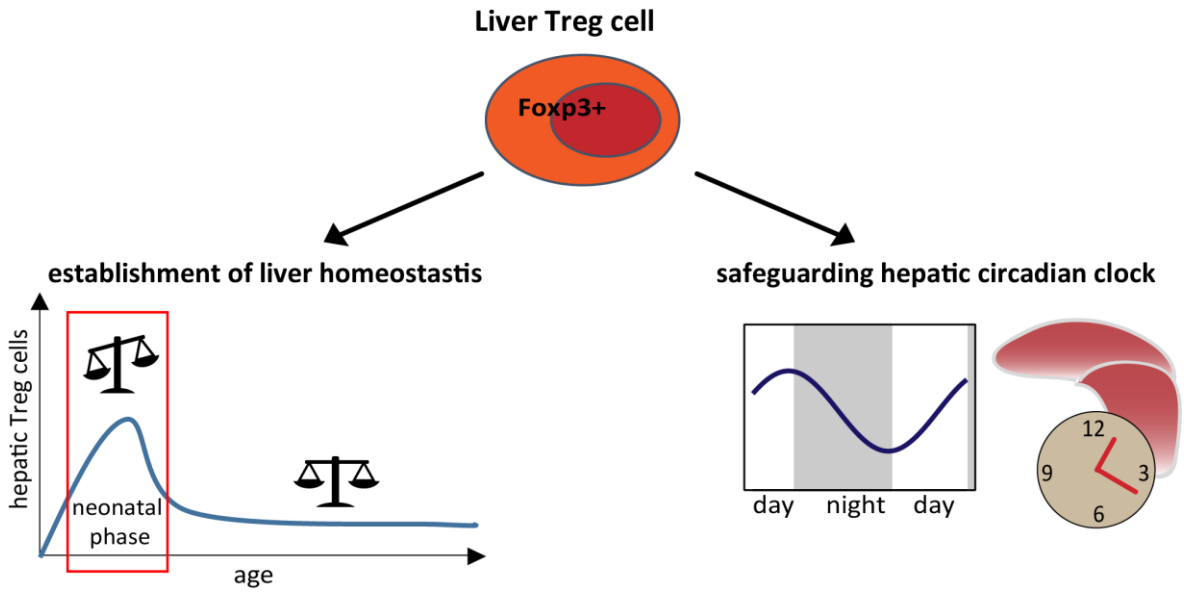

Figure 39: Identification of two new non-classical functions of T_{reg} cells in the liver tissue. Left side: T_{reg} cells help to establish liver tissue homeostasis by helping the liver to develop from a stressed and immature state to a full developed mature organ. During this neonatal and immature phase, the immature liver is in a transition state, characterized by highly proliferating hepatocytes and under-represented cell clusters, partly involved in metabolic function. Right side: T_{reg} cells secure the hepatic clock to regulate circadian expression in the liver, since loss of T_{reg}-mediating liver control leads to a disrupted circadian rhythmicity.

9 References

Abbas, A. K., C. Benoist, J. A. Bluestone, D. J. Campbell, S. Ghosh, S. Hori, S. Jiang, V. K. Kuchroo, D. Mathis, M. G. Roncarolo, A. Rudensky, S. Sakaguchi, E. M. Shevach, D. A. Vignali, and S. F. Ziegler. 2013. 'Regulatory T cells: recommendations to simplify the nomenclature', *Nat Immunol*, 14: 307-8.

Abu-Bakar, A., D. M. Arthur, S. Aganovic, J. C. Ng, and M. A. Lang. 2011. 'Inducible bilirubin oxidase: a novel function for the mouse cytochrome P450 2A5', *Toxicol Appl Pharmacol*, 257: 14-22.

Adachi, O., T. Kawai, K. Takeda, M. Matsumoto, H. Tsutsui, M. Sakagami, K. Nakanishi, and S. Akira. 1998. 'Targeted disruption of the MyD88 gene results in loss of IL-1- and IL-18-mediated function', *Immunity*, 9: 143-50.

Adkins, B., C. Leclerc, and S. Marshall-Clarke. 2004. 'Neonatal adaptive immunity comes of age', *Nat Rev Immunol*, 4: 553-64.

Akira, S., S. Uematsu, and O. Takeuchi. 2006. 'Pathogen recognition and innate immunity', *Cell*, 124: 783-801.

Alberts, B., Johnson, A., Lewis, J., Raff, M., Roberts, K. and Walter, P. 2008. ´Molecular Biology of The Cell´,Garland Science.

Ando, H., M. Kumazaki, Y. Motosugi, K. Ushijima, T. Maekawa, E. Ishikawa, and A. Fujimura. 2011. 'Impairment of peripheral circadian clocks precedes metabolic abnormalities in ob/ob mice', *Endocrinology*, 152: 1347-54.

Annayev, Y., S. Adar, Y. Y. Chiou, J. D. Lieb, A. Sancar, and R. Ye. 2014. 'Gene model 129 (Gm129) encodes a novel transcriptional repressor that modulates circadian gene expression', *J Biol Chem*, 289: 5013-24.

Arjona, A., and D. K. Sarkar. 2006. 'The circadian gene mPer2 regulates the daily rhythm of IFN-gamma', *J Interferon Cytokine Res*, 26: 645-9.

Arjona, A., A. C. Silver, W. E. Walker, and E. Fikrig. 2012. 'Immunity's fourth dimension: approaching the circadian-immune connection', *Trends Immunol*, 33: 607-12.

Arpaia, N., J. A. Green, B. Moltedo, A. Arvey, S. Hemmers, S. Yuan, P. M. Treuting, and A. Y. Rudensky. 2015. 'A Distinct Function of Regulatory T Cells in Tissue Protection', *Cell*, 162: 1078-89.

Asano, M., M. Toda, N. Sakaguchi, and S. Sakaguchi. 1996. 'Autoimmune disease as a consequence of developmental abnormality of a T cell subpopulation', *J Exp Med*, 184: 387-96.

Baaten, B. J., C. R. Li, M. F. Deiro, M. M. Lin, P. J. Linton, and L. M. Bradley. 2010. 'CD44 regulates survival and memory development in Th1 cells', *Immunity*, 32: 104-15.

Bamboat, Z. M., J. A. Stableford, G. Plitas, B. M. Burt, H. M. Nguyen, A. P. Welles, M. Gonen, J. W. Young, and R. P. DeMatteo. 2009. 'Human liver dendritic cells promote T cell hyporesponsiveness', *J Immunol*, 182: 1901-11.

Beaule, C., and S. Amir. 1999. 'Photic entrainment and induction of immediate-early genes within the rat circadian system', *Brain Res*, 821: 95-100.

Bendelac, A., P. B. Savage, and L. Teyton. 2007. 'The biology of NKT cells', *Annu Rev Immunol*, 25: 297-336.

Bennett, C. L., J. Christie, F. Ramsdell, M. E. Brunkow, P. J. Ferguson, L. Whitesell, T. E. Kelly, F. T. Saulsbury, P. F. Chance, and H. D. Ochs. 2001. 'The immune dysregulation, polyendocrinopathy, enteropathy, X-linked syndrome (IPEX) is caused by mutations of FOXP3', *Nat Genet*, 27: 20-1.

Bilgir, F., O. Bilgir, L. Kebapcilar, M. Calan, F. Ozdemirkiran, T. Cinali, and G. Bozkaya. 2012. 'Soluble CD40 ligand, high sensitive C-reactive protein and fetuin-A levels in patients with essential thrombocythemia', *Transfus Apher Sci*, 46: 67-71.

Bode, J. G., U. Albrecht, D. Haussinger, P. C. Heinrich, and F. Schaper. 2012. 'Hepatic acute phase proteins--regulation by IL-6- and IL-1-type cytokines involving STAT3 and its crosstalk with NF-kappaB-dependent signaling', *Eur J Cell Biol*, 91: 496-505.

Bollinger, T., A. Leutz, A. Leliavski, L. Skrum, J. Kovac, L. Bonacina, C. Benedict, T. Lange, J. Westermann, H. Oster, and W. Solbach. 2011. 'Circadian clocks in mouse and human CD4+ T cells', *PLoS One*, 6: e29801.

Bonder, C. S., M. U. Norman, M. G. Swain, L. D. Zbytnuik, J. Yamanouchi, P. Santamaria, M. Ajuebor, M. Salmi, S. Jalkanen, and P. Kubes. 2005. 'Rules of recruitment for Th1 and Th2 lymphocytes in inflamed liver: a role for alpha-4 integrin and vascular adhesion protein-1', *Immunity*, 23: 153-63.

Bone-Larson, C. L., C. M. Hogaboam, H. Evanhoff, R. M. Strieter, and S. L. Kunkel. 2001. 'IFN-gamma-inducible protein-10 (CXCL10) is hepatoprotective during acute liver injury through the induction of CXCR2 on hepatocytes', *J Immunol*, 167: 7077-83.

Brunkow, M. E., E. W. Jeffery, K. A. Hjerrild, B. Paeper, L. B. Clark, S. A. Yasayko, J. E. Wilkinson, D. Galas, S. F. Ziegler, and F. Ramsdell. 2001. 'Disruption of a new forkhead/winged-helix protein, scurfin, results in the fatal lymphoproliferative disorder of the scurfy mouse', *Nat Genet*, 27: 68-73.

Burghardt, S., B. Claass, A. Erhardt, K. Karimi, and G. Tiegs. 2014. 'Hepatocytes induce Foxp3(+) regulatory T cells by Notch signaling', *J Leukoc Biol*, 96: 571-7.

Burzyn, D., C. Benoist, and D. Mathis. 2013. 'Regulatory T cells in nonlymphoid tissues', *Nat Immunol*, 14: 1007-13.

Burzyn, D., W. Kuswanto, D. Kolodin, J. L. Shadrach, M. Cerletti, Y. Jang, E. Sefik, T. G. Tan, A. J. Wagers, C. Benoist, and D. Mathis. 2013. 'A special population of regulatory T cells potentiates muscle repair', *Cell*, 155: 1282-95.

Campbell, D. J., and M. A. Koch. 2011. 'Phenotypical and functional specialization of FOXP3+ regulatory T cells', *Nat Rev Immunol*, 11: 119-30.

Camus-Randon, A. M., F. Raffalli, J. C. Bereziat, D. McGregor, M. Konstandi, and M. A. Lang. 1996. 'Liver injury and expression of cytochromes P450: evidence that regulation of CYP2A5 is different from that of other major xenobiotic metabolizing CYP enzymes', *Toxicol Appl Pharmacol*, 138: 140-8.

Cavadini, G., S. Petrzilka, P. Kohler, C. Jud, I. Tobler, T. Birchler, and A. Fontana. 2007. 'TNF-alpha suppresses the expression of clock genes by interfering with E-box-mediated transcription', *Proc Natl Acad Sci U S A*, 104: 12843-8.

Chaves, I., G. T. van der Horst, R. Schellevis, R. M. Nijman, M. G. Koerkamp, F. C. Holstege, M. P. Smidt, and M. F. Hoekman. 2014. 'Insulin-FOXO3 signaling modulates circadian rhythms via regulation of clock transcription', *Curr Biol*, 24: 1248-55.

Cho, H., X. Zhao, M. Hatori, R. T. Yu, G. D. Barish, M. T. Lam, L. W. Chong, L. DiTacchio, A. R. Atkins, C. K. Glass, C. Liddle, J. Auwerx, M. Downes, S. Panda, and R. M. Evans. 2012. 'Regulation of circadian behaviour and metabolism by REV-ERB-alpha and REV-ERB-beta', *Nature*, 485: 123-7.

Cipolletta, D., M. Feuerer, A. Li, N. Kamei, J. Lee, S. E. Shoelson, C. Benoist, and D. Mathis. 2012. 'PPAR-gamma is a major driver of the accumulation and phenotype of adipose tissue Treg cells', *Nature*, 486: 549-53.

Cookson, S., and D. Reen. 2003. 'IL-15 drives neonatal T cells to acquire CD56 and become activated effector cells', *Blood*, 102: 2195-7.

Crispe, I. N. 2003. 'Hepatic T cells and liver tolerance', *Nat Rev Immunol*, 3: 51-62.

Depres-Brummer, P., P. Bourin, N. Pages, G. Metzger, and F. Levi. 1997. 'Persistent T lymphocyte rhythms despite suppressed circadian clock outputs in rats', *Am J Physiol*, 273: R1891-9.

Dibner, C., and U. Schibler. 2015. 'METABOLISM. A pancreatic clock times insulin release', *Science*, 350: 628-9.

Dimitrov, S., C. Benedict, D. Heutling, J. Westermann, J. Born, and T. Lange. 2009. 'Cortisol and epinephrine control opposing circadian rhythms in T cell subsets', *Blood*, 113: 5134-43.

Duguay, D., and N. Cermakian. 2009. 'The crosstalk between physiology and circadian clock proteins', *Chronobiol Int*, 26: 1479-513.

Dujardin, H. C., O. Burlen-Defranoux, L. Boucontet, P. Vieira, A. Cumano, and A. Bandeira. 2004. 'Regulatory potential and control of Foxp3 expression in newborn CD4+ T cells', *Proc Natl Acad Sci U S A*, 101: 14473-8.

Dutton, R. W., L. M. Bradley, and S. L. Swain. 1998. 'T cell memory', *Annu Rev Immunol*, 16: 201-23.

Eckel-Mahan, K. L., V. R. Patel, S. de Mateo, R. Orozco-Solis, N. J. Ceglia, S. Sahar, S. A. Dilag-Penilla, K. A. Dyar, P. Baldi, and P. Sassone-Corsi. 2013. 'Reprogramming of the circadian clock by nutritional challenge', *Cell*, 155: 1464-78.

Edgar, R. S., E. W. Green, Y. Zhao, G. van Ooijen, M. Olmedo, X. Qin, Y. Xu, M. Pan, U. K. Valekunja, K. A. Feeney, E. S. Maywood, M. H. Hastings, N. S. Baliga, M. Merrow, A. J. Millar, C. H. Johnson, C. P. Kyriacou, J. S. O'Neill, and A. B. Reddy. 2012. 'Peroxiredoxins are conserved markers of circadian rhythms', *Nature*, 485: 459-64.

Edwards-Smith, C., S. Goto, R. Lord, Y. Shimizu, F. Vari, and N. Kamada. 1996. 'Allograft acceptance and rejection, mediated by a liver suppressor factor, LSF-1, purified from serum of liver transplanted rats', *Transpl Immunol*, 4: 287-92.

Eghtesad, S., S. Jhunjhunwala, S. R. Little, and P. R. Clemens. 2011. 'Rapamycin ameliorates dystrophic phenotype in mdx mouse skeletal muscle', *Mol Med*, 17: 917-24.

Erhardt, A., M. Biburger, T. Papadopoulos, and G. Tiegs. 2007. 'IL-10, regulatory T cells, and Kupffer cells mediate tolerance in concanavalin A-induced liver injury in mice', *Hepatology*, 45: 475-85.

Ermolaeva, M. A., M. C. Michallet, N. Papadopoulou, O. Utermohlen, K. Kranidioti, G. Kollias, J. Tschopp, and M. Pasparakis. 2008. 'Function of TRADD in tumor necrosis factor receptor 1 signaling and in TRIF-dependent inflammatory responses', *Nat Immunol*, 9: 1037-46.

Ferrell, J. M., and J. Y. Chiang. 2015. 'Circadian rhythms in liver metabolism and disease', *Acta Pharm Sin B*, 5: 113-22.

Feuerer, M., L. Herrero, D. Cipolletta, A. Naaz, J. Wong, A. Nayer, J. Lee, A. B. Goldfine, C. Benoist, S. Shoelson, and D. Mathis. 2009. 'Lean, but not obese, fat is enriched for a unique population of regulatory T cells that affect metabolic parameters', *Nat Med*, 15: 930-9.

Feuerer, M., J. A. Hill, K. Kretschmer, H. von Boehmer, D. Mathis, and C. Benoist. 2010. 'Genomic definition of multiple ex vivo regulatory T cell subphenotypes', *Proc Natl Acad Sci U S A*, 107: 5919-24.

Feuerer, M., J. A. Hill, D. Mathis, and C. Benoist. 2009. 'Foxp3+ regulatory T cells: differentiation, specification, subphenotypes', *Nat Immunol*, 10: 689-95.

Fickert, P., A. Fuchsbichler, M. Wagner, G. Zollner, A. Kaser, H. Tilg, R. Krause, F. Lammert, C. Langner, K. Zatloukal, H. U. Marschall, H. Denk, and M. Trauner. 2004. 'Regurgitation of bile acids from leaky bile ducts causes sclerosing cholangitis in Mdr2 (Abcb4) knockout mice', *Gastroenterology*, 127: 261-74.

Floess, S., J. Freyer, C. Siewert, U. Baron, S. Olek, J. Polansky, K. Schlawe, H. D. Chang, T. Bopp, E. Schmitt, S. Klein-Hessling, E. Serfling, A. Hamann, and J. Huehn. 2007. 'Epigenetic control of the foxp3 locus in regulatory T cells', *PLoS Biol*, 5: e38.

Fontenot, J. D., J. L. Dooley, A. G. Farr, and A. Y. Rudensky. 2005. 'Developmental regulation of Foxp3 expression during ontogeny', *J Exp Med*, 202: 901-6.

Fontenot, J. D., M. A. Gavin, and A. Y. Rudensky. 2003. 'Foxp3 programs the development and function of CD4+CD25+ regulatory T cells', *Nat Immunol*, 4: 330-6.

Fortier, E. E., J. Rooney, H. Dardente, M. P. Hardy, N. Labrecque, and N. Cermakian. 2011. 'Circadian variation of the response of T cells to antigen', *J Immunol*, 187: 6291-300.

Gachon, F., N. Leuenberger, T. Claudel, P. Gos, C. Jouffe, F. Fleury Olela, X. de Mollerat du Jeu, W. Wahli, and U. Schibler. 2011. 'Proline- and acidic amino acid-rich basic leucine zipper proteins modulate peroxisome proliferator-activated receptor alpha (PPARalpha) activity', *Proc Natl Acad Sci U S A*, 108: 4794-9.

Garcia, A. M., S. A. Fadel, S. Cao, and M. Sarzotti. 2000. 'T cell immunity in neonates', *Immunol Res*, 22: 177-90.

Gibbs, J. E., S. Beesley, J. Plumb, D. Singh, S. Farrow, D. W. Ray, and A. S. Loudon. 2009. 'Circadian timing in the lung; a specific role for bronchiolar epithelial cells', *Endocrinology*, 150: 268-76.

Godfrey, V. L., J. E. Wilkinson, E. M. Rinchik, and L. B. Russell. 1991. 'Fatal lymphoreticular disease in the scurfy (sf) mouse requires T cells that mature in a sf thymic environment: potential model for thymic education', *Proc Natl Acad Sci U S A*, 88: 5528-32.

Gondek, D. C., L. F. Lu, S. A. Quezada, S. Sakaguchi, and R. J. Noelle. 2005. 'Cutting edge: contact-mediated suppression by CD4+CD25+ regulatory cells involves a granzyme B-dependent, perforin-independent mechanism', *J Immunol*, 174: 1783-6.

Grossman, W. J., J. W. Verbsky, B. L. Tollefsen, C. Kemper, J. P. Atkinson, and T. J. Ley. 2004. 'Differential expression of granzymes A and B in human cytotoxic lymphocyte subsets and T regulatory cells', *Blood*, 104: 2840-8.

Guerau-de-Arellano, M., M. Martinic, C. Benoist, and D. Mathis. 2009. 'Neonatal tolerance revisited: a perinatal window for Aire control of autoimmunity', *J Exp Med*, 206: 1245-52.

Hai, T., C. D. Wolfgang, D. K. Marsee, A. E. Allen, and U. Sivaprasad. 1999. 'ATF3 and stress responses', *Gene Expr*, 7: 321-35.

Hashiramoto, A., T. Yamane, K. Tsumiyama, K. Yoshida, K. Komai, H. Yamada, F. Yamazaki, M. Doi, H. Okamura, and S. Shiozawa. 2010. 'Mammalian clock gene Cryptochrome regulates arthritis via proinflammatory cytokine TNF-alpha', *J Immunol*, 184: 1560-5.

Haspel, J. A., S. Chettimada, R. S. Shaik, J. H. Chu, B. A. Raby, M. Cernadas, V. Carey, V. Process, G. M. Hunninghake, E. Ifedigbo, J. A. Lederer, J. Englert, A. Pelton, A. Coronata, L. E. Fredenburgh, and A. M. Choi. 2014. 'Circadian rhythm reprogramming during lung inflammation', *Nat Commun*, 5: 4753.

Haxhinasto, S., D. Mathis, and C. Benoist. 2008. 'The AKT-mTOR axis regulates de novo differentiation of CD4+Foxp3+ cells', *J Exp Med*, 205: 565-74.

Hayashi, M., S. Shimba, and M. Tezuka. 2007. 'Characterization of the molecular clock in mouse peritoneal macrophages', *Biol Pharm Bull*, 30: 621-6.

Hori, S. 2011. 'Stability of regulatory T-cell lineage', *Adv Immunol*, 112: 1-24.

Hori, S., T. Takahashi, and S. Sakaguchi. 2003. 'Control of autoimmunity by naturally arising regulatory CD4+ T cells', *Adv Immunol*, 81: 331-71.

Horibata, Y., H. Ando, M. Itoh, and H. Sugimoto. 2013. 'Enzymatic and transcriptional regulation of the cytoplasmic acetyl-CoA hydrolase ACOT12', *J Lipid Res*, 54: 2049-59.

Hsieh, C. S., H. M. Lee, and C. W. Lio. 2012. 'Selection of regulatory T cells in the thymus', *Nat Rev Immunol*, 12: 157-67.

Hughes, C. S., S. Foehr, D. A. Garfield, E. E. Furlong, L. M. Steinmetz, and J. Krijgsveld. 2014. 'Ultrasensitive proteome analysis using paramagnetic bead technology', *Mol Syst Biol*, 10: 757.

Hughes, M. E., J. B. Hogenesch, and K. Kornacker. 2010. 'JTK_CYCLE: an efficient nonparametric algorithm for detecting rhythmic components in genome-scale data sets', *J Biol Rhythms*, 25: 372-80.

Hugill, A. J., M. E. Stewart, M. A. Yon, F. Probert, I. J. Cox, T. A. Hough, C. L. Scudamore, L. Bentley, G. Wall, S. E. Wells, and R. D. Cox. 2015. 'Loss of arylformamidase with reduced thymidine kinase expression leads to impaired glucose tolerance', *Biol Open*, 4: 1367-75.

Itoh, M., T. Takahashi, N. Sakaguchi, Y. Kuniyasu, J. Shimizu, F. Otsuka, and S. Sakaguchi. 1999. 'Thymus and autoimmunity: production of CD25+CD4+ naturally anergic and suppressive T cells as a key function of the thymus in maintaining immunologic self-tolerance', *J Immunol*, 162: 5317-26.

Jenkins, M. R., and G. M. Griffiths. 2010. 'The synapse and cytolytic machinery of cytotoxic T cells', *Curr Opin Immunol*, 22: 308-13.

Jenne, C. N., and P. Kubes. 2013. 'Immune surveillance by the liver', *Nat Immunol*, 14: 996-1006.

Josefowicz, S. Z., L. F. Lu, and A. Y. Rudensky. 2012. 'Regulatory T Cells: Mechanisms of Differentiation and Function', *Annual Review of Immunology, Vol 30*, 30: 531-64.

Kandula, S., and C. Abraham. 2004. 'LFA-1 on CD4+ T cells is required for optimal antigen-dependent activation in vivo', *J Immunol*, 173: 4443-51.

Katzenellenbogen, M., L. Mizrahi, O. Pappo, N. Klopstock, D. Olam, J. Jacob-Hirsch, N. Amariglio, G. Rechavi, E. Domany, E. Galun, and D. Goldenberg. 2007. 'Molecular mechanisms of liver carcinogenesis in the mdr2-knockout mice', *Mol Cancer Res*, 5: 1159-70.

Keller, M., J. Mazuch, U. Abraham, G. D. Eom, E. D. Herzog, H. D. Volk, A. Kramer, and B. Maier. 2009. 'A circadian clock in macrophages controls inflammatory immune responses', *Proc Natl Acad Sci U S A*, 106: 21407-12.

Kelley-Loughnane, N., G. E. Sabla, C. Ley-Ebert, B. J. Aronow, and J. A. Bezerra. 2002. 'Independent and overlapping transcriptional activation during liver development and regeneration in mice', *Hepatology*, 35: 525-34.

Kim, J. M., J. P. Rasmussen, and A. Y. Rudensky. 2007. 'Regulatory T cells prevent catastrophic autoimmunity throughout the lifespan of mice', *Nat Immunol*, 8: 191-7.

Kim, S. D., M. Antenos, E. J. Squires, and G. M. Kirby. 2013. 'Cytochrome P450 2A5 and bilirubin: mechanisms of gene regulation and cytoprotection', *Toxicol Appl Pharmacol*, 270: 129-38.

Klein, L., B. Kyewski, P. M. Allen, and K. A. Hogquist. 2014. 'Positive and negative selection of the T cell repertoire: what thymocytes see (and don't see)', *Nat Rev Immunol*, 14: 377-91.

Koboziev, I., F. Karlsson, D. V. Ostanin, L. Gray, M. Davidson, S. Zhang, and M. B. Grisham. 2012. 'Role of LFA-1 in the activation and trafficking of T cells: implications in the induction of chronic colitis', *Inflamm Bowel Dis*, 18: 2360-70.

Koch, M. A., G. Tucker-Heard, N. R. Perdue, J. R. Killebrew, K. B. Urdahl, and D. J. Campbell. 2009. 'The transcription factor T-bet controls regulatory T cell homeostasis and function during type 1 inflammation', *Nat Immunol*, 10: 595-602.

Kohsaka, A., A. D. Laposky, K. M. Ramsey, C. Estrada, C. Joshu, Y. Kobayashi, F. W. Turek, and J. Bass. 2007. 'High-fat diet disrupts behavioral and molecular circadian rhythms in mice', *Cell Metab*, 6: 414-21.

Kolodin, D., N. van Panhuys, C. Li, A. M. Magnuson, D. Cipolletta, C. M. Miller, A. Wagers, R. N. Germain, C. Benoist, and D. Mathis. 2015. 'Antigen- and cytokine-driven accumulation of regulatory T cells in visceral adipose tissue of lean mice', *Cell Metab*, 21: 543-57.

Kon, N., T. Hirota, T. Kawamoto, Y. Kato, T. Tsubota, and Y. Fukada. 2008. 'Activation of TGF-beta/activin signalling resets the circadian clock through rapid induction of Dec1 transcripts', *Nat Cell Biol*, 10: 1463-9.

Koppaka, V., D. C. Thompson, Y. Chen, M. Ellermann, K. C. Nicolaou, R. O. Juvonen, D. Petersen, R. A. Deitrich, T. D. Hurley, and V. Vasiliou. 2012. 'Aldehyde dehydrogenase inhibitors: a comprehensive review of the pharmacology, mechanism of action, substrate specificity, and clinical application', *Pharmacol Rev*, 64: 520-39.

Korn, T., E. Bettelli, M. Oukka, and V. K. Kuchroo. 2009. 'IL-17 and Th17 Cells', *Annu Rev Immunol*, 27: 485-517.

Lan, R. Y., C. Cheng, Z. X. Lian, K. Tsuneyama, G. X. Yang, Y. Moritoki, Y. H. Chuang, T. Nakamura, S. Saito, S. Shimoda, A. Tanaka, C. L. Bowlus, Y. Takano, A. A. Ansari, R. L. Coppel, and M. E. Gershwin. 2006. 'Liver-targeted and peripheral blood alterations of regulatory T cells in primary biliary cirrhosis', *Hepatology*, 43: 729-37.

Lathrop, S. K., S. M. Bloom, S. M. Rao, K. Nutsch, C. W. Lio, N. Santacruz, D. A. Peterson, T. S. Stappenbeck, and C. S. Hsieh. 2011. 'Peripheral education of the immune system by colonic commensal microbiota', *Nature*, 478: 250-4.

Lee, H. M., J. L. Bautista, and C. S. Hsieh. 2011. 'Thymic and peripheral differentiation of regulatory T cells', *Adv Immunol*, 112: 25-71.

Li-Hawkins, J., E. G. Lund, S. D. Turley, and D. W. Russell. 2000. 'Disruption of the oxysterol 7alpha-hydroxylase gene in mice', *J Biol Chem*, 275: 16536-42.

Li, W., S. Zhu, J. Li, Y. Huang, R. Zhou, X. Fan, H. Yang, X. Gong, N. T. Eissa, W. Jahnen-Dechent, P. Wang, K. J. Tracey, A. E. Sama, and H. Wang. 2011. 'A hepatic protein, fetuin-A, occupies a protective role in lethal systemic inflammation', *PLoS One*, 6: e16945.

Liang, B., C. Workman, J. Lee, C. Chew, B. M. Dale, L. Colonna, M. Flores, N. Li, E. Schweighoffer, S. Greenberg, V. Tybulewicz, D. Vignali, and R. Clynes. 2008. 'Regulatory T cells inhibit dendritic cells by lymphocyte activation gene-3 engagement of MHC class II', *J Immunol*, 180: 5916-26.

Loikkanen, I., S. Haghighi, S. Vainio, and A. Pajunen. 2002. 'Expression of cytosolic acetyl-CoA synthetase gene is developmentally regulated', *Mech Dev*, 115: 139-41.

Lopez, M., D. Meier, A. Muller, P. Franken, J. Fujita, and A. Fontana. 2014. 'Tumor necrosis factor and transforming growth factor beta regulate clock genes by controlling the expression of the cold inducible RNA-binding protein (CIRBP)', *J Biol Chem*, 289: 2736-44.

Luster, A. D. 2002. 'The role of chemokines in linking innate and adaptive immunity', *Curr Opin Immunol*, 14: 129-35.

MacDonald, H. R. 2002. 'Development and selection of NKT cells', *Curr Opin Immunol*, 14: 250-4.

Maria, A., K. A. English, and J. D. Gorham. 2014. 'Appropriate development of the liver Treg compartment is modulated by the microbiota and requires TGF-beta and MyD88', *J Immunol Res*, 2014: 279736.

Mauad, T. H., C. M. van Nieuwkerk, K. P. Dingemans, J. J. Smit, A. H. Schinkel, R. G. Notenboom, M. A. van den Bergh Weerman, R. P. Verkruisen, A. K. Groen, R. P. Oude Elferink, and et al. 1994. 'Mice with homozygous disruption of the mdr2 P-glycoprotein gene. A novel animal model for studies of nonsuppurative inflammatory cholangitis and hepatocarcinogenesis', *Am J Pathol*, 145: 1237-45.

McAlister, G. C., D. P. Nusinow, M. P. Jedrychowski, M. Wuhr, E. L. Huttlin, B. K. Erickson, R. Rad, W. Haas, and S. P. Gygi. 2014. 'MultiNotch MS3 enables accurate, sensitive, and multiplexed detection of differential expression across cancer cell line proteomes', *Anal Chem*, 86: 7150-8.

Mellor, A. L., and D. H. Munn. 2004. 'IDO expression by dendritic cells: tolerance and tryptophan catabolism', *Nat Rev Immunol*, 4: 762-74.

Miller, J. F. 2011. 'The golden anniversary of the thymus', *Nat Rev Immunol*, 11: 489-95.

Min, B., R. McHugh, G. D. Sempowski, C. Mackall, G. Foucras, and W. E. Paul. 2003. 'Neonates support lymphopenia-induced proliferation', *Immunity*, 18: 131-40.

Molyneux, P. C., L. A. Pyle, M. Dillon, and M. E. Harrington. 2015. 'A Mouse Primary Hepatocyte Culture Model for Studies of Circadian Oscillation', *Curr Protoc Mouse Biol*, 5: 311-29.

Moran, A. E., K. L. Holzapfel, Y. Xing, N. R. Cunningham, J. S. Maltzman, J. Punt, and K. A. Hogquist. 2011. 'T cell receptor signal strength in Treg and iNKT cell development demonstrated by a novel fluorescent reporter mouse', *J Exp Med*, 208: 1279-89.

Murphy, K., P. Travers, and M. Walport. 2008. *Janeway's Immuno Biology* (Garland Science).

Nemeth, E., A. W. Baird, and C. O'Farrelly. 2009. 'Microanatomy of the liver immune system', *Semin Immunopathol*, 31: 333-43.

Nguyen, K. D., S. J. Fentress, Y. Qiu, K. Yun, J. S. Cox, and A. Chawla. 2013. 'Circadian gene Bmal1 regulates diurnal oscillations of Ly6C(hi) inflammatory monocytes', *Science*, 341: 1483-8.

Noshiro, M., E. Usui, T. Kawamoto, H. Kubo, K. Fujimoto, M. Furukawa, S. Honma, M. Makishima, K. Honma, and Y. Kato. 2007. 'Multiple mechanisms regulate circadian expression of the gene for cholesterol 7alpha-hydroxylase (Cyp7a), a key enzyme in hepatic bile acid biosynthesis', *J Biol Rhythms*, 22: 299-311.

Notas, G., T. Kisseleva, and D. Brenner. 2009. 'NK and NKT cells in liver injury and fibrosis', *Clin Immunol*, 130: 16-26.

Oberle, N., N. Eberhardt, C. S. Falk, P. H. Krammer, and E. Suri-Payer. 2007. 'Rapid suppression of cytokine transcription in human CD4+CD25 T cells by CD4+Foxp3+ regulatory T cells: independence of IL-2 consumption, TGF-beta, and various inhibitors of TCR signaling', *J Immunol*, 179: 3578-87.

Ohkura, N., M. Hamaguchi, H. Morikawa, K. Sugimura, A. Tanaka, Y. Ito, M. Osaki, Y. Tanaka, R. Yamashita, N. Nakano, J. Huehn, H. J. Fehling, T. Sparwasser, K. Nakai, and S. Sakaguchi. 2012. 'T cell receptor stimulation-induced epigenetic changes and Foxp3 expression are independent and complementary events required for Treg cell development', *Immunity*, 37: 785-99.

Oishi, K., N. Amagai, H. Shirai, K. Kadota, N. Ohkura, and N. Ishida. 2005. 'Genome-wide expression analysis reveals 100 adrenal gland-dependent circadian genes in the mouse liver', *DNA Res*, 12: 191-202.

Partch, C. L., C. B. Green, and J. S. Takahashi. 2014. 'Molecular architecture of the mammalian circadian clock', *Trends Cell Biol*, 24: 90-9.

Pikarsky, E., R. M. Porat, I. Stein, R. Abramovitch, S. Amit, S. Kasem, E. Gutkovich-Pyest, S. Urieli-Shoval, E. Galun, and Y. Ben-Neriah. 2004. 'NF-kappaB functions as a tumour promoter in inflammation-associated cancer', *Nature*, 431: 461-6.

Poltorak, A., X. He, I. Smirnova, M. Y. Liu, C. Van Huffel, X. Du, D. Birdwell, E. Alejos, M. Silva, C. Galanos, M. Freudenberg, P. Ricciardi-Castagnoli, B. Layton, and B. Beutler. 1998. 'Defective LPS signaling in C3H/HeJ and C57BL/10ScCr mice: mutations in Tlr4 gene', *Science*, 282: 2085-8.

Pusterla, T., J. Nemeth, I. Stein, L. Wiechert, D. Knigin, S. Marhenke, T. Longerich, V. Kumar, B. Arnold, A. Vogel, A. Bierhaus, E. Pikarsky, J. Hess, and P. Angel. 2013. 'Receptor for advanced glycation endproducts (RAGE) is a key regulator of oval cell activation and inflammation-associated liver carcinogenesis in mice', *Hepatology*, 58: 363-73.

Ripperger, J. A., L. P. Shearman, S. M. Reppert, and U. Schibler. 2000. 'CLOCK, an essential pacemaker component, controls expression of the circadian transcription factor DBP', *Genes Dev*, 14: 679-89.

Ritchie, M. E., B. Phipson, D. Wu, Y. Hu, C. W. Law, W. Shi, and G. K. Smyth. 2015. 'limma powers differential expression analyses for RNA-sequencing and microarray studies', *Nucleic Acids Res*, 43: e47.

Salomon, B., D. J. Lenschow, L. Rhee, N. Ashourian, B. Singh, A. Sharpe, and J. A. Bluestone. 2000. 'B7/CD28 costimulation is essential for the homeostasis of the CD4+CD25+ immunoregulatory T cells that control autoimmune diabetes', *Immunity*, 12: 431-40.

Sana, G., C. Lombard, O. Vosters, N. Jazouli, F. Andre, X. Stephenne, F. Smets, M. Najimi, and E. M. Sokal. 2014. 'Adult human hepatocytes promote CD4(+) T-cell hyporesponsiveness via interleukin-10-producing allogeneic dendritic cells', *Cell Transplant*, 23: 1127-42.

Scharschmidt, T. C., K. S. Vasquez, H. A. Truong, S. V. Gearty, M. L. Pauli, A. Nosbaum, I. K. Gratz, M. Otto, J. J. Moon, J. Liese, A. K. Abbas, M. A. Fischbach, and M. D. Rosenblum. 2015. 'A Wave of Regulatory T Cells into Neonatal Skin Mediates Tolerance to Commensal Microbes', *Immunity*, 43: 1011-21.

Scheiermann, C., Y. Kunisaki, and P. S. Frenette. 2013. 'Circadian control of the immune system', *Nat Rev Immunol*, 13: 190-8.

Schreiber, H. A., J. Loschko, R. A. Karssemeijer, A. Escolano, M. M. Meredith, D. Mucida, P. Guermonprez, and M. C. Nussenzweig. 2013. 'Intestinal monocytes and macrophages are required for T cell polarization in response to Citrobacter rodentium', *J Exp Med*, 210: 2025-39.

Seki, E., and D. A. Brenner. 2008. 'Toll-like receptors and adaptor molecules in liver disease: update', *Hepatology*, 48: 322-35.

Sekiya, T., I. Kashiwagi, R. Yoshida, T. Fukaya, R. Morita, A. Kimura, H. Ichinose, D. Metzger, P. Chambon, and A. Yoshimura. 2013. 'Nr4a receptors are essential for thymic regulatory T cell development and immune homeostasis', *Nat Immunol*, 14: 230-7.

Shinkai, Y., G. Rathbun, K. P. Lam, E. M. Oltz, V. Stewart, M. Mendelsohn, J. Charron, M. Datta, F. Young, A. M. Stall, and et al. 1992. 'RAG-2-deficient mice lack mature lymphocytes owing to inability to initiate V(D)J rearrangement', *Cell*, 68: 855-67.

Sieber, J., C. Hauer, M. Bhuvanagiri, S. Leicht, J. Krijgsveld, G. Neu-Yilik, M. W. Hentze, and A. E. Kulozik. 2016. 'Proteomic analysis reveals branch-specific regulation of the unfolded protein response by nonsense-mediated mRNA decay', *Mol Cell Proteomics*.

Solt, L. A., Y. Wang, S. Banerjee, T. Hughes, D. J. Kojetin, T. Lundasen, Y. Shin, J. Liu, M. D. Cameron, R. Noel, S. H. Yoo, J. S. Takahashi, A. A. Butler, T. M. Kamenecka, and T. P. Burris. 2012. 'Regulation of circadian behaviour and metabolism by synthetic REV-ERB agonists', *Nature*, 485: 62-8.

Sookoian, S., G. Castano, C. Gemma, T. F. Gianotti, and C. J. Pirola. 2007. 'Common genetic variations in CLOCK transcription factor are associated with nonalcoholic fatty liver disease', *World Journal of Gastroenterology*, 13: 4242-48.

Stefan, N., and H. U. Haring. 2013. 'The role of hepatokines in metabolism', *Nat Rev Endocrinol*, 9: 144-52.

Storch, K. F., O. Lipan, I. Leykin, N. Viswanathan, F. C. Davis, W. H. Wong, and C. J. Weitz. 2002. 'Extensive and divergent circadian gene expression in liver and heart', *Nature*, 417: 78-83.

Sugimoto, N., T. Oida, K. Hirota, K. Nakamura, T. Nomura, T. Uchiyama, and S. Sakaguchi. 2006. 'Foxp3-dependent and -independent molecules specific for CD25+CD4+ natural regulatory T cells revealed by DNA microarray analysis', *Int Immunol*, 18: 1197-209.

Suri-Payer, E., A. Z. Amar, A. M. Thornton, and E. M. Shevach. 1998. 'CD4+CD25+ T cells inhibit both the induction and effector function of autoreactive T cells and represent a unique lineage of immunoregulatory cells', *J Immunol*, 160: 1212-8.

Tai, X., M. Cowan, L. Feigenbaum, and A. Singer. 2005. 'CD28 costimulation of developing thymocytes induces Foxp3 expression and regulatory T cell differentiation independently of interleukin 2', *Nat Immunol*, 6: 152-62.

Taniguchi, H., A. F. Fernandez, F. Setien, S. Ropero, E. Ballestar, A. Villanueva, H. Yamamoto, K. Imai, Y. Shinomura, and M. Esteller. 2009. 'Epigenetic inactivation of the circadian clock gene BMAL1 in hematologic malignancies', *Cancer Res*, 69: 8447-54.

Taniuchi, I. 2009. 'Transcriptional regulation in helper versus cytotoxic-lineage decision', *Curr Opin Immunol*, 21: 127-32.

Thaben, P. F., and P. O. Westermark. 2014. 'Detecting rhythms in time series with RAIN', *J Biol Rhythms*, 29: 391-400.

Thornton, A. M., P. E. Korty, D. Q. Tran, E. A. Wohlfert, P. E. Murray, Y. Belkaid, and E. M. Shevach. 2010. 'Expression of Helios, an Ikaros transcription factor family member, differentiates thymic-derived from peripherally induced Foxp3+ T regulatory cells', *J Immunol*, 184: 3433-41.

Tidball, J. G., and S. A. Villalta. 2010. 'Regulatory interactions between muscle and the immune system during muscle regeneration', *Am J Physiol Regul Integr Comp Physiol*, 298: R1173-87.

Tiegs, G., and A. W. Lohse. 2010. 'Immune tolerance: what is unique about the liver', *J Autoimmun*, 34: 1-6.

Toyabe, S., S. Seki, T. Iiai, K. Takeda, K. Shirai, H. Watanabe, H. Hiraide, M. Uchiyama, and T. Abo. 1997. 'Requirement of IL-4 and liver NK1+ T cells for concanavalin A-induced hepatic injury in mice', *J Immunol*, 159: 1537-42.

Turek, F. W., C. Joshu, A. Kohsaka, E. Lin, G. Ivanova, E. McDearmon, A. Laposky, S. Losee-Olson, A. Easton, D. R. Jensen, R. H. Eckel, J. S. Takahashi, and J. Bass. 2005. 'Obesity and metabolic syndrome in circadian Clock mutant mice', *Science*, 308: 1043-5.

Turman, M. A., T. Yabe, C. McSherry, F. H. Bach, and J. P. Houchins. 1993. 'Characterization of a novel gene (NKG7) on human chromosome 19 that is expressed in natural killer cells and T cells', *Hum Immunol*, 36: 34-40.

Unitt, E., S. M. Rushbrook, A. Marshall, S. Davies, P. Gibbs, L. S. Morris, N. Coleman, and G. J. Alexander. 2005. 'Compromised lymphocytes infiltrate hepatocellular carcinoma: the role of T-regulatory cells', *Hepatology*, 41: 722-30.

Vetrone, S. A., E. Montecino-Rodriguez, E. Kudryashova, I. Kramerova, E. P. Hoffman, S. D. Liu, M. C. Miceli, and M. J. Spencer. 2009. 'Osteopontin promotes fibrosis in dystrophic mouse muscle by modulating immune cell subsets and intramuscular TGF-beta', *J Clin Invest*, 119: 1583-94.

Vignali, D. A., L. W. Collison, and C. J. Workman. 2008. 'How regulatory T cells work', *Nat Rev Immunol*, 8: 523-32.

Villalta, S. A., W. Rosenthal, L. Martinez, A. Kaur, T. Sparwasser, J. G. Tidball, M. Margeta, M. J. Spencer, and J. A. Bluestone. 2014. 'Regulatory T cells suppress muscle inflammation and injury in muscular dystrophy', *Sci Transl Med*, 6: 258ra142.

Vinas, O., R. Bataller, P. Sancho-Bru, P. Gines, C. Berenguer, C. Enrich, J. M. Nicolas, G. Ercilla, T. Gallart, J. Vives, V. Arroyo, and J. Rodes. 2003. 'Human hepatic stellate cells show features of antigen-presenting cells and stimulate lymphocyte proliferation', *Hepatology*, 38: 919-29.

Wang, Y., T. Liu, W. Tang, B. Deng, Y. Chen, J. Zhu, and X. Shen. 2016. 'Hepatocellular Carcinoma Cells Induce Regulatory T Cells and Lead to Poor Prognosis via Production of Transforming Growth Factor-beta1', *Cell Physiol Biochem*, 38: 306-18.

Ward, S. M., B. C. Fox, P. J. Brown, J. Worthington, S. B. Fox, R. W. Chapman, K. A. Fleming, A. H. Banham, and P. Klenerman. 2007. 'Quantification and localisation of FOXP3+ T lymphocytes and relation to hepatic inflammation during chronic HCV infection', *J Hepatol*, 47: 316-24.

Warren, A., D. G. Le Couteur, R. Fraser, D. G. Bowen, G. W. McCaughan, and P. Bertolino. 2006. 'T lymphocytes interact with hepatocytes through fenestrations in murine liver sinusoidal endothelial cells', *Hepatology*, 44: 1182-90.

Watts, T. H. 2005. 'TNF/TNFR family members in costimulation of T cell responses', *Annu Rev Immunol*, 23: 23-68.

Winau, F., G. Hegasy, R. Weiskirchen, S. Weber, C. Cassan, P. A. Sieling, R. L. Modlin, R. S. Liblau, A. M. Gressner, and S. H. Kaufmann. 2007. 'Ito cells are liver-resident antigen-presenting cells for activating T cell responses', *Immunity*, 26: 117-29.

Wohlfert, E. A., J. R. Grainger, N. Bouladoux, J. E. Konkel, G. Oldenhove, C. H. Ribeiro, J. A. Hall, R. Yagi, S. Naik, R. Bhairavabhotla, W. E. Paul, R. Bosselut, G. Wei, K. Zhao, M. Oukka, J. Zhu, and Y. Belkaid. 2011. 'GATA3 controls Foxp3(+) regulatory T cell fate during inflammation in mice', *J Clin Invest*, 121: 4503-15.

Wong, J., B. Johnston, S. S. Lee, D. C. Bullard, C. W. Smith, A. L. Beaudet, and P. Kubes. 1997. 'A minimal role for selectins in the recruitment of leukocytes into the inflamed liver microvasculature', *J Clin Invest*, 99: 2782-90.

Yadav, M., C. Louvet, D. Davini, J. M. Gardner, M. Martinez-Llordella, S. Bailey-Bucktrout, B. A. Anthony, F. M. Sverdrup, R. Head, D. J. Kuster, P. Ruminski, D. Weiss, D. Von Schack, and J. A. Bluestone. 2012. 'Neuropilin-1 distinguishes natural and inducible regulatory T cells among regulatory T cell subsets in vivo', *J Exp Med*, 209: 1713-22, S1-19.

Yadav, M., S. Stephan, and J. A. Bluestone. 2013. 'Peripherally induced tregs - role in immune homeostasis and autoimmunity', *Front Immunol*, 4: 232.

Yang, S., N. Fujikado, D. Kolodin, C. Benoist, and D. Mathis. 2015. 'Regulatory T cells generated early in life play a distinct role in maintaining self-tolerance', *Science*, 348: 589-94.

Yoshitane, H., H. Ozaki, H. Terajima, N. H. Du, Y. Suzuki, T. Fujimori, N. Kosaka, S. Shimba, S. Sugano, T. Takagi, W. Iwasaki, and Y. Fukada. 2014. 'CLOCK-controlled polyphonic regulation of circadian rhythms through canonical and noncanonical E-boxes', *Mol Cell Biol*, 34: 1776-87.

Yu, X., D. Rollins, K. A. Ruhn, J. J. Stubblefield, C. B. Green, M. Kashiwada, P. B. Rothman, J. S. Takahashi, and L. V. Hooper. 2013. 'TH17 cell differentiation is regulated by the circadian clock', *Science*, 342: 727-30.

Zhang, Y., B. Fang, M. J. Emmett, M. Damle, Z. Sun, D. Feng, S. M. Armour, J. R. Remsberg, J. Jager, R. E. Soccio, D. J. Steger, and M. A. Lazar. 2015. 'GENE REGULATION. Discrete functions of nuclear receptor Rev-erbalpha couple metabolism to the clock', *Science*, 348: 1488-92.

Zheng, Y., A. Chaudhry, A. Kas, P. deRoos, J. M. Kim, T. T. Chu, L. Corcoran, P. Treuting, U. Klein, and A. Y. Rudensky. 2009. 'Regulatory T-cell suppressor program co-opts transcription factor IRF4 to control T(H)2 responses', *Nature*, 458: 351-6.

Zheng, Y., S. Josefowicz, A. Chaudhry, X. P. Peng, K. Forbush, and A. Y. Rudensky. 2010. 'Role of conserved non-coding DNA elements in the Foxp3 gene in regulatory T-cell fate', *Nature*, 463: 808-12.

Zhou, B., Y. Zhang, F. Zhang, Y. Xia, J. Liu, R. Huang, Y. Wang, Y. Hu, J. Wu, C. Dai, H. Wang, Y. Tu, X. Peng, Y. Wang, and Q. Zhai. 2014. 'CLOCK/BMAL1 regulates circadian change of mouse hepatic insulin sensitivity by SIRT1', *Hepatology*, 59: 2196-206.

Zhou, Y., L. Jiang, and L. Rui. 2009. 'Identification of MUP1 as a regulator for glucose and lipid metabolism in mice', *J Biol Chem*, 284: 11152-9.

10 Appendix

Table 11: Comparison of Cyp proteins expressed in the liver of neonatal versus adult mice assessed by quantitative mass spectrometry analysis

Cyp family	ratio 10 d vs. 6 w (log2)
Cyp3a16	2.673902854
Cyp8b1	0.916744235
Cyp2b10	0.87522133
Cyp2e1	0.850513161
Cyp2c68	0.53333506
Cyp20a1	0.195852667
Cyp2a22	0.154792124
Cyp2a12	-0.051992553
Cyp2j6	-0.079158093
Cyp4f13	-0.214579863
Cyp3a11	-0.263317076
Cyp17a1	-0.27450794
Cyp39a1	-0.360867147
Cyp2b9	-0.433282307
Cyp3a41a	-0.442877703
Cyp2d26	-0.509703585
Cyp3a13	-0.56086937
Cyp2c70	-0.605611663
Cyp4v3	-0.625837743
Cyp3a25	-0.627110026
Cyp2c40	-0.807309813
Cyp2c44	-0.817228558
Cyp4f15	-0.875600994
Cyp2j5	-0.887598566
Cyp2d22	-1.09655644
Cyp4a14	-1.098618187
Cyp2c69	-1.118264309
Cyp4b1	-1.262737809
Cyp2c39	-1.311468046
Cyp2c29	-1.315866345
Cyp2f2	-1.514013273
Cyp1a2	-1.563276638
Cyp2c37	-1.591945
Cyp51a1	-1.705518188
Cyp27a1	-1.796582324
Cyp4a10	-1.85196221
Cyp2c55	-1.960053735
Cyp2d10	-2.12992269

Cyp7b1	-2.426508991
Cyp2c50	-2.482782026
Cyp2b13	-2.616427292
Cyp2a4	-3.038459349
Cyp2c54	-3.12188461
Cyp2a5	-3.921219474

Table 12: List of cluster of genes following the dysregulated pattern of *Per1* expression during T_{reg} cell depletion

Gene name	Probe ID
PER1	ILMN_2813484
PER1	ILMN_2813487
1110020G09RIK	ILMN_1237830
DAAM1	ILMN_1246330
ZFP238	ILMN_2459155
PTP4A1	ILMN_1223414
ASGR2	ILMN_2613758
SEMA4G	ILMN_2718314
MAGIX	ILMN_2705203
PPP1R15B	ILMN_1239754
DUSP16	ILMN_3112011
ACO1	ILMN_1216382
SYNPO	ILMN_2422982
ACOX1	ILMN_2771368
PDXP	ILMN_1228470
PER2	ILMN_2987863
TMEM150	ILMN_2653395
BHLHB2	ILMN_1249378
4931406C07RIK	ILMN_2612325
TMEM57	ILMN_2657921
VPS4B	ILMN_2455501

Table 13: List of cluster of genes following the dysregulated pattern of *Rev-Erb-α* expression during T_{reg} cell depletion

Gene name	Probe ID
REV-ERBA-a	ILMN_2749669
LOC100047427	ILMN_1229091
DBP	ILMN_2616226
FAM102A	ILMN_1225348
CIART	ILMN_3102736
CIART	ILMN_1236079
CCDC85B	ILMN_1220846
PCSK4	ILMN_2629776
CIART	ILMN_3029489
REV-ERBA-b	ILMN_2798993
CDV3	ILMN_2673894
SLC5A6	ILMN_1225056
PIK3AP1	ILMN_1257623
A730054J21RIK	ILMN_2447991
CPOX	ILMN_2972755
RRP12	ILMN_2728118
RGS16	ILMN_2600744
LRP4	ILMN_1244134
PER2	ILMN_2987862
PCSK4	ILMN_1252464
RPA2	ILMN_2597840

11 Abbreviations

%	**Percent**
°C	Degree Celsius
µg	Micro gram
µl	Micro liter
µm	Micro meter
µM	Micro Molar
Acadsb	Acyl-CoA dehydrogenase
ACK buffer	Ammonium chloride–potassium bicarbonate cell lysis buffer
Acot	Acyl-CoA thioesterase
Acot12	Acyl-CoA thioesterase 12
Acss2	Acetyl-coenzyme A synthetase
Afmid	Arylformamidase
Afp	Alpha-fetoprotein
Ahsg	Alpha2-HS
AIV	Autoimmune hepatitis
Aldh	Aldehyde dehydrogenase
ALT	Alanine-aminotransferase
APC	Antigen presenting cell
AST	Aspartate transaminase
Atf3	Activating transcription factor 3
Birc5	Survivin
Bmal1	Brain and muscle Arnt-like 1
BSA	Bovine serum albumin

Ca^{2+}	Calcium
cAMP	Second messenger cyclic adenosine monophosphate
CD	Clusters of differentiation
CD11a	Lymphocyte function-associated antigen 1 (LFAT)
Ciart	Circadian associated repressor of transcription
Clock	Circadian locomotor output cycles kaput
CLPs	Common lymphoid progenitors
CNS3	Conserved non-coding sequence 3
Cry	Cryptochrome
Csad	Cysteine sulfinic acid decarboxylase
cTECs	Cortical thymic epithelial cells
CTL	Cytotoxic T lymphocyte
CTLA-4	Cytotoxic T lymphocyte associated antigen 4
Cyp	Cytochrome P450
Dbp	Albumin D-box binding protein
DC	Dendritic cell
Ddo	D-aspartate oxidase
DMB	Human Duchenne muscular dystrophy
DMEM	Dulbecco‘s Modified Eagle‘s Medium
DMSO	Dimethyl sulfoxide
DN cell	CD4 and CD8 double-negative cell
DNA	Deoxyribonucleic acid
DP cell	CD4 and CD8 double-positive cell
DT	Diphtheria toxin
DTR	Diphteria toxin receptor

E-box	Canonical Enhancer box
EDTA	Ethylenediaminetetraacetic acid
EGF-R	Epidermal growth factor receptor
FACS	Fluorescence activated cell sorting
FBS	Fetal bovine serum
FC	Fold change
FDR	False discovery rates
Fen1	Flap structure-specific endonuclease 1
FITC	Fluorescein isothiocyanate
Foxo3	Insulin-phosphatidylinositol 3-kinase-Forkhead box class O3a
FOXP3	Forkhead box 3
GFP	Green fluorescent protein
Glul	Glutamine synthetase
GO	Gene Ontology
HCC	Hepatocellular cancer
HCV	Hepatitis C virus
HEPES	4-(2-hydroxylethyl)-1-piperazineethanesulfonic acid
HSCs	Hematopoietic stem cells
IDO	Indoleamine 2, 3-dioxygenase
IFN-γ	Interferon γ
Ig	Immunoglobulin
IL	Interleukin
IPEX	Immunodysregulation polyendocrinopathy, enteropathy X-linked
iT_{reg} cell	(in vitro) Induced regulatory T cell
Junb	Jun B proto-oncogene

LAG3	CD4 homologue lymphocyte activation gene 3
LC-ESI-MS/MS	Liquid chromatography-electrospray ionization -tandem MS
Lig1	Ligase 1
LSECs	Liver sinusoidal endothelium cells
Mcm	Members of the DNA helicase complex
mdx	Muscular dystrophy
MHC	Major histocompatibility complex
min	Minutes
ml	Milliliter
mM	Milli Molar
MS	Mass spectrometry
mTEC	Medullary thymic epithelial cell
Mup	Major urinary family
NK cell	Natural killer cell
Nkg7	Natural killer cell protein 7
NKT cell	Natural killer T cell
Nr4a1	Nuclear receptor 4a1
Nrp1	Neuropilin 1
Otc	Ornithine transcarbamylase
PBC	Primary biliary cirrhosis
PBS	Phosphate buffered saline
PCR	Polymerase chain reaction
Per	Period
PH	Primary hepatocytes
Ppar-g	Peroxisome proliferator-activated receptor-g

PRRs	Pattern-recognition receptors
pT_{reg} cell	Peripheral induced regulatory T cell
qPCR	Quantitative real-time PCR
RNA	Ribonucleic acid
Rora	Nuclear retinoid-related orphan receptor a
Rore	Ror response element
rpm	Rounds per minute
RT	Room temperature
SCN	Suprachiasmatic nucleus
T_{conv} cell	Conventional T cell
TCR	T cell receptor
TGF-β	Transforming growth factor β
T_H cell	T helper cell
TLR	Toll-like-receptor
Top2a	DNA topoisomerase 2-alpha
T_{reg} cell	Regulatory T cell
TSDR	T_{reg}-specific demethylation region
tT_{reg} cell	Thymic derived regulatory T cell
VAT	Visceral adipose tissue
α	alpha
β	beta
γ	gamma
δ	delta

12 Acknowledgments

I want to take the opportunity to say **THANK YOU** to the people and institutions contributed to the success of my PhD studies.

I want to thank my advisor Dr. Markus Feuerer for giving me the opportunity to work in his laboratory, for his supervision of my work during my PhD project, and for his scientific advice and help. I really enjoyed my time in the lab!

Thanks to Ulrike Träger for proof reading this work, discussing with me in the lab and answering all my questions!!!

Thanks to all members of the Immune tolerance group, it was always a pleasure to work with you: David Richards, Melanie Barra, Michael Delacher, Ulrike Träger, Dany Kägebein, Sabine Schmitt and Kristin Lobbes! Additionally, I would like to thank my interns for the help on my PhD project: Alexandra Schnell and Ayse Menevse. I had a lot of fun with you two!
Julia, Eva, Ulrike, Kristin and Fabian: Thanks for the nice lunch or coffee breaks!!!

The Flow Cytometry core facility, the Animal core facility as well as the Genomics and Proteomics core facility at the DKFZ always provided excellent assistance.
I want to thank the members of my thesis defence and thesis advisory committees for their support: Prof. Dr. Peter Angel, Prof. Dr. Viktor Umansky, Prof. Dr. Ana Martin-Villalba and Dr. Jeroen Krijgsveld. Additionally, I want to thank all of our collaborators for their knowledge and support. Thank you!
This work was financially supported by a stipend from the DKFZ-MOST (Ministry of Science, Culture and Sport) program.

A warm Thank you to my parents Renate and Norbert Joschko, my sister Natalie, my husband Sebastian Hofer and the Hofer family for supporting me in any way during the past years. You are the best!